DEVELOPMENT OF DRUG CONJUGATES FOR CANCER THERAPY AND EVALUATION OF DUAL SIRNA SILENCING EFFECT ON BREAST CANCER GROWTH AND INVASION

A DISSERTATION IN
Pharmaceutical Science
and
Chemistry

Presented to the Faculty of the University of
Missouri-Kansas City in partial fulfillment of
the requirements for the degree

DOCTOR OF PHILOSOPHY

by
WANYI TAI

B.S., China Pharmaceutical University, 2004
M.S., Shanghai Institute of Materia Medica, Chinese Academy of Sciences, 2007

Kansas City, Missouri
2012

DEVELOPMENT OF DRUG CONJUGATES FOR CANCER THERAPY AND EVALUATION OF DUAL SIRNA SILENCING EFFECT ON BREAST CANCER GROWTH AND INVASION

Wanyi Tai, Candidate for the Doctor of Philosophy Degree

University of Missouri-Kansas City, 2012

ABSTRACT

The objective of this dissertation is to present various approaches for treatment cancer, which is the leading cause of death worldwide. Compared to other disease, cancer has many unique biological characteristics that can be exploited for its therapy. In chapter 1 and 2, its molecular characteristics and microenvironments, as well as the corresponding therapeutic strategies, are summarized.

In chapter 3, we developed a peptide drug conjugate to specifically deliver TGX-221 to HER2 overexpressed prostate cancer cells. TGX-221 is a highly potent phosphoinositide 3-kinases β (PI3Kβ) inhibitor that holds great promise as a novel chemotherapy agent for prostate cancer. However, poor solubility and lack of targetability limit its therapeutic applications. The peptide drug conjugate was proven to be gradually cleaved by PSA to release TGX-D1 (TGX-221 analogue). Both the peptide drug conjugate and its cleaved products demonstrate a comparable activity to the parent drug, TGX-D1. Moreover, cellular uptake of the peptide drug conjugate and its cleaved product SL-TGX were significantly higher in prostate cancer cells compared to the parent drug. The high cellular uptake of dipeptide drug conjugate SL-TGX might be mediated by peptide transporters in prostate cancer cells. However, the expression of

peptide transporters in prostate cancer cell lines has not been reported before. Therefore, in Chapter 4, the expression profile and functional activity of peptide transporters were investigated in the prostate cancer cell lines LNCaP, PC-3 and DU145. Peptide transporter 1 (PEPT1) is found overexpressed in PC-3 cells, and peptide transporter 2 (PEPT2) is upregulated in LNCaP cells.

We also developed another approach to enhance water solubility and targetability of hydrophobic drugs. In Chapter 5, we developed a polymer-rapamycin conjugate using a novel, linear and PEG based multiblock copolymer (Mw ~ 32 kDa). Rapamycin has demonstrated potent anti-tumor activity in preclinical and clinical studies. However, the clinical development of its formulations has been hampered due to its poor solubility and undesirable distribution *in vivo*. The polymer-rapamycin conjugate provided enhanced solubility in water compared with free rapamycin and shows a profound activity against a panel of human cancer cell lines. This polymer-rapamycin conjugate also presented high drug loading capacity (wt% ~ 28%) when GlyGlyGly was used as a linker. The uptake study further indicated that the lysosome is the major site of intracellular localization of polymer drug conjugate. Thus, these preclinical data suggested that polymer rapamycin conjugate is a novel anti-cancer agent that holds great promising for treatment of a wide variety of tumors.

Macromolecules such as siRNA can also be used as anticancer drugs. In chapter 6, we designed nine HER2 siRNAs and ten VEGF siRNAs and identified potent siRNA that can silence the target gene up to 75-83%. The most potent HER2 and VEGF siRNAs were used to conduct functional studies in HER2 positive breast cancer cells. Combination of HER2 and VEGF siRNAs demonstrated synergistic silencing effect on VEGF. Both HER2 siRNA and

VEGF siRNA showed significant inhibition on cell migration and proliferation. HER2 siRNA also demonstrated dramatic suppression of cell spreading and adhesion to ECM, as well as induction of apoptosis. Dual silencing of HER2 and VEGF led to significant cell morphology change and substantial suppression on migration, spreading, cell adhesion, and proliferation.

APPROVAL PAGE

The Faculty listed below, appointed by the Dean of the School of Graduate Studies, have examined a dissertation titled "Development of Drug Conjugates in Cancer Therapy and Evaluation of Dual siRNA Silencing Effect on Breast Cancer Growth and Invasion", presented by Wanyi Tai, candidate for the Doctor of Philosophy, and certify that in their opinion it is worthy of acceptance.

Supervisory Committee

Kun Cheng, Ph.D., Committee Chair
Division of Pharmaceutical Sciences

Ashim K. Mitra, Ph.D.
Division of Pharmaceutical Sciences

Mridul Mukherji, Ph.D.
Division of Pharmaceutical Sciences

Zhonghua Peng, Ph.D.
Department of Chemistry

David Van Horn, Ph.D.
Department of Chemistry

TABLE OF CONTENTS

LIST OF ILLUSTRATIONS

LIST OF TABLES

ACKNOWLEDGEMENTS

I would like to express my greatest gratitude to my advisor Dr. Kun Cheng for his patient guidance, continuous support and persistent encouragement during my Ph.D. study. His prompt feedback and valuable suggestion always accelerate my research work.

I also would like to thank Dr. Ashim K. Mitra, Dr. Mridul Mukherji, Dr. Zhonghua Peng and Dr. David Van Horn for their kindly serving on my supervisory committee. Their valuable discussion, insightful comments and helpful assistance motivate me to excel my study throughout my graduate research work at University of Missouri-Kansas City.

I wish to thank Dr. William G. Gutheil and Dr. Ravinder Earla for their help of LC-MS/MS. My acknowledgement also goes to Bin Qin, Rubi Mahato, Ravi K Shukla, Zhijin Chen and Wei Jin for their time, help, discussion and cooperation in my research.

I also would like to thank all other professors and all the graduate students in our division for their help and friendship. My sincerest gratitude also goes to Joyce Johnson, Sharon Self and Nancy Bahner for their help over the past five years.

I would like to give my deepest thanks to my wife, Fei Chen, for her encouragement, support and love. I also thank my parents and my sister for their understanding and sacrifices during my graduate study.

CHAPTER 1

INTRODUCTION

1.1. Overview

Cancer is a leading cause of death worldwide and accounted for approximately 13% of all human deaths in 2008 (7.6 million) [1]. GLOBOCAN 2008 estimated that there were approximately 12.7 million cancer cases in 2008. Because the human population is continually growing and aging, the incidence of cancer is becoming even more common, and approximately 12 million cancer-related deaths are estimated in 2030 (World Health Organization). Moreover, environmental factors, which are a major cause of cancer, are likely to contribute to increased cancer mortality in the future because people are more exposed to tobacco, poor diet, obesity, infection, radiation and environmental pollutants [2]. The global burden of cancer continues to rise in both economically developing and developed countries.

Characterized by uncontrollable and abnormal cell growth in the body, cancer is a large class of very difficult diseases to treat. Cancers are primarily caused by genetic mutations that alter cell growth and mediate invasion and metastasis. These genetic mutations often either up-regulate oncogenes or silence tumor suppressor genes. Compared to normal cells, cancer cells have many unique biological characteristics that can be exploited as therapeutic targets. For example, over-expressed receptors in cancer cells could be targeted by monoclonal antibodies for cancer therapy or targeted drug delivery, while over-activated proteases could be employed to specifically activate prodrugs at tumor sites. Moreover, solid tumors develop a tumor microenvironment that is favorable for targeted drug delivery. This microenvironment is characterized by large fenestration, lack of smooth muscle layers, and ineffective lymphatic

drainage, and therefore, it helps to accumulate nanoscale particles and macromolecules in tumor tissues rather than in normal tissues. This passive targeting phenomenon is termed the "enhanced permeability and retention (EPR) effect". Both active targeting and passive targeting therapies have been extensively utilized in translational research of advanced drug delivery in cancer therapy.

1.2. Statement of the Problem

TGX-221 is a novel, potent, isoform-specific, and cell-permeable small molecule inhibitor of PI3K-p110β. It exhibits a significant suppression of the p110β activity in prostate cancer cell lines as well as prostate cancer animal model [3]. However, assessment of the therapeutic potential was halted due to its very poor solubility. Organic solvent is required for the intravenous administration of TGX-221, which may cause significant toxicities [3]. Therefore, a water soluble formulation of this compound is highly desirable for its future therapeutic application.

Rapamycin is a well-known immunosuppressant drug that has been widely used in organ transplantation. Besides its immunosuppressant function, rapamycin is a potent mTOR (mammalian target of rapamycin) inhibitor. mTOR is closely related to the phosphoinositide 3-kinase (PI3K) pathway and acts as a central modulator of cell growth, motility and survival. Rapamycin has demonstrated potent anti-tumor activity in preclinical and clinical studies. However, the clinical development of its formulations has been hampered due to its poor solubility and undesirable distribution *in vivo*. Chemical modification of rapamycin may present an opportunity to overcome the obstacles and improving its therapeutic index.

In order to circumvent the problems of TGX-221 and rapamycin, two novel drug conjugates have been designed and synthesized. A multi-functional peptide was conjugated with TGX-D1 (a derivative of TGX-221) to increase its solubility and targetability. Rapamycin was conjugated with a novel hydrophilic polymer to improve the solubility and distribution profile of rapamycin. Both these two drug conjugate hold great promise for cancer therapy.

1.3. Objective

The objectives of this dissertation are:

(1). To develop a peptide drug conjugate for prostate cancer. A multi-functional peptide is conjugated with drug TGX-D1. This peptide contains a HER2 binding ligand and a Prostate Specific Antigen (PSA) cleavable linker. After conjugated with TGX-D1, the peptide can specifically deliver the drug to HER2 overexpressed prostate cancer cells and release the parent drug by PSA specific cleavage.

(2). To explore the expression profile and functional activity of peptide transporters in prostate cancer cell lines; To explore mRNA and protein expression profile of peptide transporters in prostate cancer cell lines by qRT-PCR and western blot analysis; To examine transport activity by radiolabeled Gly-Sar and *L*-Histidine.

(3). To synthesize and evaluate a polymer rapamycin conjugate for cancer therapy; To design and synthesize a novel, linear poly(ethylene glycol) multiblock copolymer; To conjugate the polymer with rapamycin and evaluate the bioconjugate's bioacitivity; To track the cellular uptake and distribution of the polymer drug conjugate in cancer cell.

(4). To inhibit breast cancer cell growth and invasiveness by dual silencing of HER2 and VEGF; To screen the most potent HER2 siRNA and VEGF siRNA by real time PCR and ELISA; To examine the synergic effect of HER2 siRNA and VEGF siRNA on cell growth, migration, spreading, attachment and apoptosis.

CHAPTER 2

REVIEW OF LITERATURE

2.1. Biological Characteristics of Cancer

Molecular characteristics

Cancers have unique molecular characteristics that make their cells different from normal cells and unique to each other. All of the unique molecular characteristics are related to genomic instability and mutations. Genomic instability and its mutations directly drive the process of cancer development. The molecular characteristics of cancers can be classified into two phenotypes: the over-expression of oncogenes and the down-regulation of tumor suppressor genes. This section is mainly focused on oncogenes because over-expressed oncogenes are the most popular target for cancer drug therapy. Oncogenes and their pathways, such as sonic hedgehog, Wnt, Transforming growth factor β (TGFβ), and Hippo signaling pathways are overexpressed or activated in cancer cells, but they are mainly used as targets for cancer therapy rather than for targeted drug delivery. In this section, two types of oncogenes, oncogenic receptors and oncogenic enzymes, will be discussed in detail.

Over-expression of cell signaling receptors is one of the most common oncogenic alterations in cancer. When the receptors are over-expressed, the downstream signaling pathways are hyperactivated, and tumors are generated with unlimited proliferation potential and an unstable genotype. Human epidermal growth factor receptor 2 (HER2) is a well-known oncogenic receptor that is over-expressed in many cancers. Approximately 25% of all breast cancer cases are associated with HER2 over-expression [4]. The expression level of HER2 in breast cancer cells is generally 10 to 100-fold higher than in normal tissues [5]. Over-expression

of HER2 significantly promotes the formation of HER2 hetero dimers, which activates the HER2 signaling cascades, including the phosphoinositide phospholipase C γ (PLCγ), phosphatidylinositol 3 kinases (PI3K), and mitogen-activated protein kinases (MAPK) pathways. As an oncogenic membrane receptor, overexpressed HER2 is a reasonable target for cancer therapy and targeted drug delivery. Several HER2 specific antibodies and antibody-drug conjugates have been developed in clinical research [4]. Besides HER2, prostate-specific membrane antigen (PSMA) in prostate cancer, CD33 in relapsed acute myeloid leukaemia, epidermal growth factor receptor (EGFR) in lung cancer, and mesothelin in pancreatic cancer are also commonly altered molecular characteristics of cancers.

Oncogenic enzymes, including kinases and digestive enzymes, have been found to be over-expressed in many human cancers. Kinases represent one of the largest enzyme families, and there are more than 500 kinases encoded in the human genome [6, 7]. Kinases regulate most of the important intracellular signal transduction pathways and directly control cell proliferation and biological responses to environmental stimuli. Numerous kinases, especially the key components of signal transduction pathways, are attractive targets for cancer chemotherapy. These kinases include the PI3K family, AGC kinase family, CMGC kinase family, Abelson cytoplasmic tyrosine kinase (AbI), aurora kinase, and cyclin-dependent kinase (CDK) [8-10]. Small molecule drugs, rather than antibodies, are the most successful inhibitors to modulate kinase activities due to their high penetration ability, potency and selectivity. Digestive enzymes are another type of enzymes over-expressed in many human cancers. For example, matrix metalloproteinase (MMP) is a zinc-dependent endopeptidase that degrades all types of extracellular matrix proteins. Degradation of the extracellular matrix is crucial for malignant

tumor growth, angiogenesis, invasion and metastasis. Elevated MMP expression has been detected in the serum and tumor tissues of patients with advanced cancer. Prostate specific antigen (PSA) and PSMA are two enzymes commonly over-expressed in prostate cancer. PSA is a small proteinase produced by the prostate gland. Elevated levels of PSA have been associated with prostate cancer. Consequently, PSA testing is considered the most effective assay for the early detection of prostate cancer [11]. PSMA is a zinc metalloenzyme that localizes in the cell membrane. It catalyzes the hydrolysis of N-acetylaspartylglutamate (NAAG) to glutamate and N-acetylaspartate. Although PSMA is expressed in many tissues, it is strongly expressed in human prostate cancer. PSMA is expressed 100-fold greater in prostate cancer than in most other tissues and 8 to 12-fold above over non-cancerous prostate tissue [12]. Digestive enzymes in cancer tissues are usually exploited to activate prodrugs by cleaving the peptide linker of the prodrug. After cleavage, the parent drug is released and elicits its therapeutic effect at the tumor site where the digestive enzyme is over-expressed. A number of these prodrugs are under preclinical or clinical evaluations [13-16].

Tumor angiogenesis

Angiogenesis is the physiological process involving the formation of new blood vessels from pre-existing vessels. Angiogenesis is important in embryogenesis, development, wound healing, tumor growth, and metastasis. In tumors, angiogenesis is essentially required for the transition of tumor cells from a dormant state to a malignant state. When a solid tumor is smaller than 2 mm in diameter, oxygen and nutrients can easily diffuse from a nearby blood supply into its center [17]. However, neoangiogenesis is required to form an independent blood supply

within solid tumors larger than 2 mm in diameter. Tumors easily become hypoxic when they outgrow the existing blood supply. As a result, tumor angiogenesis is initiated by the hypoxic microenvironment that switches the balance between anti- and pro-antiogenic factors in favor of angiogenesis [18]. Hypoxia promotes the production of pro-angiogeneic factors such as vascular endothelial growth factor (VEGF), platelet-derived growth factor (PDGF), basic fibroblastic growth factor (bFGF), nitric oxide synthase, and TGF α and β. Among them, VEGF is the most important factor for regulating tumor angiogenesis [19]. Pro-angiogenic factors diffuse across the extratumoral matrix and activate pre-existing vascular endothelial cells, which migrate toward the solid tumor and form new vessel lumen [20]. Other precursor cells such as bone marrow-derived EPCs (endothelial progenitor cells), tissue-derived EPCs, and hematopoietic stem cells also contribute to the formation of the tumor-associated endothelial cells [21]. The establishment of neovasculature inside the tumors shifts them from having a non-angiogenic to an angiogenic phenotype. This process, also termed the "angiogenic switch", is a hallmark of cancer progression [22].

The tumor vasculature is structurally and functionally abnormal compared to normal vessels in healthy tissues (**Figure 1**). Tumor vessels are unevenly distributed, heterogeneous, chaotic, irregularly branched, tortuous, leaky, thin-walled, and pericyte-depleted [23]. In contrast to quiescent endothelial cells, activated tumor endothelial cells can lose their polarity and detach from the basement membrane. Because of its wide junctions and multiple fenestrations that range from 10 to 1000 nm, the tumor vasculature is often leaky [24]. Macromolecules or particles ranging from 20 to 200 nm tend to extravasate and accumulate inside the interstitial space, which has been called the EPR effect [25]. In addition, abnormal tumor vessels also function poorly.

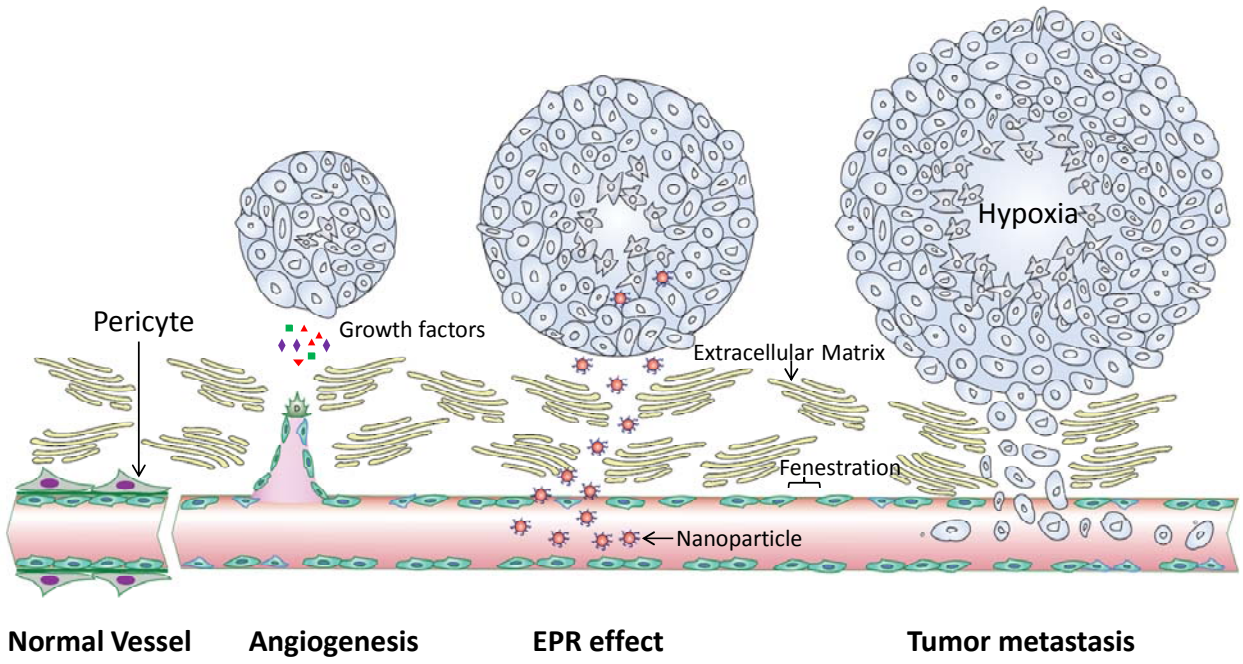

Figure 1. Tumor microenvironment. The tumor vasculature is structurally different from normal vessels in healthy tissues. In normal vessels, endothelial cells are well-aligned along the vessel wall, which is surrounded by pericytes. The walls of tumor vessels have fenestrations and they are not protected by pericytes. The abnormal structure of tumor vasculature leads to the accumulation of macromolecules or particles in tumor tissue, which is called the EPR effect. Tumor cells secrete endothelial growth factors and induce the angiogenesis. Tumor cells also metastasize to other organs through tumor vessels.

Due to the chaotic network and uneven distribution of abnormal tumor vessels, the blood flow is chaotic and even stagnant in some areas. The blood flow direction is also unpredictable, and in a given vessel, blood can flow in both directions [26]. Moreover, because of the leakiness of tumor vessels, the escaping fluid increases the interstitial fluid pressure.

Tumor microenvironment

Tumor hypoxia occurs when a portion of tumor cells undergo oxygen deprivation due to a disordered vasculature. As tumors grow rapidly, high levels of cell proliferation consume oxygen and nutrients at an accelerated rate, which leads to a significantly lower concentration of oxygen in the tumor hypoxic zone than in healthy tissues. Hypoxic tumor cells are relatively quiescent, which renders them resistant to chemotherapy and radiotherapy. Tumor cells in the hypoxic zone are thought to be susceptible to additional genetic mutations that make them resistant to traditional therapy, ultimately contributing to relapse and treatment failure [27]. In clinics, hypoxia has been demonstrated to positively correlate with cancer progression and therapeutic relapse [28]. Tumor hypoxia has therefore been considered to be a potential therapeutic target for cancer. Hypoxic cytotoxins selectively kill the oxygen-deficient tumor cells and have demonstrated potent anticancer activities in a number of preclinical and clinical studies [29, 30].

As a consequence of anaerobic metabolism and poor perfusion, solid tumors exhibit lower external pH than normal tissues. The external pH of a solid tumor is acidic and in the range of 6.0-7.0, whereas the pH in normal tissues and blood is approximately 7.4 [31]. According to the Warburg effect, tumor cells predominantly produce energy by aerobic glycolysis unlike normal cells, which undergo mitochondrial oxidative phosphorylation [32]. Most tumor cells undergo the high rate of glycolysis that generates lactic acids by lactic acid fermentation. Moreover, both hypoxia and genetic mutations promote the expression of lactate dehydrogenase A and decrease the activation of pyruvate dehydrogenase, both of which drive the accumulation of lactatic acid. To favor metabolic flux and avoid cytotoxicity, lactate is then

exported from the cytoplasm with one proton by monocarboxylate transporters [33]. The acidification of the extracellular space is also exacerbated by the over-expression of carbonic anhydrase IX in hypoxic tumor cells. Carbonic anhydrase IX converts CO_2 into a proton and bicarbonate. The bicarbonate anion is subsequently taken up into the cytoplasm by the anion Cl^- /Bicarbonate exchanger, while the proton is kept and contributes to the acidification [34]. This acidic microenvironment is common in solid tumors but rare in healthy tissues, and it therefore provides a potential strategy for stimuli-responsive nanomedicines. The low pH-cleavable PEG-lipid has been used in liposomes and micelles to increase drug half-life without compromising cellular uptake [35].

Interstitial hypertension is another general characteristic of solid tumors. It is the phenomenon that occurs when interstitial fluid pressure in solid tumors is elevated due to the high permeability of the blood vessels. In normal tissues, the pressure in healthy blood vessels is higher than the fluid pressure in the interstitial space. However, in tumors, the fluid escapes from the blood vessels and accumulates in the tumor tissues, leading to a slightly higher pressure in the interstitial space than that in the blood vessel [36]. Interstitial hypertension has been recognized as a significant cause of the poor drug-delivery efficiency in radiotherapy and chemotherapy. Interstitial tumor hypertension reduces drug diffusion and penetration but increases drug efflux, which leads to a poor uptake of anti-cancer drugs, especially large therapeutic agents [37].

Cancer metastasis

As one of the most important hallmarks of malignancy, cancer metastasis is the process by which malignant tumor cells spread from the original site to other non-adjacent organs. A primary tumor generally develops from a single genetically damaged cancer stem cell, which presents the malignant phenotype. The cancer stem cell undergoes unlimited proliferation to produce excessive cancer cells and form the primary tumor in the local area. In some cases, primary tumors can progress into malignant cancers, which are often caused by genetic mutations in the tumor cells. The metastatic process can be classified into several basic steps: local invasion, intravasation, survival in circulation, distant organ infiltration, and colonization [38]. Local invasion starts with activation of metastasis initiation genes that allow primary tumor cells to invade the surrounding tissues. These genes increase cell motility, elevate the expression of proteases to degrade extracellular matrices and promote angiogenesis. Metastasis genes drive cancer cells to invade through the basement membrane, penetrate blood vessels, and enter the circulation. Circulating tumor cells are subjected to additional mechanical stresses, including the shear stress from the circulation system. The number of cells that survive in such a microenvironment is very small, and the circulating tumor cells are at a concentration of approximately 10^3 cells per liter of blood [39]. However, these cells always display a more aggressive phenotype. Distant organ infiltration and colonization by circulating tumor cells involves a reverse procedure of intravasation. Because the microenvironment of each organ is different, circulating tumor cells need to infiltrate through different barriers, survive in that specific microenvironment, and finally overtake that tissue. Different types of tumor cells can colonize the same distant organs, but some tumor cells prefer to metastasize into restricted sites. For example, prostate cancer mostly metastasizes to the bone, while ocular melanoma metastasis

is largely confined to the liver. Colorectal and pancreatic cancer cells often colonize in the liver and lung. Breast and lung carcinoma usually spread to the bone, liver, brain and the adrenal gland [38]. It still remains unclear which genes contribute to the organ-specific metastasis.

2.2. HER2 in Breast Cancer and Prostate Cancer

In normal cells, HER2 plays important roles in all stages of cell development. However, the mutation or overexpression of HER2 could directly lead to tumorigenesis as well as metastasis. Although mutation of the neu gene (rodent HER2 gene) is required for tumorigenesis in rodents, human HER2 appears to hold tumorigenic potential through overexpression of the wild-type HER2 gene. Overexpression of HER2 enhances and prolongs signals that trigger cells' transformation. In human cancers, HER2 is frequently overexpressed in breast cancer, gastric cancer, ovarian cancer and prostate cancer.

HER2 in breast cancer

Overexpression of HER2 usually results in malignant transformation of cells and accounts for ~25% of all breast cancer cases. It is always associated with more aggressive tumor phenotypes, greater likelihood of lymph node involvement, and increased resistance to endocrine therapy [40]. The overall survival rate and relapse time for HER2 positive breast cancer patients are significantly shorter than patients without HER2 overexpression. *In vitro* studies showed that inhibition of HER2 expression induced significant apoptosis in breast cancer cells [41, 42]. Thereafter, HER2 is a logical target for breast cancer therapy. Both prognostic and therapeutic values of HER2 in breast cancer have been established [43]. Most notably, the monoclonal

humanized antibody against HER2 (Trastuzumab) was approved in 1998 by FDA for the treatment of HER2 positive breast cancer [44]. In addition, it has been shown *in vitro* that reduction of HER2 expression by antisense or siRNA resulted in growth inhibition and apoptosis in HER2 positive breast cancer cells [42, 45, 46]. All these data indicate the essential role of HER2 in proliferation and anti-apoptosis in HER2 positive breast cancer.

HER2 in prostate cancer

HER2 also plays pivotal roles in prostate cancer and many efforts have been made to examine the HER2 expression in prostate cancer, albeit the results are somewhat contradictory and confusing [47, 48]. The disparity is partly due to the differences in tumor sample selection, the techniques used to detect HER2, and the definition of "positive" [48]. Signoretti et al. have conducted a comprehensive study to analyze the HER2 level at DNA, RNA and protein levels in tumor samples from different clinical stages. Using an absolute scoring system with a defined "positive" criteria, they found that 25% of untreated primary tumors, 59% of localized tumors after neoadjuvant hormone therapy, and 78% of castrate metastatic tumors overexpressed HER2 [47].

However, the use of antibody targeting HER2 (Trastuzumab) showed little effect on the advanced hormone-refractory prostate cancer in a phase II clinical trial [49]. One possible explanation is that HER2 was not overexpressed in those prostate cancer patients. Nevertheless, several lines of evidence have implicated HER2 as a key mediator in the recurrence of prostate cancer to a hormone-refractory, androgen-independent tumor, which is the hallmark of prostate cancer progress [50]. The driving force for prostate cancer recurrence is the reactivation of

androgen receptor (AR), which is a type of nuclear receptor, activated by steroid hormone but ablated in hormonal therapy. Phosphorylation and reactivation of AR stimulate cancer cell growth and trigger tumor progression [51]. It has been observed that overexpression of HER2 kinase enhanced AR function and hormone-independent growth in prostate tumor cells [52, 53]. It was postulated that HER2 activated AR through the MAPK pathway [53]. Additionally, the HER2/HER3 dimer increases AR protein stability and promotes the binding of AR to the promoter region of its target genes, resulting in AR activation in an androgen-depleted environment. As a result, HER2 may be a promising therapeutic target for the treatment of aggressive hormone-refractory prostate cancer [54, 55]. For example, blockage of HER2 could reverse tumor cells to androgen dependent phenotype, suggesting the combination of anti-HER2 and anti-androgen therapies might be an effective therapy for prostate cancer [56].

2.3. Bioconjugates for Cancer Therapy

Antibody-drug conjugates

Antibody-drug conjugates are constructed by covalently conjugating a recombinant antibody to a cytotoxic chemical via a synthetic linker. Antibody-drug conjugates are considered a successful combination of biological and small molecules, which potentially create highly potent targeting agents. Cytotoxic chemicals provide the pharmacological potency, while highly specific antibodies serve as the targeting agent, which also may include a carrier that increases the half-life and biocompatibility of the conjugate. The antibody-drug conjugate is one of the most popular bioconjugates in translational research. There are currently more than 15 antibody-

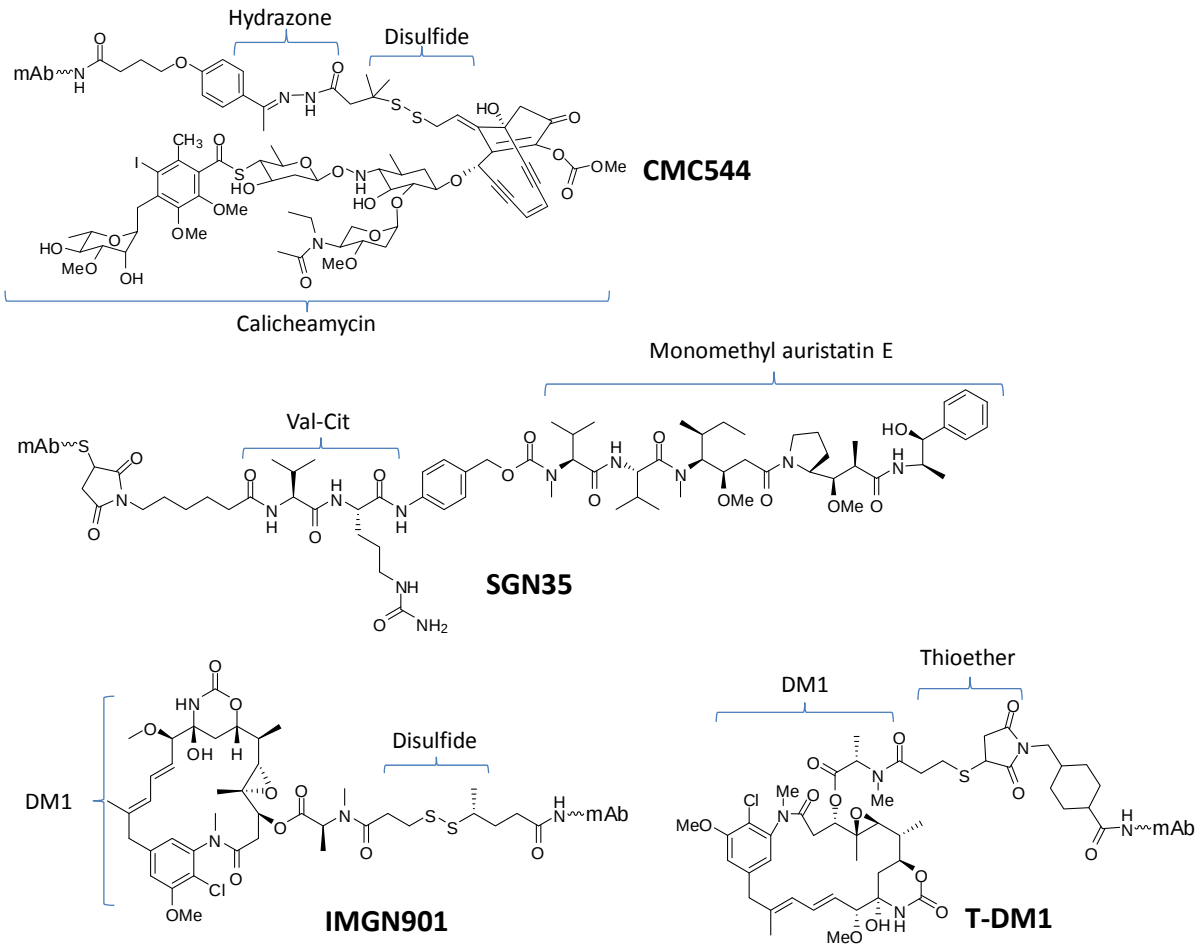

Figure 2. Structures of CMC544, SGN35, IMGN901 and T-DM1

drug conjugates that are undergoing clinical trials [57]. As listed in **Table 1**, they have different targets, cytotoxic chemicals and chemical linkers.

In cancer therapy, tumor-associated antigens are mainly selected as targets for antibody-drug conjugates. The antigens are either expressed in all tumors or in a specific type of tumor and should be well characterized in pre-clinical and clinical evaluations. The antigen must have high expression levels in cancer cells but low or no expression in normal tissues. The elevated expression level not only provides increased selectivity for the antibody-drug conjugate, but also

Table 1. Antibody-drug conjugates in cancer clinical trials.

Product Name	Target	Active Agent	Linkers	Application	Trial Phase	Company
Mylotarg	CD33	Calicheamycin	Hydrazone+disulfide	Acute myelogenous leukemia	Withdrawn 2010	Pfizer
SGN35	CD30	Monomethyl auristatin E	Val-Cit	Hodgkin lymphoma	Approved	Seattle Genetics
CMC-544	CD22	Calicheamycin	Hydrazone+disulfide	Non-Hodgkin lymphoma	Phase III terminated	Pfizer
T-DM1	HER2	DM1	Thioether	Breast cancer	Phase III	Roche
CDX-011	GPNMB	Monomethyl auristatin E	Val-Cit	Breast cancer	Phase II	Celldex
IMGN901	CD56	DM1	Disulfide	Small lung cancer	Phase II	ImmunoGen
IMGN242	CanAg	DM4	Disulfide	Gastric cancer	Phase II	ImmunoGen
HuC242-DM1	CamAg	DM1	Disulfide	Various cancers	Phase I	ImmunoGen
AVE9633	CD33	DM4	Disulfide	Acute myelogenous leukemia	Phase I	Sanofi-Aventis
IMMU-110	CD74	Doxorubicin	Hydrazone	Multiple myeloma	Phase I	Immunomedics
SGN-75	CD70	Monomethyl auristatin F	Val-Cit	Various cancers	Phase I	Seattle Genetics
IMGN388	Integrin	DM4	Disulfide	Various cancers	Phase I	ImmunoGen
SAR3419	CD19	DM4	Disulfide	Non-Hodgkin lymphoma	Phase I	Sanofi-Aventis
AGS-16M8F	AGS-16	Monomethyl auristatin F	Thioether	Renal and liver cancer	Phase I	Agensys
ASG-5ME	SLC44A4	Monomethyl auristatin E	Val-Cit	Various epithelial tumor	Phase I	Seattle Genetics
BIIB015	Cripto protein	DM4	Disulfide	Various cancers	Phase I	Biogen Idec
BT-062	CD138	DM4	Disulfide	Multiple myeloma	Phase I	Biotest
PSMA ADC	PSMA	Monomethyl auristatin E	Val-Cit	Prostate cancer	Phase I	Progenics
MEDI-547	EphA2	Monomethyl auristatin F	Thioether	Various tumors	Phase I terminated	MedImmune
MDX-1203	CD70	Duocarmycin	Val-Cit	Various cancers	Phase I	Bristol-Myers Squibb

guarantees that a sufficient amount of drug can be delivered into the tumor cells. Another critical property of the antigen is its ability to be internalized after binding of antibody-drug conjugates to tumor cells. The internalization is directly related to the therapeutic effect of antibody-drug conjugates. Depending on the chemical linker, internalization generally triggers the release of cytotoxic agents from the conjugate to elicit therapeutic effects. Internalization of antibody-drug conjugates is crucial to reduce the toxicity that is associated with the premature release of drug dose in extracellular compartments [57]. A wide variety of tumor-associated antigens have been

applied to antibody-drug conjugate in clinical trials. These antigens include CD33 for acute myeloid leukemia (AML), CD30 for Hodgkin disease, HER2, PSMA, CanAg and EGFR for solid carcinomas, and integrin for endothelial cells. A summary of these well-identified antigens and an introduction of some new potential targets have been extensively reviewed by Teicher [58].

The cytotoxic agents used in antibody-drug conjugates are numerically rare and restricted to four major families of compounds: calicheamycin, maytansinoids (DM1 and DM4), auristatins agent is the high cytotoxic potency. The IC_{50} of the cytotoxic agents is generally as low as $10^{-9} \sim 10^{-11}$M. These highly toxic drugs have very low therapeutic windows and cannot be used as a single agent for cancer therapy [59]. The high toxicity of chemical drugs is essential to enhance the potency of the antibody-drug conjugates. Theoretically, the number of antigens/targets per tumor cell is limited ($10^3 \sim 10^6$). Therefore, only thousands of antibody-drug molecules can be internalized to release the active parent drugs. The drug payload of antibody-drug conjugates is generally low, and each antibody molecule only conjugates with 1-3 cytotoxic molecules. The information described above indicates that the chemical agent must be sufficiently potent that several thousands of them can efficiently eradicate the tumor cells. The first-generation antibody-drug conjugate SNG-15, in which the antibody BR96 is conjugated with drug doxorubicin ($IC_{50} \sim 10^{-7}$ M), was significantly hampered by its low potency. Very limited anti-tumor activity was observed in the phase I and II clinical trials even at a dose of approximately 700 mg/m^2 [60, 61]. By contrast, new generation antibody-drug conjugates showed clinical activity at a dose of 3.6 mg/kg for Trastuzumab-DM1, a dose of 1.8 mg/kg for SGN-35 (Brentuximab-vedotin), and a dose of 1.3-1.8 mg/kg for MDX-1203 [62-64].

The chemical linker is also a key component of antibody-drug conjugates. A successful linker should be stable in circulation, but it should be labile when antibody-drug conjugates enter the tumor microenvironment or tumor cells. A wide variety of chemical linkers have been investigated in preclinical and clinical studies. For example, CMC-544 (Inotuzumab-ozogamicin) and IMMU-110 have an acid-labile hydrazone linker, which is stable at physiological pH (~7.4), but it is cleavable in the intracellular compartment of the lysosome due to its low pH (5.0-6.0) [65, 66]. This linker has also been successfully applied in Mylotarg (Gemtuzumab-ozogamicin) [67]. Disulfide bond-based linkers have also been used in antibody-drug conjugates [68-74]. Disulfide bonds exhibit moderate stability in the plasma but break down quickly in the cytoplasm due to the reductive intracellular environment [75]. BT-062 and SAR3419 are two typical antibody-drug conjugates that use disulfide bond-based chemical linkers [76, 77]. Non-cleavable thioether linkers have recently been proven to be superior to disulfide bonds in a preclinical study [75]. This is probably because the thioether linker has a higher degree of stability *in vivo*, which results in increased pharmacokinetic exposure and better toxicity tolerance compared to disulfide bonds. Upon internalization/endocytosis, the thioether-linked antibody undergoes lysosomal degradation to release chemical drugs. Several thioether based antibody-drug conjugates (T-DM1, AGS-16M8F and MEDI-547) are currently in clinical trials [75, 78, 79]. More recently, peptide linkers have been developed to selectively release chemical drug after cleavage by a lysosomal protease (cathepsin B). Among them, the valine-citrulline (val-cit) dipeptide linker is the most commonly used peptide linker in antibody-drug conjugates. It has been employed in SGN-35 (Brentuximab-vedotin), CDX-011 (Glembatumumab-vedotin), SGN-75, ASG-5ME, PSMA ADC, and MDX-1203 [63, 80-84].

Peptide-drug conjugates

Beside antibodies and their fragments, peptides represent another class of attractive ligands for tumor targeting. Suitable peptide ligands having a molecular weight less than 5 kDa exhibit excellent tumor penetration as well as a higher drug payload compared to antibody ligands. Because of its simple structure, a peptide-drug conjugate can be easily prepared by organic synthesis techniques. The conjugation sites of peptide ligands are always well defined, and therefore pure chemical entities can be used in cancer therapy. In the case of antibody-drug conjugates, drug molecules are always attached to antibodies by non-specific conjugation, leading to a complicated mixture of antibody-drug conjugates. The conjugation site and numbers of drug may vary dramatically between different antibody molecules and different preparation batches. Several peptide-drug conjugates have entered clinical trials (**Table 2**).

Table 2. Peptide-drug conjugates in translational cancer research.

Product Name	Peptide	Radionuclide/Drug	Target	Application	Trial Phase	Company
Octreoscan	Octreotide	^{111}In	Somatostatin receptor	Nuclear imaging	Approved	Covidien
68Ga-DOTATOC	Octreotide	^{68}Ga	Somatostatin receptor	Nuclear imaging	Phase I	European institute of oncology
^{90}Y-SMT-487	Octreotide	^{90}Y	Somatostatin receptor	Radiotherapy	Phase II	Norvatis
90Y-DOTALAN	Lanreotide	^{90}Y	Somatostatin receptor	Radiotherapy	Phase I	University of Vienna
^{177}Lu-DOTATATE	Octreotate	^{177}Lu	Somatostatin receptor	Radiotherapy	Phase III	Excel Diagnostics and Nuclear Oncology Center
^{99m}TC-BN	Bombesin	^{99m}Tc	GRP receptors	Nuclear imaging	Phase I	University "La Sapienza"
^{99m}Tc-N_3S-X-BN(2-14)	Bombesin	^{99m}Tc	GRP receptors	Nuclear imaging	Preclinical	------
ANG1005	Angiopep-2	Paclitaxel	Brain cancer	Chemotherapy	Phase I	AngioChem
SF1226	RGD	LY294002	Various cancers	Chemotherapy	Phase I	Semafore Pharmaceuticals

In translational research, peptide-drug conjugates have been successfully used for peptide receptor radiation therapy (PRRT). Regulatory peptide receptors are over-expressed in numerous human cancers, and can be used as molecular targets for tumor diagnosis and therapeutic use [85]. At the present time, the somatin receptor and gastrin-releasing peptide (GRP) receptor have been established for tumor targeting in PRRT. The peptide tracers for somatostatin receptor and GRP receptors are radiolabeled octreotide analogues and bombesin analogues, respectively. These peptide ligands are usually characterized by binding affinities in the low nanomolar range and non-immunogenicity. An octreotide (Sandostatin®) is an octapeptide that mimics natural somatostatin pharmacologically. Four radiolabeled octreotides are in clinical use. For example, ^{111}In-DTPA-octreotide (Octreostan®) is used to noninvasively image somatostatin receptor-expressing tumors [86]. As recently shown, Gallium-68 labeled octreotides (*68Ga*-DOTATOC) have high resolution and sensitivity in detecting small tumors or tumors with a low density of the receptor [87]. Octreotides can also be labeled with a radionuclide to treat neuroendocrine tumors. DOTA chelated ^{90}Y (such as ^{90}Y-SMT-487 and ^{90}Y-DOTALAN) and ^{177}Lu (such as ^{177}Lu-DOTATATE) are commonly used in the clinic [88-90]. The major difference between them lies in the somatostatin-receptor subtype affinity profiles [91]. Bombesin is a 14-mer peptide that shows high affinity for the GRP receptor. Two ^{99m}Tc-labeled bombesins are being used clinically. ^{99m}TC-BN and ^{99m}Tc-N3S-X-BN(2-14) are primarily used to identify breast and prostate primary cancer and metastases [92-94]. ^{68}Ga and ^{111}In labeled bombesins are also under preclinical evaluation [95, 96]. Besides regulatory peptides, a wide range of radiolabeled peptides are also under preclinical development. Peptide ligands such as RGD peptide, neurotensin and Tat

penetrating peptide offer promising radioligand candidates for various cancers in future radiation therapies [97].

Moreover, peptides have been used to guide chemical drugs to various tumors. ANG1005 and SF1226 are the two examples in clinical evaluations. ANG1005 is a peptide-drug conjugate engineered to deliver paclitaxel across the blood-brain barrier (BBB) for glioma therapy. The peptide Angiopep-2 is a ligand that binds to the low density lipoprotein receptor-related protein (LRP) receptor at BBB. The binding of Angiopep-2 with the LRP receptor results in crossing the BBB by receptor-mediated transport. ANG1005 is composed of Angiopep-2 linked to three molecules of paclitaxel with a cleavable succinyl ester linkage [98]. After conjugation, Angiopep-2 dramatically increases the capacity of uptake of paclitaxel into the brain. The *in vivo* uptake of ANG1005 into the brain and brain tumors is 4-54-fold higher than that of paclitaxel. Moreover, ANG1005 bypasses P-gp and resides in the brain much longer even after capillary deletion and vascular washout [99]. Phase-I clinical trials of ANG1005 were started in 2008. SF1126 is a novel RGD-conjugated LY294002 prodrug. LY294002 is a pan phosphoinositide 3-kinase (PI3K) inhibitor that shows *in vitro* and *in vivo* anti-tumor effects. However, LY294002 is not a valuable drug candidate due to its poor water-solubility and short plasma half-life. The peptide RGD was conjugated to LY294002 to increase its solubility and targetability to integrins in the tumor compartment [100]. Recent data from a phase I clinical trial reveal that SF1126 was well tolerated up to 1,110 mg/m^2 given by *i.v*. twice a week. Clinical activity was also observed in 19/33 (~58%) patients with multiple solid tumors. No significant toxicity or effect on glucose level were reported [101].

Polymer-drug conjugates

The first attempt to attach drugs to water soluble polymers was achieved in the mid-1970s [102]. Since then, polymer-drug conjugates have been extensively studied, and dozens of polymer-drug conjugates have entered clinical evaluation, several of them have been approved by the FDA for cancer therapy [103]. Conjugating with polymer carriers modulates not only the pharmacokinetics but also the water solubility and toxicity of the cytotoxic chemical. Active targeting can also be achieved when a tumor homing ligand is introduced to the same polymer carrier. Based on the types of drugs, polymer-drug conjugates can be categorized into two groups: polymer-conjugated chemical drugs and polymer-conjugated proteins.

Synthesis of polymer-conjugated chemical drugs is an active area in cancer therapy. To date, one of the polymer-conjugated chemical drugs has been approved by the FDA, and nine of them are undergoing clinical trials (**Table 3**). Among them, the poly(L-glutamic acid)-paclitaxel conjugate (CT-2103, Xyotax®, Opaxio™), in which paclitaxel is conjugated to the carboxyl group of poly(L-glutamic acid) via an ester bond, has advanced into Phase III clinical trials and been granted fast track designation by the FDA. CT-2103 shows high water solubility (>20 mg/kg) and a significantly improved pharmacokinetics profile compared to paclitaxel [104]. Preclinical studies revealed that CT-2103 could also penetrate tumors and distribute into the necrotic zone of tumors several days after injection [105]. The tumor-penetration property of the polymer-drug conjugate is probably achieved through several routes: (i) diffusion of the intact polymer-drug conjugate; (ii) diffusion of small fragments of CT-2103 such as paclitaxel, Glu-paclitaxel or Glu-Glu-paclitaxel; and (iii) re-distribution through the migration of macrophages because CT-2103 can be captured by macrophages [98]. In the phase I study, the maximal

Table 3. Polymer-drug conjugates in cancer clinical trials

Product Name	Polymer	Drug	Molecular weight	Indication	Trial Phase	Company
CT-2103	Poly(Glu)	Paclitaxel	~80 kDa	Various cancers	Approved	Cell Therapeutics
PK1	HMAP	Doxorubicin	~30 kDa	Lung and breast cancer	Phase II	Pfizer
PK2	HMAP-Galactosamine	Doxorubicin	~25 kDa	Hepatocellular carcinoma	Phase II	Pfizer
PNU166148	HMAP	Camptothecin	~18 kDa	Various cancers	Phase I terminated	Pfizer
PNU166945	HMAP	Paclitaxel	25~35 kDa	Various cancers	Phase I terminated	Pfizer
AP5346	HMAP	Oxaliplatin	~25 kDa	Various cancers	Phase II	Acess Pharmaceuticals
AP5280	HMAP	Carboplatin	22 kDa	Various cancers	Phase I	Acess Pharmaceuticals
Pegamotecan	PEG	Camptothecin	40 kDa	Solid tumors	Phase I terminated	Enzon
EZN-2208	PEG	SN-38	40 kDa	Solid tumors	Phase I	Enzon
IT-101	Cyclodextrin based polymer	Camptothecin	85±23 kDa	Solid tumors	Phase I	Insert Therapeutics
DE-310	Carboxymethyl-dextran	Exatecan	~340 kDa	Solid tumors	Phase I	Daiichi Pharmaceuticals
CT-2106	Poly(Glu)	Camptothecin	~50 kDa	Various cancers	Phase I	Cell Therapeutics
AD-70	Dextran	Doxorubicin	~70 kDa	Various cancers	Phase I	Alpha Therap

tolerated dose of CT2103 was up to 233 mg/m^2 with a 3-week schedule and 177 mg/m^2 with a 2-week schedule [106]. Moreover, the plasma half-life was approximately 185 h and the AUC of CT-2103 was about 50 times higher than that of free paclitaxel [107]. CT2103 advanced into Phase II trials for androgen-independent prostate cancer and Phase III trials for NSCLC. Besides polyglutamic acid based polymer-drug conjugates (CT2103, CT2106), various chemical drugs have been conjugated with HPMA, PEG, cyclodextrin-based polymer and carboxymethyldextran [98, 108-120].

Polymer-conjugated proteins, namely polymer-protein conjugates, have become a fast-growing field in cancer therapy. Nine of them have been approved by the FDA, and all of them use PEG as the drug carrier [103]. PEGylation of proteins results in reduced immunogenicity and

enhanced circulation time compared to native proteins. After covalent conjugation, the long, flexible and hydrophilic PEG provides a steric shield for therapeutic proteins, which reduces the opportunity to be recognized by the immune system. Moreover, PEG can dramatically increase the size of the native proteins, thereby enhancing the circulation half-life. Taking Oncaspar® as an example, 5 kDa PEG increases the half-life of L-Asparaginase from 20 hours to approximately 357 hours. PEG-INTRON, a 12 kDa PEG-conjugated Interferon α-2b, has a half-life of 48-72 hours, which is 6-10 times longer than that of the native protein. The PEG polymer along with its associated water molecules surrounds the protein drug and protects it from enzyme degradation, renal filtration and immune response, thereby dramatically amplifying the therapeutic benefits and limiting the adverse effects.

However, PEGylation may also decrease the activities and stability of a protein drug. Steric hindrance of the PEG chains could reduce the binding affinity between proteins and its antigens. Additionally, chemical modification of protein drug might cause conformational change of the protein, which always leads to activity loss and protein aggregation. However, the quality of PEG-protein conjugates could be well controlled once the standard PEGylation method is established.

2.4. HER2 siRNA Mediated RNAi for Cancer Therapy

Instead of targeting HER2 by small molecular inhibitors, gene expression can be directly inhibited by oligonucleotides including antisense oligonucleotide and siRNA. Antisense oligonucleotides act by binding to the complementary mRNA sequence through Watson-Crick base pairing, leading to its degradation by endogenous nuclease RNase H. The resulting

downregulation of HER2 mRNA causes inhibition of proliferation of HER2 overexpressing cancer cells [45, 121]. In addition, antisense oligonucleotide suppresses HER2 expression in a dose dependent, sequence specific and target specific manner [45, 122]. It has been demonstrated that the combinational therapy of antisense oligonucleotide and chemotherapy drug doxorubicin produced synergistic effect in inhibiting proliferation and activating apoptosis of HER2 overexpressing breast cancer cells [45, 121].

siRNA acts through the RNA interference mechanism where the antisense strand of siRNA binds the complementary sequence of target mRNA and triggers its degradation [123]. Potent knockdown of specific gene sequence makes siRNA a promising therapeutic approach for cancer therapy [46, 124]. Inhibition of HER2 expression by a retrovirus-mediated shRNA (short hairpin RNA) resulted in cell cycle arrest at G_0/G_1, increased apoptosis, reduced proliferation, and growth inhibition in breast and ovarian tumor cells overespressing HER2 [42]. Similar effects have been observed by other groups in HER2 positive breast cancer cells using synthetic siRNA [41, 125]. In addition, we studied the effect of HER2 siRNA on tumor cells invasiveness properties including cell morphology change, *in vitro* migration, cell spreading, and adhesion to extracellular matrix (ECM). Our data demonstrated for the first time that HER2 siRNA could inhibit cell migration and invasion abilities. The HER2 siRNA also exhibited dramatic suppression on cell spreading and adhesion to ECM [46].

CHAPTER 3

DEVELOPMENT OF A PEPTIDE DRUG CONJUGATE FOR PROSTATE CANCER THERAPY

3.1. Rationale

Phosphoinositide 3-kinases (PI3Ks) are lipid enzymes that phosphorylate the 3'-OH of the inositol ring of phosphoinositides. It has been established that PI3Ks play a pivotal role in cell growth, proliferation, and survival [126]. PI3Ks have been divided into three classes (I, II, and III) according to their different structural features and *in vitro* lipid substrate specificities [127, 128]. Interestingly, class I PI3Ks can be further divided into two subclasses (class IA p110α/β/δ and class IB p110γ) [126]. Recent emerging evidence indicates that PI3K isoforms (p110α/β/δ) possess an oncogenic potential through gain-of-function mutations or gene amplifications [129]. Their major PI3K downstream signaling effector, protein kinase B (PKB, also known as Akt), has been found to be over-activated in human cancers, such as prostate cancer [130-132]. However, a negative regulator of the PI3K signaling pathway, phosphatase and tensin homolog (PTEN), has long been reported to be inactive in most human cancers, including prostate cancer [133-135]. Conditional knockout of PTEN in mouse prostate epithelium resulted in intraepithelial neoplasia [136, 137]. PTEN-null cancers represent a significant portion (30~50%) of all prostate cancer cases[138], and they are always associated with an unfavorable prognosis [139]. In PTEN-null prostate cancers, PI3Kβ (PI3K-p110β), rather than PI3Kα, has been proven to contribute to tumoregenesis and androgen-independent progression [140]. Recently, for the first time, we have demonstrated that PI3Kβ is essential for the androgen-stimulated AR (androgen receptor) transactivation and cell proliferation [141]. We also observed

high expression of this isoform in malignant prostate tissues compared to nonmalignant compartments, and the expression level was significantly correlated with prostate cancer progression [141]. The chemical inhibition or genetic knockout of PI3Kβ is believed to prevent AR-dependent gene expression and tumor growth. Given all of the evidence described above, PI3Kβ is considered an attractive target for the development of novel anti-cancer agents for prostate cancer, which is the most common malignance in American men.

TGX-221 is a novel, potent, isoform-specific, and cell-permeable small molecule inhibitor of PI3Kβ. The inhibition effect of TGX-221 on PI3Kβ is about 1000-fold over PI3Kα and PI3Kγ, and 20-fold over PI3Kδ [142]. TGX-221 has been successfully used in animal models to suppress the PI3Kβ activity *in vivo* [3]. However, the therapeutic potential of TGX-221 in cancer therapy is halted due to its poor solubility and the wide distribution of PI3Kβ *in vivo*. Organic solvent is generally required for intravenous administration of TGX-221, which may cause significant toxicities [3]. Additionally, widely distributed PI3Kβ plays important roles in cell metabolism, growth and development [143]. For example, knockdown of PI3Kβ leads to early embryonic lethality [144], glucose intolerance[140] and platelet disaggregation [145]. As a result, an improved solubility and the targeted delivery of TGX-221 to tumor cells are two essential prerequisites for its successful application in prostate cancer therapy.

Peptide-drug conjugation is a promising strategy for the targeted delivery of chemotherapy drugs. Unlike an antibody-drug conjugate, a peptide-drug conjugate is small in size, which results in excellent cell permeability and a high drug-loading capability. In our approach, a HER2 (Human Epidermal growth factor Receptor 2)-specific peptide was conjugated to TGX-D1, a TGX-221 derivative, and the drug was specifically delivered to the prostate cancer

cells. HER2, a well-known membrane receptor in breast cancer, is also overexpressed in many prostate cancers [48]. It has been revealed that 25% of untreated primary prostate tumors, 59% of localized tumors after hormone treatment, and 78% of castrate metastatic tumors overexpress the HER2 protein [47, 146, 147]. Although the monoclonal anti-HER2 antibody has not shown a significant therapeutic effect in prostate cancer [49], the overexpressed HER2 on prostate cancers does provide a promising molecular target for targeted drug delivery systems. To further increase the tumor specificity, a PSA (prostate specific antigen) cleavable peptide (SSKYQ) was incorporated as a linker between the anti-HER2 peptide and TGX-D1. PSA is a prostate tissue-specific serine protease that is often over-expressed in prostate cancer cells, but not in other normal cells [148]. In this study, the peptide conjugated TGX-D1 was specifically delivered to prostate cancer cells, and then cleaved by PSA to release the parent drug, which led to high cellular uptake of TGX-D1 by tumor cells.

3.2. Materials and Methods

Materials

All starting reagents listed below were obtained from commercial sources and used without further purification. 2-amino-3-bromo-5-methylpyridine was purchased from Oakwood Products, Inc. (West Columbia, SC). Piperidine, malonyl dichloride, methanesulfonyl chloride, aniline, 4-aminophenethyl alcohol, 2-aminophenethyl alcohol, 3-aminobenzyl alcohol and butyl vinyl ether were obtained from Sigma-Aldrich (St Louis, MO). Morpholine was purchased from Ricca chemical company (Arlington, Texas). Triisopropylsilane (TIPS), trifluoroacetic acid (TFA), triethylamine, N, N-diisopropylethylamine (DIPEA), 4-dimethyl-aminopyridine (DMAP)

and dichloro 1,1'-bis(diphenylphosphino)ferrocene palladium ($PdCl_2$(dppf)) were purchased from Acros Organics (Morris Plains, NJ). 2-(7-Aza-1H-benzotriazole-1-yl)-1,1,3,3-tetramethyluronium hexafluorophosphate (HATU) was ordered from Genscript Inc. (Piscataway, NJ). Thiazolyl Blue was obtained from RPI Corp. (Prospect, IL). All the amino acids used in solid phase peptide synthesis were obtained from Anaspec Inc. (Fremont, CA). All the organic solvents for synthesis and HPLC were ordered from Fisher Scientific Inc. and used as received.

Synthesis of TGX-221, TGX-D2, TGX-D3 and TGX-D4

Compounds 2, 3, and 4 were synthesized from commercially available 2-amino-3-bromo-5-methylpyridine (1) following Jackson's report [149]. For the synthesis of TGX-221 and its derivatives, compound 4 (1 mmol) was suspended in 20 mL of dry toluene. After adding 3 g of molecular sieves (4Å) and 3 mmol of aniline or its derivatives, the reaction was refluxed for 4 hours under nitrogen. The molecular sieves were removed, and the filtrate was concentrated under vacuum. The residue was re-dissolved in methanol, followed by adding 20mg of $NaBH_4$ at $0^{\circ}C$. The reaction was continuously stirred for another hour at room temperature. After quenching the reaction with 10 mL of saturated NH_4Cl aqueous solution, the product was extracted with $CHCl_3$. The organic phase was then washed with brine, dried and concentrated under vacuum. The final product was purified by silica gel chromatography ($CHCl_3$/methanol, 50/1) to give a yield of 50~80%.

TGX-221: ^1H NMR (400 MHz, $CDCl_3$) δ8.62 (s, 1H), 7.61(s, 1H), 7.13(m, 2H), 6.68(t, 1H), 6.45(d, 2H), 5.63(s, 1H), 5.15(q, 1H), 3.80(m, 4H), 3.65(m, 5H), 2.25(s, 3H), 1.54(d, 3H). ESI-MS calcd. for $C_{21}H_{24}N_4O_2$ 364.4; found, 365.4 $[M + 1]^{1+}$.

TGX-D2: ^{1}H NMR (400 MHz, $CDCl_3$) δ8.63(s, 1H), 7.57(s, 1H), 7.08(d, 1H), 7.00(t, 1H), 6.68(t, 1H), 6.25(d, 1H), 5.65(s, 1H), 5.18(m, 1H), 3.80(m, 6H), 3.65(m, 6H), 2.63(s, 1H), 1.6(d, 3H). ESI-MS calcd. for $C_{23}H_{28}N_4O_3$ 408.5; found 409.3 $[M + 1]^{1+}$.

TGX-D3: ^{1}H NMR (400 MHz, $CDCl_3$) δ8.65 (s, 1H), δ7.57 (s, 1H), δ7.09 (t, 1H), δ6.68 (d, 1H), δ6.55 (s, 1H), δ6.34 (d, 1H), δ5.66 (s, 1H), δ5.12 (m, 1H), δ3.93 (m, 1H), δ3.79 (m, 4H), δ6.67 (m, 4H), δ3.60 (m, 2H), δ3.27 (s, 3H), δ1.50 (d, 3H). ESI-MS calcd. for $C_{22}H_{26}N_4O_3$ 394.5; found, 395.3 $[M + 1]^{1+}$.

TGX-D4: ^{1}H NMR (400 MHz, $CDCl_3$) δ8.65(s, 1H), 7.60(s,1H), 6.94(d, 2H), 6.41(d, 2H), 5.63(s, 1H), 5.09(q, 1H), 3.80(m, 6H), 3.65(m, 4H), 2.71(t, 2H), 2.30(s, 3H), 1.58(d, 3H). ESI-MS calcd. for $C_{23}H_{28}N_4O_3$ 408.5; found, 409.4 $[M + 1]^{1+}$.

Synthesis of compound 5

Methyl bromoacetate (5 mmol) and N,N-diisopropylethylamine (5 mmol) were added into a solution of TGX-221 (364 mg, 1 mmol) in CH_3CN (50 mL), and the reaction mixture was stirred at 85°C for 24 hours. After cooling to room temperature, the reaction mixture was concentrated under vacuum. The remaining brown residue was dissolved with $CHCl_3$ and then washed with water, brine and dried over Na_2SO_4. After concentration, the residue was purified by silica gel chromatography (chloroform/methanol, 100/1, yield ≈ 60%). ^{1}H NMR (400 MHz, $CDCl_3$) δ8.65(s, 1H), 7.58(s, 1H), 7.10(t, 2H), 6.70(t, 1H), 6.46(d, 2H), 5.64(s, 1H), 5.13(q, 1H), 4.20(s, 3H), 3.80(m, 4H), 3.65(m, 6H), 2.25(s, 3H), 1.57(d, 3H). ESI-MS calcd. for $C_{24}H_{28}N_4O_4$ 436.5; found 437.3 $[M + 1]^{1+}$.

Synthesis of TGX-D1

LiCl (5 mmol) and $NaBH_4$ (5mmol) were added to a solution of compound **5** (1 mmol) in THF (10 mL). After stirring at room temperature for 10 minutes, 20 mL of anhydrous ethanol was added to the reaction mixture. After twelve hours, an additional 5 mmol of LiCl and $NaBH_4$ were added to the reaction mixture and stirred for another 12 hours. The reaction was quenched with saturated NH_4Cl aqueous solution and then extracted with $CHCl_3$. The organic layer was washed with water, brine, and dried over Na_2SO_4. After concentration, the residue was purified by silica gel chromatography (chloroform/methanol, 50/1, yield ≈ 50%). ^1H NMR (400 MHz, $CDCl_3$) δ8.64 (s, 1H), δ7.43 (s, 1H), δ7.20 (t, 2H), δ6.86 (d, 2H), δ6.76 (t, 1H), δ5.60 (s, 1H), δ3.81 (t, 1H), δ3.60 (m, 5H), δ3.51 (m, 2H), δ3.42 (t, 2H), δ3.37 (m, 2H), δ2.33 (s, 3H), δ1.63 (d, 2H). ESI-MS calcd. for $C_{23}H_{28}N_4O_3$ 408.5; found 409.5 $[M + 1]^{1+}$.

Synthesis of NH_2-L-TGX

Fmoc-Leu-OH (100 mg) and EDCI (50 mg) were added to TGX-D1 (1mmol) in dichloromethane (DCM), and the reaction was initiated by adding DMAP and stirring at room temperature overnight. After that time, water was added to the reaction, and the organic phase was separated, washed, and dried with Na_2SO_4. The intermediate was purified by silica gel chromatography ($CHCl_3$/methanol, 100/1). To remove the Fmoc protecting groups, the intermediate was dissolved in 1.8 mL DCM, followed by adding 200 μL of piperidine. The reaction mixture was stirred at room temperature for 30 minutes. Finally, the solvent was evaporated under vacuum, and the residue was purified with silica gel chromatography ($CHCl_3$/ethanol, 50/2.5). ESI-MS calcd. for $C_{29}H_{39}N_5O_4$ 521.6; found 522.4 $[M + 1]^{1+}$.

Synthesis of NH_2-SL-TGX

HATU (10 mg) and Boc-Ser(OtBu)-OH (20 mg) were dissolved in 5 mL of dried DMF under nitrogen, followed by adding 10 μL of DIPEA. After 10 minutes, NH_2-L-TGX was added to initiate the coupling reaction. After 12 hours, the organic solvent was evaporated and the residue was purified by silica gel chromatography. The purified intermediate was then dissolved in the mixture of TFA/DCM/TIPS (v/v/v, 50/45/5). The mixture was stirred for 3 hours, followed by concentration and purification with HPLC (Abs. 268nm). ESI-MS calcd. for $C_{32}H_{44}N_6O_6$ 608.7; found 609.6 $[M + 1]^{1+}$.

Synthesis of the peptide-drug conjugate

Undeprotected peptide synthesis. All undeprotected peptide intermediates were synthesized by an Fmoc solid-phase peptide synthesis method. The resin used for peptide synthesis was 2-chlorotrityl resin. HATU was used as the coupling reagent and DIPEA served as the base. The undeprotected peptides were cleaved from the resin by acetic acid/trifluoroethanol/DCM (v/v/v, 10/20/70) at room temperature after 2 hours. After removing the resin by filtration, the reaction was concentrated under vacuum at room temperature. The crude products were purified by small silica gel chromatography ($CHCl_3$/Methanol, 50/2.5~50/10).

Coupling and deprotection. The un-deprotected peptides (0.02 mmol) and purified NH_2-L-TGX-D1 (0.01 mmol) were dissolved in 3 mL of dried DMF. Two equivalents of HATU (0.02 mmol) and four equivalents of DIPEA (0.04 mmol) were added to the solution. After stirring at

room temperature overnight, the reaction was quenched by a saturated NH_4Cl aqueous solution. The solvent was then removed, and the brown residue was reconstituted in 20 mL of $CHCl_3$, followed by washing with water. After concentration under vacuum, the crude product was purified by silica gel chromatography ($CHCl_3$/methanol, 50/2.5~50/10). The residual protecting groups in the peptide drug conjugate were removed by acidic cleavage. Briefly, the purified compound was dissolved in a mixture of DCM and TFA (1 mL/1 mL) and stirred for 2 hours at room temperature. To increase the yield, 50 μL of scavenging agent such as triisopropylsilane (TIPS) was added into the reaction. The reaction mixture was then concentrated, and the final product was purified by reverse phase HPLC. The molecular weight was confirmed by LC/MS.

Ac-SSKYQSL-TGX**:** ESI-MS calcd. for $C_{60}H_{85}N_{13}O_{16}$ 1244.4; found 1245.2 $[M + 1]^{1+}$.

Ac-KCCYSLGGGSSKYQSL-TGX-D1 (KCC-TGX)**:** ESI-MS calcd. for $C_{96}H_{141}N_{23}O_{27}S_2$ 2113.4; found 705.5 $(M+3)^{3+}$; 1056.4 $(M+2)^{2+}$.

Cytotoxicity assay

LNCaP cells were seeded in 96-well plates at a density of 1×10^4 cells/well (DU145 cells were seeded at a density of 3×10^3 cells/well due to its fast growth rate). After 24 hours, TGX-221 and its derivatives (TGX-D1, TGX-D2, TGX-D3 and TGX-D4) were added, and the cells were incubated at 37°C for 72 hours. The relative viable cell numbers were determined using a MTT assay. IC_{50} was calculated by fitting a concentration-response curve using Graphpad Prism 5 (GraphPad Software, Inc.).

Androgen induced proliferation assay

LNCaP cells were seeded in 96-well plates 12 hours before the assay. The medium was changed to serum-free medium containing 1 nM of R1881 (a synthetic androgen), followed by adding TGX-221 and its derivatives. After incubation for 72 hours, the proliferation rate was examined by the Alamar Blue-based proliferation assay (Promega Corp., WI).

Androgen induced gene expression assay

The luciferase reporter plasmid controlled by a synthetic androgen response element (ARE-LUC) has been described previously [141]. LNCaP cells were seeded in 6-well plates and transfected with 1.0 μg of ARE-LUC using Lipofectamine on the following day. After 24 hours, the medium was changed to RPMI-1640 containing 2% FBS and R1881 (1.0nM). TGX-221 and TGX-D1 were added to the cells and incubated for 24 hours. After washing with PBS, the cells were lysed, and the total protein concentration of the cell lysate was measured by a BCA protein assay (Pierce Biotech., IL). Luciferase activity of each sample was determined and normalized to the protein concentration.

***In vitro* release of TGX-D1 from the peptide-drug conjugate**

Drug release from NH_2-SL-TGX. Stock solution of NH_2-SL-TGX (10 mM in DMSO, 0.5% formic acid) was diluted to a final concentration of 100 μM with buffer (50 mM Tri-Cl, 100 mM NaCl, pH 7.4) and then incubated at 37 °C. At selected time intervals, a 50 μL aliquot was removed and mixed with 50 μl of 0.1% TFA to quench the reaction. The samples were stored at -30 °C for HPLC analysis.

Drug release from Ac-SSKYQSL-TGX. Ac-SSKYQSL-TGX was mixed with freshly prepared PSA solution (10 μg/mL) in buffer (50 mM Tri-Cl, 100mM NaCl, pH 7.4) to give a final concentration of 100 μM. The mixture was incubated at 37 °C, and 50 μl aliquot were quenched with an equal volume of 0.1% TFA in methanol at selected time intervals. After incubation at room temperature for 10 minutes, the samples were centrifuged at 12,000g for 10 minutes, and the supernatant was collected for HPLC analysis.

The samples were assayed by a Waters HPLC system (717 plus autosampler, 600 controller pump, 486 tunable absorbance detector) on a C-18 reverse phase column (4.6×250mm, 5μm). The mobile phase was methanol/water (65/35, v/v) in 0.1% formic acid, and the flow rate was set at 1.0 mL/min. Samples were tested as 30 μL injections, and the drug concentration was monitored by UV detector at 268nm.

Immunostaining

LNCaP cells cultured on 96-well plates were fixed in ice-cold acetone/methanol (1/1, v/v) for 10 minutes, followed by blocking with 1% BSA for 1 hour. The cells were then incubated with the biotinylated peptides for 1 hour in TBST buffer (0.1% Tween-20 in 0.1M Tri-Cl, pH 7.4). After washing to remove the unbound peptides, streptavidin-FITC (Pierce, Rockford, IL) was added, and the cells were examined with a Leica DMI3000 fluorescence microscope (Leica Microsystems GmbH, Wetzlar, Germany).

Aqueous solubility assay

The aqueous solubilities of TGX-221, TGX-D1 and KCC-TGX were assayed by the thermodynamic method. Briefly, 1 mg of TGX-221, TGX-D1, or KCC-TGX was suspended in 100 μL of water, and the mixture was shaken at room temperature for 3 days. The un-dissolved drug crystals were removed by centrifugation at 12,000 *g* for 10 minutes. The supernatant was diluted, and the drug concentration was quantified by HPLC.

Stability assay of KCC-TGX

The stability of KCC-TGX was analyzed in PBS, cell culture medium and mouse serum. KCC-TGX was diluted to 5 μM in PBS (pH 7.5), cell culture medium (10% FBS in RMPI 1640) or 50% mouse serum. Next, the solutions were incubated at 37°C for their indicated time interval. A 20-μl aliquot was mixed with 60 μL of acetonitrile containing 0.1% formic acid to precipitate the proteins. The samples were centrifuged at 12,000g for 10 minutes, and 50μl of the supernatant was collected for HPLC quantification.

Cellular uptake study

LNCaP cells were plated in 24-well plates at a density of 2×10^5 cells/well and incubated for 12 hours before the study. The cells were washed once with PBS and incubated with freshly prepared drug solutions in RPMI-1640 medium at 37°C. One hour after the incubation, the drug was removed and the cells were washed three times with cold PBS. The cells were then harvested and kept at -80°C for the LC-MS/MS assay. The total protein concentration of the cell lysate was quantified by a BCA protein assay kit (Pierce, Rockford, IL), and the cellular uptake was normalized to the total amount of protein for each sample.

In vitro competitive receptor binding assay

To inhibit the uptake of KCC-TGX by the anti-HER2 ligand Ac-KCCYSL, LNCaP cells were pre-incubated with the indicated concentrations of Ac-KCCYSL at 37°C for 1 hour. KCC-TGX was then added and incubated with the cells for another 30 minutes. The cells were finally washed and lysed as described above. Cellular uptake of KCC-TGX was analyzed by LC-MS/MS.

LC-MS/MS analysis of TGX-221 derivatives and the peptide-drug conjugate

Drug molecules were extracted from the cells using a liquid-liquid extraction technique as reported [150]. TGX-221 was used as the internal standard during the extraction and analysis. Ethyl acetate (AcOEt) was utilized to extract the drug from the aqueous layer. All samples were hydrolyzed to release the parent drug TGX-D1 for LC-MS/MS analysis. Briefly, the cells were lysed by three cycles of a freeze-thaw procedure, and 100 μL of the clear cell suspension was incubated with 34 μL of 4N NaOH for 1 hour. Phosphate buffer (68 μL, 2N) was then added to neutralize the pH. After adding the internal standard TGX-221, each sample was vortexed with 200 μL of AcOEt for 5 minutes. The organic layer was separated from the aqueous layer by centrifugation, and 150 μL of the organic layer were transferred to a tube and dried under vacuum. The residue was reconstituted with 50 μL of acetonitrile for LC-MS/MS analysis.

LC-MS/MS analysis was performed on a QTrap® 3200 LC/MS/MS mass spectrometer equipped with a Shimadzu Prominence HPLC system. Detection was operated in the multiple-reaction monitoring (MRM) mode. The precursor and product ions were 409.1/272.1 for TGX-

D1, and 365.1/272.1 for TGX-221. The turbo ion spray setting and collision gas pressure were optimized (IS Voltage of 5500V; temperature of 300 ^{o}C; nebulizer gas of 40 psi; curtain gas of 40 psi). Ion source parameters employed a declustering potential (DP) of 31 V; collision energy (CE) of 16 V; entrance potential (EP) of 5 V; and collision cell exit potential (CXP) of 4V. The detection limit of TGX-D1 was 10 nM.

Statistical Analysis

Data were expressed as the mean ± standard deviation (SD). Difference between any two groups was determined by ANOVA. $P<0.05$ was considered statistically significant.

3.3. Results

Structure of the peptide-drug conjugate

The chemical structure of the peptide-drug conjugate (KCC-TGX) is depicted in **Figure 3A**. This peptide-drug conjugate consists of five parts: i) the parent drug TGX-D1; ii) a self-cyclizing linker (SL); iii) the PSA cleavable peptide (SSKYQ); iv) a peptide spacer (GGG); and iv) a HER2-targeting peptide (KCCYSL). The peptide-drug conjugate could be activated by PSA cleavage to release the parent drug TGX-D1.

Figure 3B illustrates the release of TGX-D1 from KCC-TGX upon binding to HER2 on prostate cancer cells. Briefly, KCC-TGX was specifically delivered to the prostate cancer cells, and cleaved by PSA to form NH_2-SL-TGX which was further cleaved by self-cyclization to release the active parent drug TGX-D1. PSA's enzymatic activity only exists in the microenvironment of the prostate cancer cells, but not in systemic circulation due to the presence

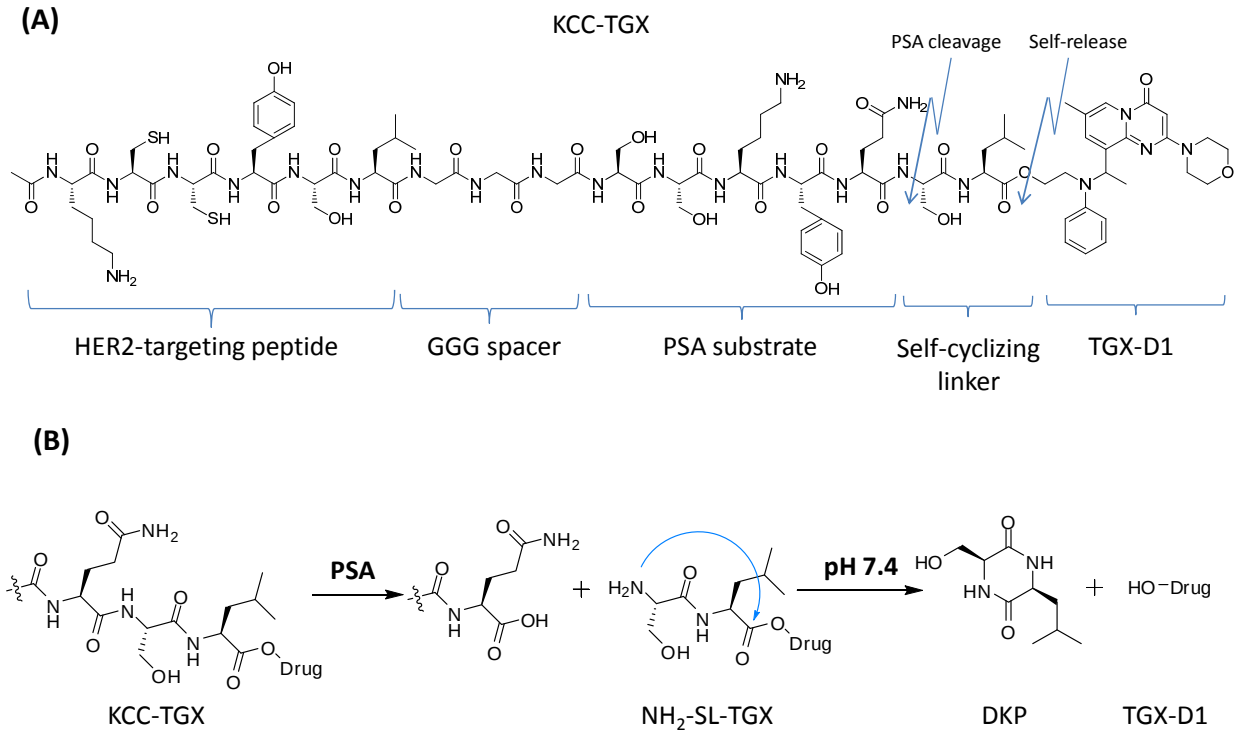

Figure 3. KCC-TGX and its drug release mechanism. (A) Structure of the peptide-drug conjugate KCC-TGX. KCC-TGX contains a HER2-targeting peptide, a GGG spacer, a PSA cleavable substrate, a self-cyclizing linker and the parent drug TGX-D1. (B) The activation mechanism of KCC-TGX. KCC-TGX is expected to be cleaved at the Gln-Ser site by PSA to release NH_2-SL-TGX. The free amino group of Ser (S) in NH_2-SL-TGX attacks the ester carbonyl group and releases the parent drug TGX-D1. The dipeptide Ser-Leu self-cyclizes to form diketopiperazines (DKP).

of PSA inhibitors (α1-antichymotrypsin and α2-macroglobulin) in the blood [151]. Therefore, the PSA-cleavable linker was expected to remain stable in systemic circulation.

Synthesis of the TGX-221 derivatives

Because TGX-221 does not contain any functional groups for conjugation with peptides, we synthesized four TGX-221 derivatives (TGX-D1, TGX-D2, TGX-D3, and TGX-D4) with additional hydroxyl groups, as illustrated in **Figure 4**. Compounds 2, 3, and 4 were synthesized

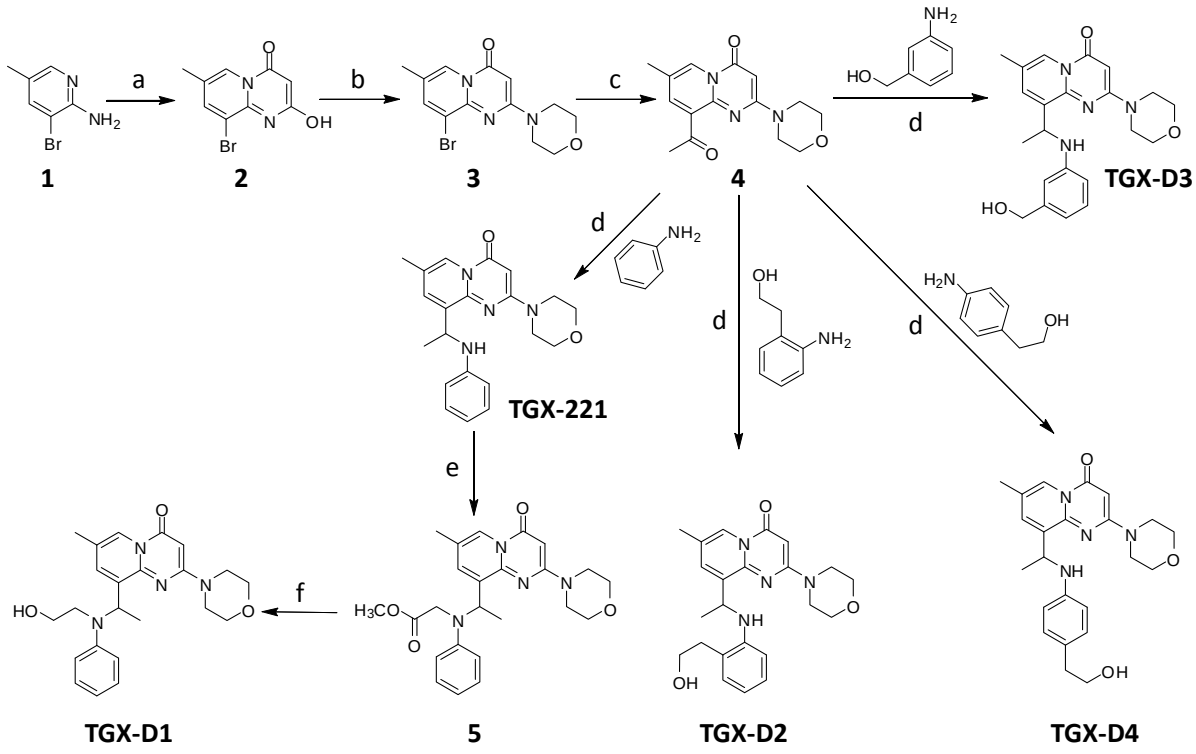

Figure 4. Synthesis of TGX-221 and its derivatives. Reagents and conditions: (a) malonyl dichloride, DCM, rt; (b) CH_3SO_2Cl, Et_3N, morpholine; (c) I. $PdCl_2$(dppf), DIPEA, butyl vinyl ether; II. 1N HCl, rt; (d) I. 4Å MS, toluene, reflux; II. $NaBH_4$, methanol; (e) methyl bromoacetate, DIPEA, CH_3CN; (f) LiCl, $NaBH_4$, THF/EtOH.

from compound 1, as reported [149]. TGX-221 was synthesized according to the same report with a modification. In line with the reported procedure, the Schiff base was generated successfully after refluxing in toluene [3]. However, the reported conditions ($NaBH_4$ in toluene) could not reduce the Schiff base to the amine, even after increasing the temperature to 100°C. This result is probably due to the poor solubility of $NaBH_4$ in toluene. After changing the solvent from toluene to methanol, a complete conversion was achieved in 30 minutes at room temperature. TGX-D2, TGX-D3 and TGX-D4 were also prepared by the same route. Compound

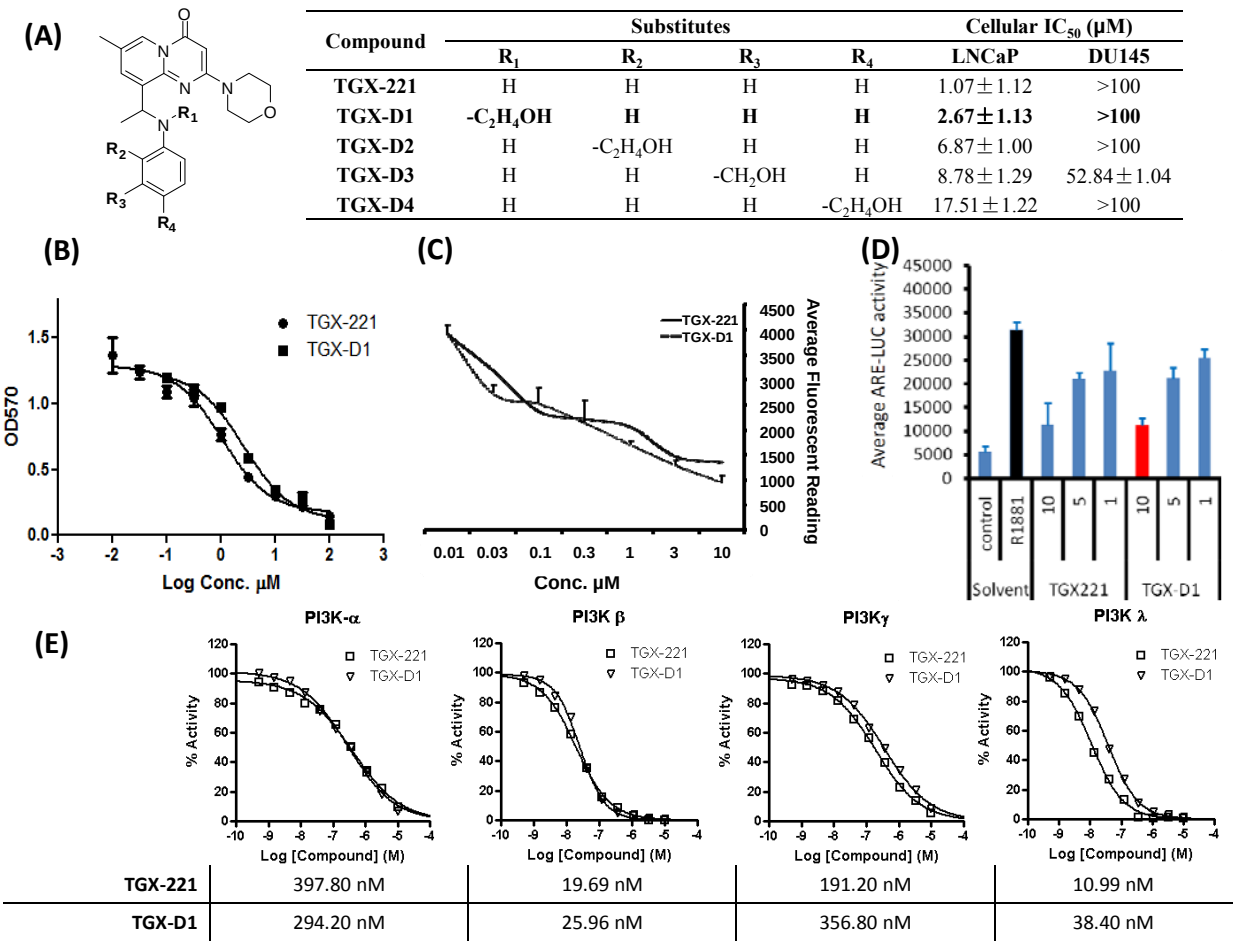

Compound	Substitutes				Cellular IC_{50} (μM)	
	R_1	R_2	R_3	R_4	LNCaP	DU145
TGX-221	H	H	H	H	1.07±1.12	>100
TGX-D1	**$-C_2H_4OH$**	**H**	**H**	**H**	**2.67±1.13**	**>100**
TGX-D2	H	$-C_2H_4OH$	H	H	6.87±1.00	>100
TGX-D3	H	H	$-CH_2OH$	H	8.78±1.29	52.84±1.04
TGX-D4	H	H	H	$-C_2H_4OH$	17.51±1.22	>100

	PI3K-α	PI3K β	PI3Kγ	PI3K λ
TGX-221	397.80 nM	19.69 nM	191.20 nM	10.99 nM
TGX-D1	294.20 nM	25.96 nM	356.80 nM	38.40 nM

Figure 5. Bioactivity screening of TGX-221 and its derivatives. TGX-D1 showed comparable effects as TGX-221 in cytotoxicity,the inhibition of androgen-induced cell proliferation and gene expression. (A) Structures of the TGX-221 derivatives and their IC_{50} values in LNCaP (PTEN-null) and DU145 (PTEN-wild) cells. (B) Cytotoxicities of TGX-221 and TGX-D1 are examined on LNCaP cells by MTT assay. (C) Both TGX-221 and TGX-D1 inhibit androgen-induced cell proliferation. LNCaP cells were treated with TGX-221 and TGX-D1 in R1881-containing serum-free mediumfor 3 days before the Alarm Blue assay. (D) Both TGX-221 and TGX-D1 inhibit androgen-induced gene expression. The ARE-LUC reporter was transfected into LNCaP cells and the cells were stimulated with R1881 (1.0 nM) in the presence or absence of TGX-221 or TGX-D1 for 24 hours before being subjected to the luciferase assay. The results are represented as the mean ± SD (n=3). (E). The response of enzyme activity of PI3K isoforms to the treatment of TGX-221 and TGX-D1.

5 was synthesized from TGX-221 by substituting the secondary aniline with a methyl acetate. to do this conversion, the ester group of compound 5 was converted to a primary alcohol (TGX-D1) by LiCl/$NaBH_4$ with a yield of 40~60%.

Bioactivity screening of the TGX-221 derivatives

We next examined the bioactivities of these TGX-221 derivatives in two prostate cancer cell lines, LNCaP and DU145. LNCaP represents a PTEN-null prostate cancer cell line that is sensitive to TGX-221 treatment, while DU145 is PTEN-wild and unresponsive to TGX-221. As shown in **Figure 5A** and **B**, TGX-221 exhibits the highest activity in LNCaP cells with an IC_{50} of 1.07 μM. Among the four TGX-221 derivatives, TGX-D1 showed the best activity (IC_{50}=2.67 μM) in LNCaP cells. Both TGX-221 and TGX-D1 showed a negligible activity in DU145 cells (IC_{50}>100 μM). TGX-D2, TGX-D3 and TGX-D4 also demonstrated activities in the LNCaP cells with IC_{50} of 6.9 μM, 8.8 μM, and 17.5 μM, respectively. DU145 cells did not respond to these derivatives with the exception of TGX-D3, which had an IC_{50} of 52.9 μM.

PI3Kβ has been reported to be essential for androgen-stimulated AR transactivation and cell proliferation in prostate cancer cells.[141] Androgen-stimulated cell proliferation and gene expression are dramatically reduced by silencing the PI3Kβ gene with siRNA or inhibiting its activity with the PI3Kβ-selective inhibitor TGX-221.[141] TGX-D1 demonstrated comparable effects as TGX-221 on the inhibition of androgen-induced cell proliferation (**Figure 5C**) and gene expression (**Figure 5D**), suggesting that TGX-D1 has a similar potency to TGX-221 to specifically inhibit PI3Kβ activity. As a result, TGX-D1 was selected for conjugation with the peptide promoiety.

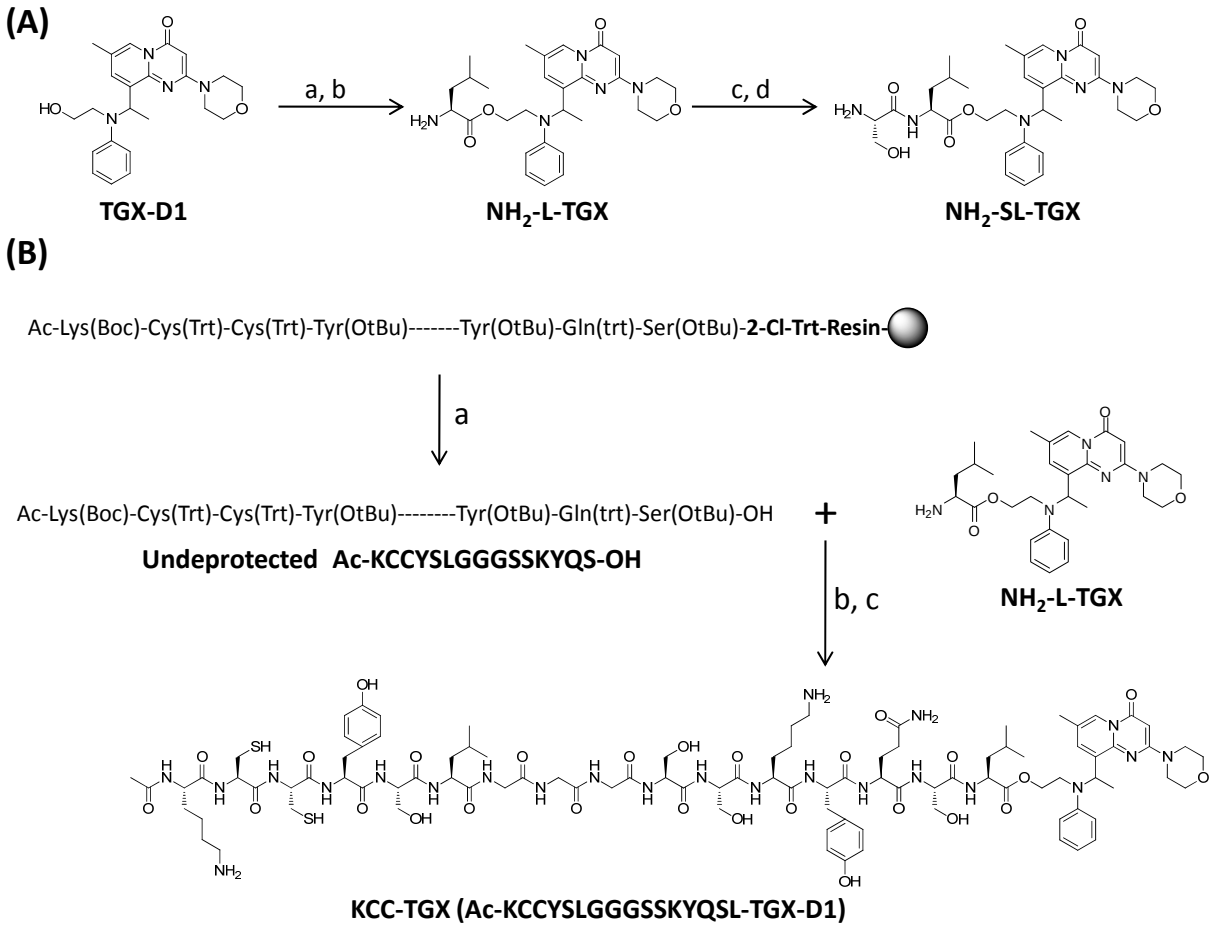

Figure 6. Synthesis of the peptide-drug conjugate. (A) Synthesis of NH_2-SL-TGX. Reaction conditions: (a) Fmoc-Leu-OH, EDCI, DMAP (cat), DCM; (b) 20% piperidine in DCM; (c) Boc-Ser(OtBu)-OH, EDCI, DMAP (cat), DCM; (d) 50% TFA in DCM. (B) Synthesis of KCC-TGX. Reaction conditions: (a) AcOH/trifluroethanol/DCM (10/20/70), rt; (b) HATU, DIPEA, NMP; (c) TFA/DCM/TIPS (47.5/47.5/5), rt.

Synthesis of the peptide-drug conjugate

Synthesis of NH_2-SL-TGX is depicted in **Figure 6A**. Fmoc-Leu-OH was conjugated to the hydroxyl group of TGX-D1 via an ester bond. After deprotection, Boc-Ser(tBu)-OH was coupled to the amino group of the NH_2-L-TGX. The dipeptide-drug conjugate (NH_2-SL-TGX)

was obtained by deprotecting the peptide and purifying it by HPLC using acidic conditions. Neutral and basic environments were avoided for NH_2-SL-TGX because of its instability.

For the synthesis of KCC-TGX, undeprotected peptide KCCYSLGGGSSKYQS including the PSA substrate, a GGG spacer, and the HER2-specific peptide was synthesized independently, and then coupled to NH_2-L-TGX (**Figure 6B**). The undeprotected peptide KCCYSLGGGSSKYQS was constructed on 2-Cl-Trt-resin using solid-phase synthesis. The N-terminus of the peptide was protected with an acetyl group to enhance the stability of the peptide-drug conjugate. Coupling reagent HATU was used to increase the yield and suppress the racemization. The undeprotected peptide-drug conjugate (KCC-TGX) was isolated by silica gel column, followed by de-protection and purification by HPLC. The peptide-drug conjugate exhibited good solubility, and no organic solvent was required in its drug release and bioactivity studies.

Drug release from the peptide-drug conjugate

Release of the parent drug from the peptide-drug conjugate is essential to elicit the therapeutic effect in prostate cancer cells. According to our hypothesis, KCC-TGX (Ac-KCCYSLGGGSSKYQSL-TGX) would be delivered to prostate cancer cells and cleaved on the cell surface by PSA. Additionally, the released NH_2-SL-TGX would undergo a self-cyclization reaction to release the parent drug TGX-D1 in physiological pH (Figure 5A). To test this hypothesis, we monitored the release of TGX-D1 from NH_2-SL-TGX *in vitro* by HPLC. The data presented in **Figure 7B** and **C** illustrated that TGX-D1 dissociated readily from the

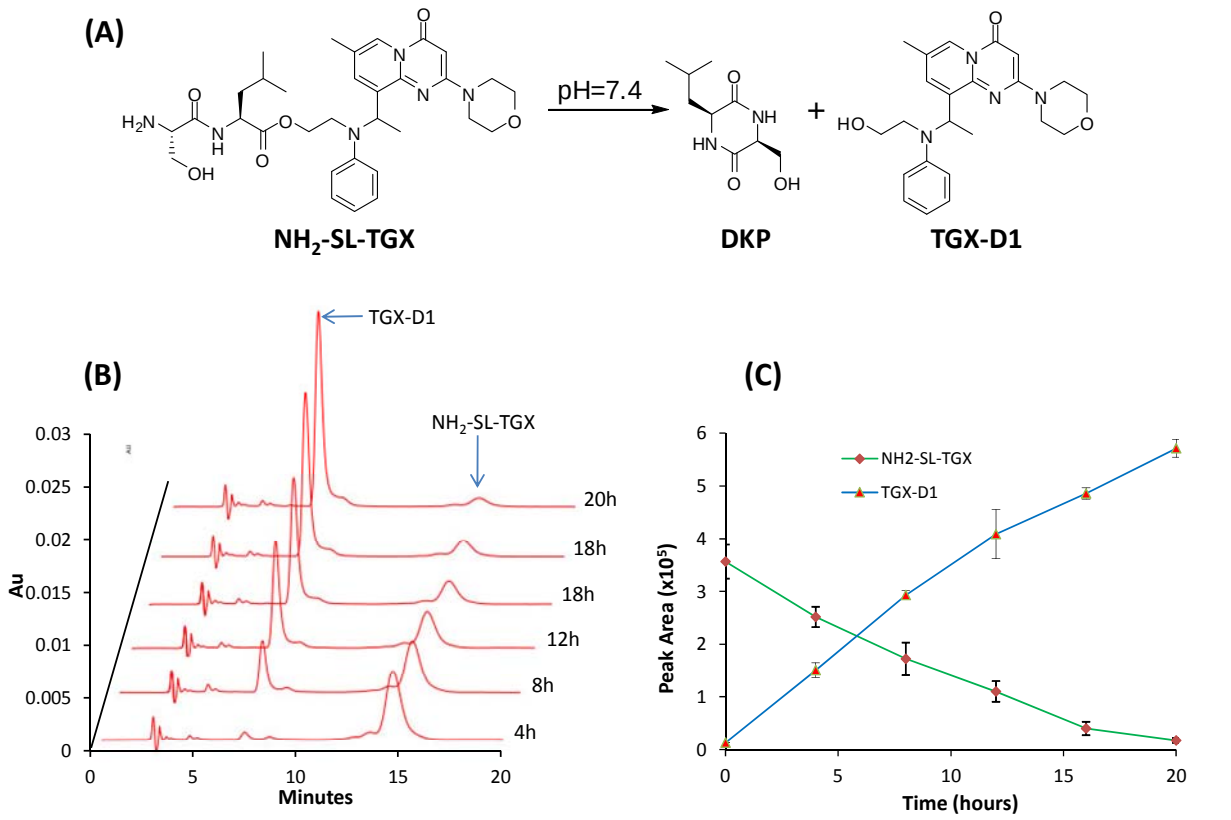

Figure 7. *In vitro* drug release from the intermediate NH_2-SL-TGX. NH_2-SL-TGX underwent self-cyclization to release the parent drug TGX-D1. The dipeptide Ser-Leu self-cyclizes to form DKP in a neutral pH. (A) Illustration of the self-cyclization reaction. (B) HPLC chromatogram monitored at 268nm. (C) Release profile of TGX-D1 from NH_2-SL-TGX. The results are represented as the mean ± SD (n=3).

dipeptide-drug conjugate NH_2-SL-TGX in PBS buffer (pH 7.4) at 37 °C. The release profile followed zero-order kinetics with a half-life of 8 hours.

We further examined the hypothesis using Ac-SSKYQSL-TGX that only contained the PSA cleavable peptide sequence SSKYQ [152]. PSA enzymes expressed in prostate cancers recognize SSKYQ and cleave it between the residues Gln (Q) and Ser (S) to form the dipeptide-drug conjugate (NH_2-SL-TGX) which undergoes a self-cyclization reaction to release the parent drug TGX-D1 in a physiological pH (**Figure 8A**). Our selection of the dipeptide SL as the linker

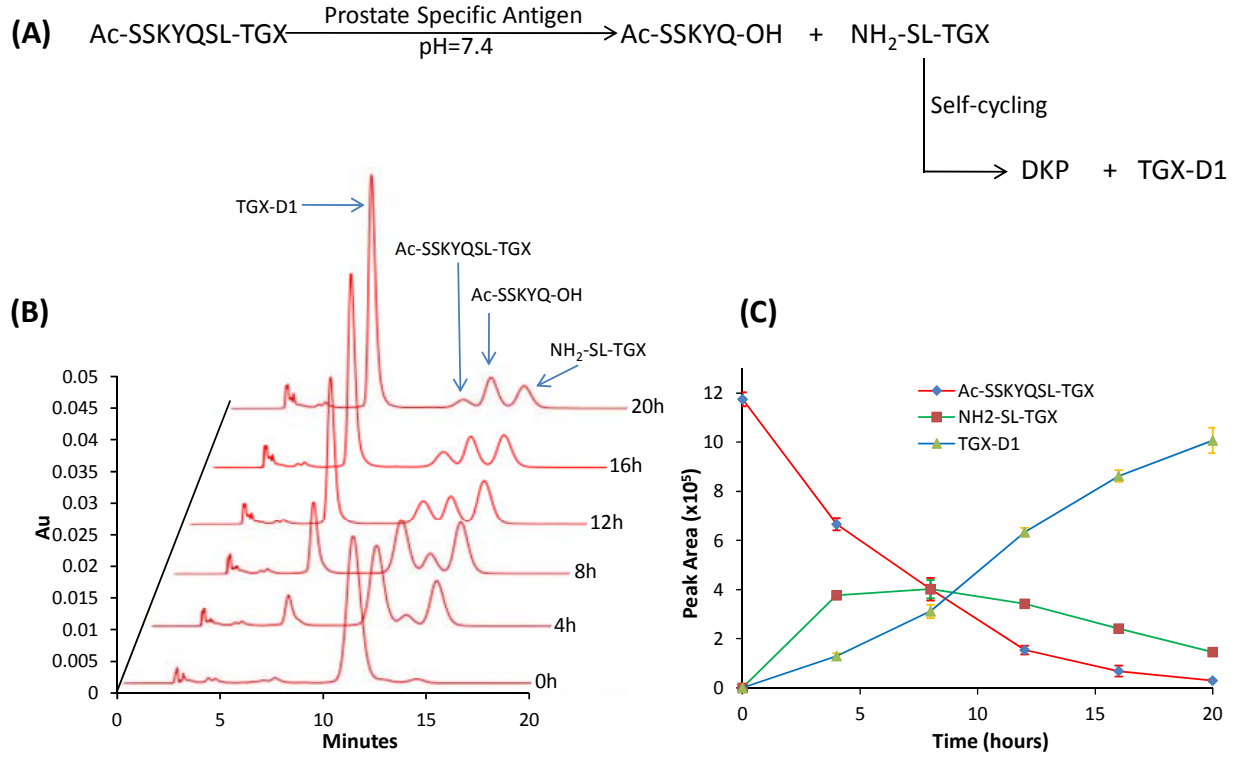

Figure 8. PSA-mediated drug release from the peptide-drug conjugate (Ac-SSKYQSL-TGX). Ac-SSKYQSL-TGX was cleaved by PSA to release the intermediate NH_2-SL-TGX which underwent self-cyclization to release the parent drug TGX-D1. (A) Illustration of PSA activation of the peptide-drug conjugate. (B) HPLC chromatogram monitored at 268nm. (C) Release profile of TGX-D1 from Ac-SSKYQSL-TGX. The results are represented as the mean ± SD (n=3).

between the PSA substrate and TGX-D1 was not only for the self-cyclizaiton reaction, it was also because the most efficient PSA cleavage occurs between Gln (Q) and Ser (S) that are followed by Leu (L) [13]. To monitor the PSA cleavage and drug release, the peptide-drug conjugate Ac-SSKYQSL-TGX was incubated with PSA at 37°C and then assayed by HPLC. As **Figure 8B** and **C** depict, Ac-SSKYQSL-TGX was gradually cleaved by PSA to release the intermediate NH_2-SL-TGX. The generation of NH_2-SL-TGX by PSA cleavage was faster than

the self-cyclization rate at the beginning, leading to an increase of NH_2-SL-TGX. However, a gradual and steady release of the parent drug TGX-D1 was also observed, suggesting that the peptide-drug conjugate could readily release the active TGX-D1 in prostate cancer cells.

Cytotoxicity of the peptide-drug conjugates

We next examined whether the released parent drug TGX-D1 was still active to induce cytotoxicity in the prostate cancer cells. As demonstrated in **Figure 9**, NH_2-SL-TGX, Ac-SSKYQSL-TGX and KCC-TGX induced similar cytotoxicities in the LNCaP cells. The IC_{50} values for NH_2-SL-TGX, Ac-SSKYQSL-TGX and KCC-TGX obtained were 5.54 μM, 4.20 μM and 5.27 μM, respectively, which are close to the IC_{50} (2.67 μM) of the parent drug TGX-D1. These results clearly indicated the efficient release of the parent drug TGX-D1 from the peptide-drug conjugate.

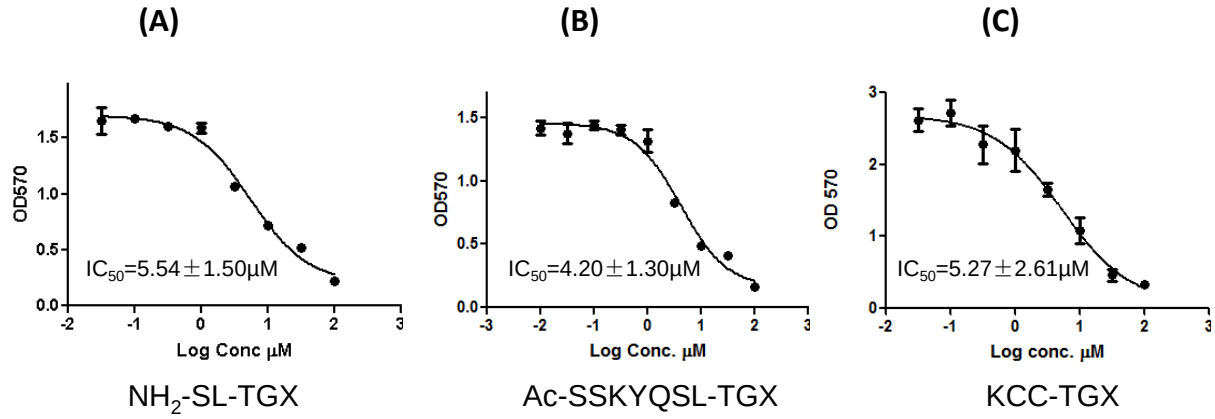

Figure 9. Cytotoxicity of NH_2-SL-TGX (A), Ac-SSKYQSL-TGX (B) and KCC-TGX (C) in LNCaP cells. LNCaP cells were incubated with the peptide-drug conjugates for 72 hours, and cytotoxicity was measured by a MTT assay. The results are represented as the mean ± SD (n=3).

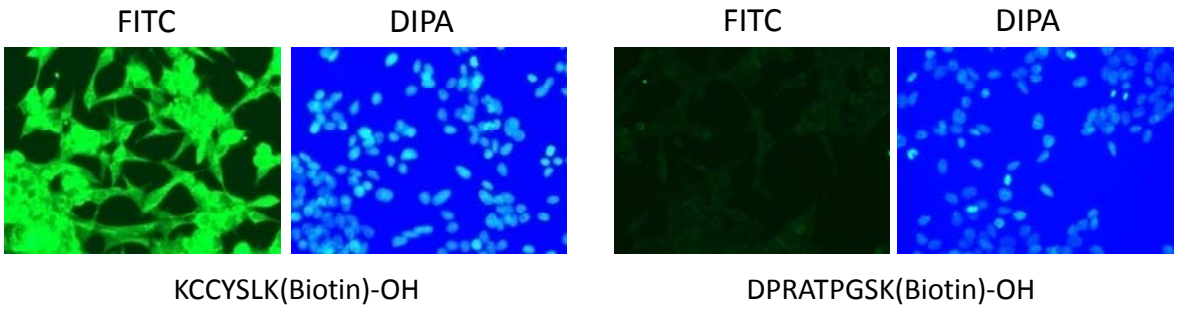

Figure 10. Immunostaining of LNCaP cells with biotinylated anti-HER2 peptide. After blocking with 1% BSA in PBS, the fixed LNCaP cells were incubated with the biotinylated peptide for 1 hour in TBST buffer. After washing with TBS, the cells were incubated with streptavidin-FITC for 20 minutes and the nucleus was stained with DIPA for cell tracking. The cells were visualized using a Leica DMI3000 microscope at a 200x magnification.

High affinity of the HER2-targeting peptide with LNCaP cells

It has been demonstrated that HER2 is highly expressed in a significant proportion of prostate cancer cells including LNCaP cells [153, 154]. KCCYSL is a HER2-targeting peptide that was generated against HER2-positive breast cancer cells using phage display technology [155]. KCCYSL is relatively small, and its affinity to the HER2 receptor is well defined [155, 156]. To verify its affinity to LNCaP cells, C-terminus biotinylated KCCYSL was incubated with LNCaP cells and then stained with streptavidin-FITC. KCCYSL exhibited high-affinity binding on the LNCaP cells at a low concentration (10 μM) in comparison to the control peptide DPRATPGSK (**Figure 10**). No significant fluorescence was observed for this control peptide even when the concentration was increased to 100 μM (data not shown). These results further

support the rationale of using the HER2-targeting peptide for targeted drug delivery to prostate cancer cells.

Cellular uptake of KCC-TGX

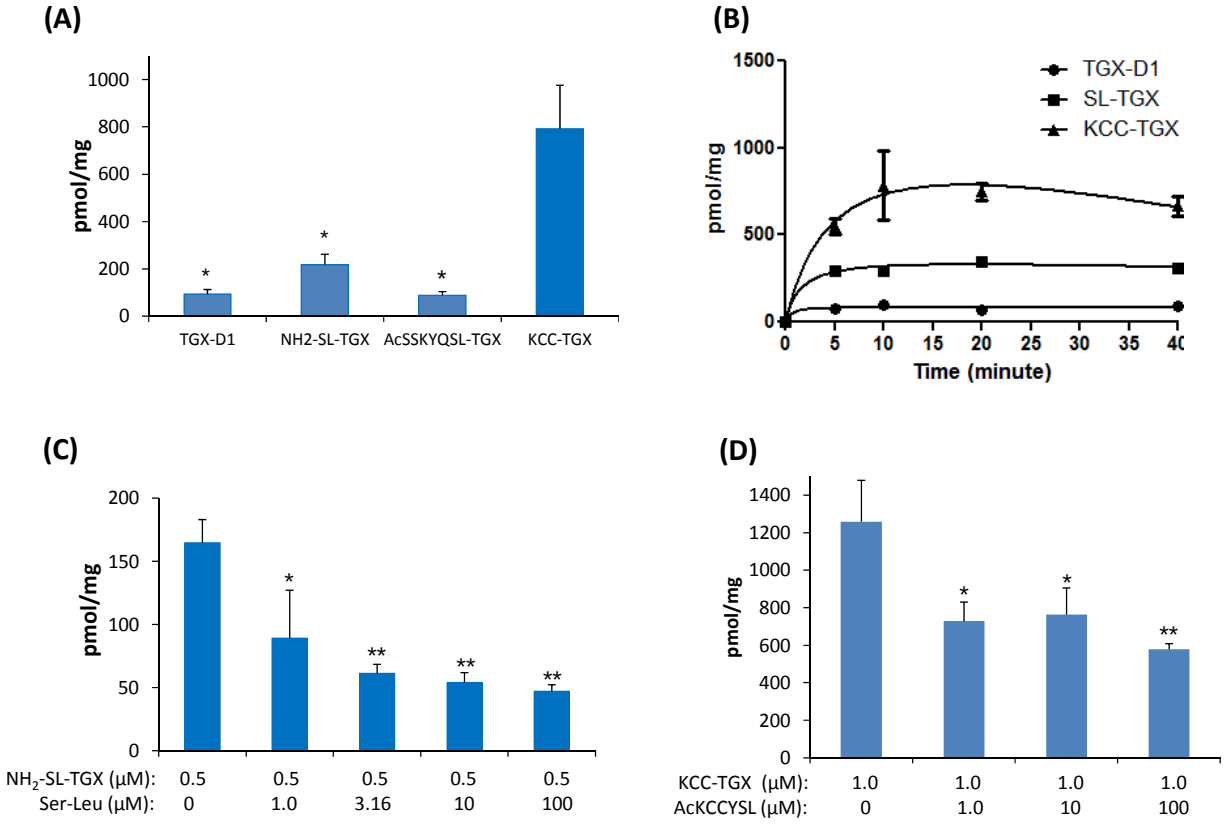

Figure 11. Cellular uptake of the peptide-drug conjugates in LNCaP cells. (A) Cellular uptake in LNCaP cells at a concentration of 0.5 μM. (B) The time-course of cellular uptake in LNCaP cells. (C) Dipeptide Ser-Leu concentration-dependent inhibition of the uptake of NH_2-SL-TGX. (D). The HER2- specific ligand AcKCCYSL inhibits the uptake of KCC-TGX in LNCaP cells. The results are represented as the mean ± SD (n=3). (* $P < 0.05$; ** $P < 0.01$).

We finally investigated whether the HER2-targeting peptide enhanced the delivery of the peptide-drug conjugate, KCC-TGX, to prostate cancer cells. Cellular uptake of TGX-D1 and its peptide conjugates were first evaluated on LNCaP cells at a concentration of 0.5μM after 1 hour of incubation (**Figure 11A**). Both TGX-D1 and Ac-SSKYQSL-TGX showed low uptake in LNCaP cells, while NH_2-SL-TGX showed a high uptake. By contrast, KCC-TGX, whichcontains the HER2 targeting peptide, exhibited the highest uptake, indicating that the HER2-specific peptide (KCCYSL) dramatically increased the cellular uptake of KCC-TGX. The time-course of drug uptake in LNCaP cells was also studied (**Figure 11B**). While KCC-TGX showed the highest uptake extent, the uptake rate was comparable to that of TGX-D1 and NH_2-SL-TGX, suggesting that coupling of the anti-HER2 peptide increases the drug affinity to prostate cancer cells without compromising its uptake rate.

It is interesting to note that NH_2-SL-TGX demonstrated a higher cellular uptake in comparison to Ac-SSKYQSL-TGX and TGX-D1. The possible explanation might be that NH_2-SL-TGX can be taken up through peptide transporters that are expressed on many cancer cells.[157] In line with this hypothesis, Ac-SSKYQSL-TGX did not show increased uptake either because only di- and tri-peptide can be actively transported by peptide transporters.[158] However, to test this hypothesis, LNCaP cells were incubated with 0.5μM of NH_2-SL-TGX in the presence of dipeptide Ser-Leu (0, 3.16, 10, and 100 μM) at 37°C for 1 hour. As Figure 9C revealed, the uptake of NH_2-SL-TGX showed a concentration-dependent decrease after co-incubation with the dipeptide Ser-Leu, which competed for the same transporters on the prostate cancer cells. The peptide transporters were almost completely saturated by Ser-Leu at 10 μM, and the uptake of NH_2-SL-TGX was accordingly inhibited by 75%.

To demonstrate whether the uptake of KCC-TGX by LNCaP cells is mediated by the anti-HER2 peptide ligand, we pre-incubated the cells with the anti-HER2 peptide and then applied KCC-TGX to the cells. As Figure 9D revealed, the uptake of Ac-KCCYSL was significantly inhibited by the pre-incubation with the HER2-specific ligand, which confirmed the specific binding of KCC-TGX to LNCaP cells via the recognition of the anti-HER2 peptide.

Aqueous solubility and stability of KCC-TGX

It is interesting to note that NH_2-SL-TGX demonstrated a higher cellular uptake in comparison to Ac-SSKYQSL-TGX and TGX-D1. The possible explanation might be that NH_2-SL-TGX can be taken up through peptide transporters that are expressed on many cancer cells [157]. In line with this hypothesis, Ac-SSKYQSL-TGX did not show increased uptake either because only di- and tri-peptide can be actively transported by peptide transporters [158]. However, to test this hypothesis, LNCaP cells were incubated with 0.5μM of NH_2-SL-TGX in the presence of dipeptide Ser-Leu (0, 3.16, 10, and 100 μM) at 37°C for 1 hour. As **Figure 11C** revealed, the uptake of NH_2-SL-TGX showed a concentration-dependent decrease after co-incubation with the dipeptide Ser-Leu, which competed for the same transporters on the prostate cancer cells. The peptide transporters were almost completely saturated by Ser-Leu at 10 μM, and the uptake of NH_2-SL-TGX was accordingly inhibited by 75%.

To demonstrate whether the uptake of KCC-TGX by LNCaP cells is mediated by the anti-HER2 peptide ligand, we pre-incubated the cells with the anti-HER2 peptide and then applied KCC-TGX to the cells. As **Figure 11D** revealed, the uptake of Ac-KCCYSL was significantly inhibited by the pre-incubation with the HER2-specific ligand, which confirmed the specific

Table 4. Solubilities of TGX-221, TGX-D1 and KCC-TGX.

Compound	Aqueous solubility	
	μg/ml	μM
TGX-221	147.5±17.6	405.2±48.2
TGX-D1	33.5±6.6	82.1±16.2
KCC-TGX	≥9899.1±465.4	≥4684.9±220.3

binding of KCC-TGX to LNCaP cells via the recognition of the anti-HER2 peptide.

Aqueous solubility and stability of KCC-TGX

The aqueous solubility of KCC-TGX was assayed by the thermodynamic method at room temperature. The aqueous solubility of TGX-221 is approximately 147.5 μg/mL which is considered to be water-insoluble according to the United States Pharmacopeia (USP) (**Table 4**). Surprisingly, the solubility of TGX-D1 is only 33.5 μg/mL which is much lower than that of TGX-221. However, after conjugating to the peptide promoiety, its solubility increased to more than 9.895 mg/mL, which is 60-fold higher than that of TGX-D1 in terms of molarity. The substantial increase in aqueous solubility is probably due to the hydrophilic peptide promeity Ac-KCCYSLGGGSSKYQSL-OH in KCC-TGX.

The stability of KCC-TGX was measured in three different solutions. KCC-TGX was found to be relatively stable in PBS and cell culture medium at 37°C. After 4 hours of incubation, 7% and 12% of KCC-TGX were found to be degraded in PBS and cell culture medium, respectively (**Figure 12**). However, KCC-TGX was quickly degraded in mouse serum with a half-life of 15 minutes, and nearly 83% of the KCC-TGX molecules were degraded in mouse

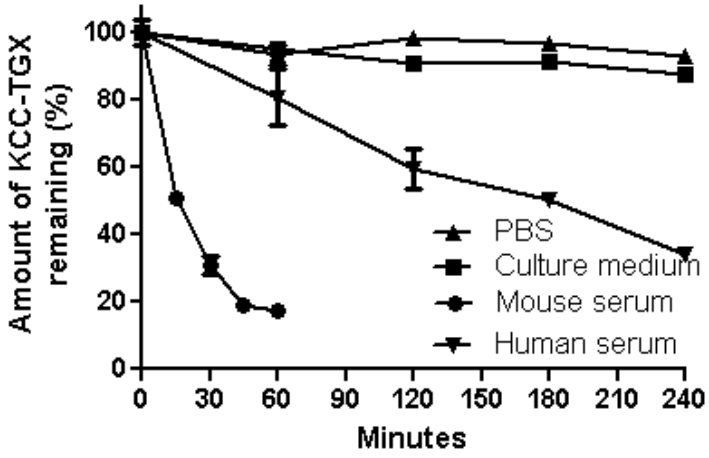

Figure 12. The stability of KCC-TGX in PBS, cell culture medium, human and mouse serum. Results were represented as mean ± SD (n=3).

serum after 60 minutes. The quick degradation of KCC-TGX is probably due to the labile ester linker was used between the peptide and TGX-D1. However, it should be noted that the hydrolysis rate of the ester linker is species dependent, and the stability is much higher in human plasma than that in mouse serum [159]. Therefore, the degradation of KCC-TGX in human plasma is expected to be much slower.

3.4. Discussion

In this study, we conjugated a peptide promoiety that contains a HER2-specific peptide and a PSA-cleavable substrate to TGX-221, a highly potent PI3Kβ inhibitor that shows a great promise for prostate cancer therapy. Despite the essential role of PI3Kβ in prostate cancer development, the therapeutic application of TGX-221 is limited due to its poor solubility and lack of specificity to prostate cancer cells. Therefore, the aim of this study is to overcome these

two problems by attaching a peptide promoiety to TGX-221. Targeted delivery of this peptide-conjugate drug was achieved by considering two mechanisms. First, the HER2-specific peptide binds to HER2 on the surface of prostate cancer cells. Second, PSA, which exists in the microenvironment of prostate cancer cells cleaves the peptide and releases the active parent drug.

Because TGX-221 does not contain a functional group for peptide conjugation, we first synthesized four TGX-221 derivatives (**Figure 4**) by attaching a -OH group at different sites. Among them, TGX-D1 was selected for peptide conjugation due to its similar activity compared to TGX-221 (**Figure 5A**).

HER2 has been reported to be overexpressed in many cancers such as breast cancer and prostate cancer. Although the role of its overexpression in prostate cancer is not fully understood, the HER2 receptor has been successfully exploited as a molecular target for targeted drug delivery to prostate cancer [153, 160]. Anti-HER2 antibody is the first type of targeting moiety used for an antibody-drug conjugate. However, its large size compromises its cellular uptake, and the antibody-drug conjugate is unable to reach the tumor interior readily. Furthermore, one antibody molecule can only be conjugated with 1-3 drug molecules, which leads to a low drug loading (<1%). As a result, only highly potent drugs (IC_{50}=10^{-9}-10^{-11}M) can be used for this antibody-drug approach [59]. By contrast, a peptide ligand is a more appropriate targeting moiety due to its excellent cell permeability, small molecular weight, ease of production, and flexibility in chemical conjugation [4]. The size of the peptide-drug conjugate is small enough to efficiently penetrate tissues, and drug loading can be as high as 20~30%. In this study, a 16-mer peptide (KCCYSLGGGSSKYQSL) was conjugated to TGX-D1 to form the peptide-drug conjugate (MW 2113.4), in which a drug loading of 19.4% was achieved. This 16-mer peptide promoiety is

composed of a HER2-targeting peptide, a GGG spacer, a PSA substrate peptide and a self-cycling dipeptide (**Figure 3A**).

PSA-activated peptide-drug conjugates have been well studied in recent years [13, 161]. For example, L-377202, a peptide-doxorubicin prodrug hydrolyzed by PSA, has already entered clinical trials [162]. However, none of these peptide-drug conjugates include tumor-specific ligands, which cause accumulation in the cancer cells. Here, we reported the first application of a HER2-specific ligand to deliver the PSA-activated TGX-221 prodrug to prostate cancer cells. Uptake of the peptide-drug conjugate KCC-TGX in prostate cancer cells is approximately 10-fold that of the peptide-drug conjugate (Ac-SSKYQSL-TGX) that only contains the PSA cleavage linker (**Figure 11A**). In addition, the peptide-mediated cellular uptake is fast, and equilibrium is quickly reached in less than 10 minutes, demonstrating a rapid uptake of the prodrug in prostate cancer cells (**Figure 11B**). This rapid uptake is critical to minimize the loss of the peptide-drug conjugate caused by kidney excretion after systemic administration. Compared to the quick uptake, PSA cleavage of the peptide-drug conjugate is slow in *in vitro* studies (**Figure 8**). However, a much more efficient cleavage *in vivo* is expected because the prostate cancer interstitial fluid contains a substantial level of enzymatically active PSA (50~500 μg/mL), which is 5~50 times higher than we used in the *in vitro* cleavage study [163]. As demonstrated in Garsky's study, the half-life of a similar PSA substrate peptide was reduced to 10~30 minutes when 340 μg/mL of PSA was used [13]. In comparison, the self-cyclization of NH_2-SL-TGX might be the rate-limiting step in the release of the parent drug *in vivo*.

One interesting observation was that the dipeptide-drug conjugate NH_2-SL-TGX exhibited a higher cellular uptake than TGX-D1 and Ac-SSKYQSL-TGX (Figure 9A). In other

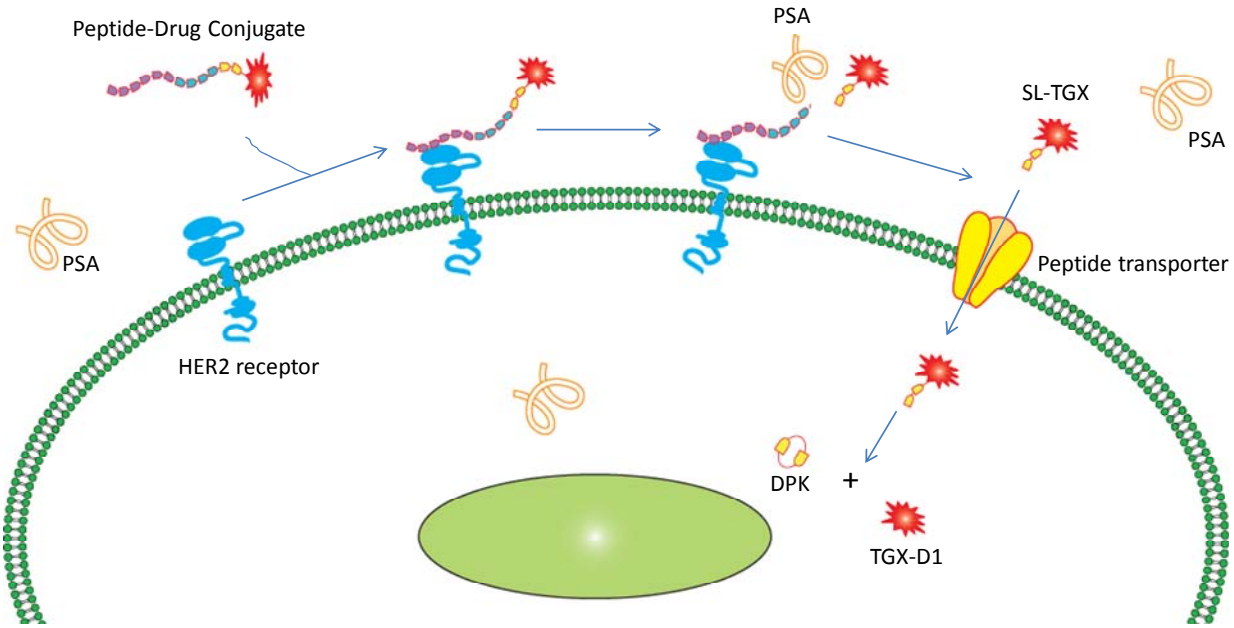

Figure 13. Delivery mechanism of peptide drug conjugate.

words, the peptide transporters that are believed to be widely expressed in various cancers could take up NH_2-SL-TGX readily [157]. In line with this hypothesis, we have found that co-incubation with the dipeptide Ser-Leu suppressed the cellular uptake of NH_2-SL-TGX (**Figure 11C**). Therefore, we reasonably believe that PSA enzymes cleave the KCC-TGX bound on the cell surface to release NH_2-SL-TGX, which are then transported into the cells through the peptide transporters. However, KCC-TGX can also be directly taken up by HER2 receptor-mediated endocytosis.

3.5. Conclusion

In summary, a multi-component peptide-drug conjugate was synthesized for TGX-221. This peptide-drug exhibits high cellular uptake in LNCaP cells. PSA enzymes activate the

peptide-drug conjugate by cleaving the PSA substrate to release NH_2-SL-TGX, which undergoes a self-cyclization to release the parent drug TGX-D1. This peptide-drug conjugate exhibits a much higher cellular uptake in prostate cancer cells in comparison to the parent drug, indicating its tremendous potential as a targeted therapy for prostate cancer patients.

CHAPTER 4

EXPRESSION PROFILE AND FUNCTIONAL ACTIVITY OF PEPTIDE TRANSPORTERS IN PROSTATE CANCER CELL LINES

4.1. Introduction

Peptide transporters, also called proton-coupled oligopeptide transporters, are membrane proteins that mediate the cellular uptake of di/tri-peptides and peptidomimetic drugs by utilizing the inwardly directed proton-motive force [164]. In mammalian cells, the peptide transporter family consists of four members, including peptide transporter 1 (PEPT1), peptide transporter 2 (PEPT2), peptide histidine transporter 1 (PHT1) and peptide histidine transporter 2 (PHT2). PEPT1 and PEPT2 are the prototype transporters of this family and have been extensively studied since their discovery in the 1980s [165-167]. In contrast, PHT1 and PHT2 are newly identified peptide transporters, and their physiological roles and functions have not yet been fully defined. PEPT1 is expressed predominantly in the small intestine and mediates transportation of nutrients (di/tri-peptide) or peptidomimetic drugs from the lumen into enterocytes, whereas PEPT2 is strongly expressed in the kidneys and mediates the renal reabsorption of filtrated nutrients and peptidomimetic drugs [168]. Due to its strong expression in the small intestine, PEPT1 has been utilized to enhance the oral absorption of poorly permeable drugs, such as β-lactam antibiotics, angiotensin-converting enzyme inhibitors and peptide prodrugs [169, 170]. The capacity of peptide transporters to transport a broad spectrum of substrates has made them an attractive target for drug delivery [170].

There has been growing interest in peptide transporters since the discovery of their high expression in cancer cells. Nakanishi et al. first reported that the human fibrosarcoma cell line

HT1080 exhibits peptide transport activity [171]. Subsequently, Gonzalez et al. observed overexpression of PEPT1 in the pancreatic carcinoma cell lines AsPc-1 and Capan-2 [172]. High expression of PEPT1 in gastric cancer cells has also been reported [173]. These findings suggest that peptide transporters might be expressed in various types of cancer cells. Considering their physiological function, it is reasonable to believe that the over-expression of peptide transporters helps cancer cells with the uptake of nutrients (di-/tri-peptide or *L*-Histidine) and supports the rapid growth of cancer cells [174]. It is also noteworthy that peptide transporters have been considered as an important target for drug delivery. By using peptide transporters in the small intestine, a variety of therapeutic agents have been efficiently transported [175]. The overexpressed peptide transporters in cancer cells therefore provide a specific pathway for therapeutic agents to enter cancer cells. However, although it is promising to utilize peptide transporters for drug delivery in cancer therapy, the expression profile and functional activity of peptide transporters are poorly elucidated in major cancer types, except pancreatic cancer and gastric cancer. Therefore, clarifying their expression patterns in new cancer types will expand the potential values of peptide transporters in cancer therapy.

Prostate cancer is the most common cancer and the second leading cause of death in American men [4, 176]. The expression profiles and functional activity of peptide transporters in prostate cancer cells have not been elucidated. In our previous study, we observed that the dipeptide prodrug Ser-Leu-TGX-D1 exhibited a three-fold greater cellular uptake when compared to the parent drug TGX-D1 in LNCaP cells. The enhanced cellular uptake indicated that LNCaP cells might express functionally active peptide transporters [177]. In the present study, we examined the gene expression profiles and functional activity of peptide transporters in

three of the most commonly used prostate cancer cell lines LNCaP, PC-3 and DU145. For the first time, we confirmed the presence of peptide transporters *in vitro* in prostate cancer cell lines PC-3 and LNCaP. Our findings demonstrated that LNCaP and PC-3 cells express functionally active peptide transporters at high levels. Moreover, we proven that these peptide transporters facilitate the transportation of the fluorescent dipeptide probe *D*-Ala-Lys-AMCA, and the inhibition of their activity can suppress the growth of prostate cancer cells. These findings indicate the promising potential of peptide transporters for prostate cancer therapy.

4.2. Materials and Methods

Materials

All reagents and solvents listed below were obtained from commercial sources and used without further purification. [^{3}H]Glycylsarcosine (0.2 Ci/mmol) and [^{3}H]*L*-Histidine (30 Ci/mmol) were purchased from Moravek Biochemicals Inc. (Brea, CA). Gly-Gly, Gly-Gly-Gly, Gly-Gly-Gly-Gly, Cefadroxil, *L*-Histidine, glycylsarcosine (Gly-Sar) and 2-Amino-2-norbornanecarboxylic acid (BCH) were obtained from Sigma-Aldrich (St. Louis, MO). PCR primers were synthesized by Integrated DNA technologies Inc. (Coralville, IA). The fluorescent dipeptide probe *D*-Ala-Lys-AMCA was purchased from Biotrend Chemicals, LLC (Destin, FL). Thiazolyl Blue was obtained from RPI Corp. (Prospect, IL). All of the organic solvents used for synthesis and HPLC were obtained from Fisher Scientific (Pittsburgh, PA).

Cell Culture

All of the cell lines used in this study were obtained from the ATCC. PC-3 cells were grown in RPMI-1640 media containing 10% Fetal Bovine Serum (FBS), 100 units/mL penicillin and 100 μg/mL streptomycin. LNCaP cells were maintained in RPMI-1640 media supplemented with 10% FBS, 100 units/mL penicillin, 100 μg/mL streptomycin, and 1 mM sodium pyruvate. Caco-2, HeLa, and DU145 cells were cultured in DMEM media supplemented with 10% FBS, 100 units/mL penicillin, and 100 μg/mL streptomycin. All cells were grown at 37°C in a humidified atmosphere containing 5% CO_2. The culture medium was changed every other day, and the cells were passaged when they reached 80-90% confluency. In the cellular uptake study, LNCaP cells were grown in Poly-*D*-Lysine coated wells to prevent detachment during washing.

Quantitative Real-Time RT-PCR (qRT-PCR, Copy number assay)

Quantification of the mRNA copy number for PEPT1, PEPT2, PHT1 and PHT2 in various cell lines was performed as reported [178]. Total RNA was isolated using TRIzol reagent (Invitrogen) according to the manufacturer's protocol. Two hundred nanograms of RNA were converted to cDNA using random hexamer primers and the MultiScribe Reverse Transcriptase Reagent (Applied Biosystems, Inc., Branchburg, NJ). Eighty nanograms of the cDNA were amplified by real time PCR using SYBR Green-1 dye universal Master Mix on a Roche LightCycler 480 system (Roche Diagnostics, Indianapolis, IN). Human genomic DNA (Promega, Madison, WI) served as the universal external standard to quantify the mRNA expressions of the four peptide transporter genes. Eighty nanograms of mRNA without reverse transcription were also directly amplified by PCR to monitor contamination of genomic DNA in the samples. Samples with no gDNA contamination (<0.3 copy/ng total RNA) were selected for qRT-PCR

analysis. The primers for PEPT1, PEPT2, PHT1 and PHT2 were designed to recognize an exon and were synthesized by Integrated DNA technologies Inc. (Coralville, IA). The primers for PEPT1 were 5'-GCAGGATGGCTGCTGACCGT-3' (forward) and 5'-GCTGAACTGGCCTGCCCCTG-3' (reverse); for PEPT2, 5'- GCGGGGTCCAGCAGATAAG CAC-3' (forward) and 5'-ACAGGGCCAGGAATTGGGGTCA-3' (reverse); for PHT1, 5'-GCTGACCATGTTTGATGCTGTGCT-3' (forward) and 5'-ACATGACAAAGAACATGCCC ACGG-3' (reverse); and for PHT2, 5'-ACATCAACAATTGCCGGATGGACC-3' (forward) and 5'-ATAGCGTCCAGCGATCCAGACAAA-3' (reverse). All groups were performed in triplicate, and the data were presented as the mean ± standard deviation (SD).

Western blot

Caco-2 cells were seeded in a 100 mm cell culture dish and cultured for 21 days. After differentiation, the Caco-2 cell monolayer was washed with PBS and lysed for 15 minutes on ice with RIPA buffer (50 mM Tris-cl pH 7.4, 150 mM NaCl, 1% NP40, 0.25% sodium deoxycholate) supplemented with protease inhibitors (Roche's complete protease inhibitor cocktail tablet). The lysate was centrifuged at 12,000 g for 10 minutes, and the supernatant was collected. Other cell lines (HeLa, LNCaP, PC-3 and Du145) were only cultured for two days before lysis. The cell lysate was prepared using the same method as described for Caco-2 cells. After measuring the total protein concentration, 20 μg of lysate was separated on a SDS-PAGE gel (10%) and transferred onto a polyvinylidene difluoride (PVDF) membrane. The membrane was blocked for 2 hours in TBST buffer (20 mM Tris, 150 mM NaCl, 0.1% Tween-20, pH 7.5) plus 5% non-fat milk. The membrane was then incubated with a primary antibody (Rabbit anti-PEPT1, Mouse

anti-PEPT2 and Rabbit anti-PHT1; Abcam, Cambridge, MA) overnight at 4°C. After rinsing three times with TBST, the membrane was incubated for 2 hours with the secondary antibody linked with horseradish peroxidase (HRP) (anti-rabbit IgG and anti-mouse IgG, Invitrogen, Grand Island, NY). After washing with the TBST buffer, the membrane was incubated with substrate and the bands were detected using FluorChem HD2 Chemiluminescent imaging system (Alpha Innotech, Santa Clara, CA).

Cellular uptake of [^{3}H]Gly-Sar and [^{3}H]*L*-Histidine

A cellular uptake study was performed on the confluent cell monolayer as described previously [172, 177]. The uptake buffer was HBSS buffer (0.952 mM $CaCl_2$, 5.36 mM KCI, 0.441 mM KH_2PO_4, 0.812 mM $MgSO_4$, 136.7 mM NaCl, 0.385 mM Na_2HPO_4, 25 mM *D*-glucose, and 10 mM HEPES) adjusted to pH 7.4. The uptake experiment was initialized by washing monolayers with pre-warmed HBSS buffer and incubating with 0.5 mL of HBSS buffer containing [^{3}H]Gly-Sar (3 μCi/mL, 15 μM) or [^{3}H]*L*-Histidine (0.5 μCi/mL, 100 μM). After 15 minute incubation at 37°C, uptake was terminated by removing the buffer and washing 5 times with ice-cold HBSS buffer. Cells were lysed overnight in 1 mL of 0.3 M NaOH/ 0.1% Triton-100, and 0.7 mL of the lysate was mixed with 3 mL of a liquid scintillation cocktail [179, 180]. The radioactivity was measured using a Beckman Multipurpose Scintillation Counter LS6500 (Beckman Coulter Inc., Brea, CA). Protein concentrations were determined using a Coomassie Protein Assay Reagent (Thermo Scientific, Rockford, IL). The active uptake, which is mediated by peptide transporters, was calculated by subtracting the passive uptake from the total uptake.

The passive uptake, which represents passive diffusion and nonspecific binding, was measured in the presence of 200 mM unlabeled Gly-Sar or *L*-Histidine.

Kinetic study of cellular uptake

To examine the uptake kinetics of Gly-Sar in prostate cancer cells, the uptake was measured in HBSS buffer (pH 7.4) over the concentration range of 62.5-2000 μM. The incubation time for the kinetic study of Gly-Sar is 30 minutes. The active uptake, which is mediated by peptide transporters, was calculated by subtracting the passive uptake from the total uptake. The passive uptake, which represents passive diffusion and nonspecific binding, was measured in the presence of 200 mM unlabeled Gly-Sar or *L*-Histidine. To obtain the kinetic parameters, the active uptake data were fitted to the Michaelis-Menten equation:

$$v = \frac{V_{max}\,[S]}{K_m + [S]}$$

Where *v* is the velocity of Gly-Sar uptake, V_{max} is the maximal velocity of Gly-Sar uptake, K_m is the Michaelis constant, and S is the Gly-Sar concentration. An Eadie-Hofstee plot was also performed to confirm a single transporter system of Gly-Sar uptake. The Eadie-Hofstee equation is:

$$v = V_{max} - K_m \frac{v}{[S]}$$

Linear and nonlinear regressions were performed using Graphpad Prism 5 (Graphpad software, Inc., La Jolla, CA). The quality of fit was determined by evaluating the correlation coefficient r^2.

The kinetic study of *L*-Histidine uptake was performed in a similar way as that of Gly-Sar, but the concentration range was 125-4000 μM, and the incubation time was reduced to 15 minutes. The active uptake data of *L*-Histidine were also fitted to the Michaelis-Menten equation and the Eadie-Hofstee equation as described above.

Uptake of the fluorescent dipeptide probe *D*-Ala-Lys-AMCA

The uptake experiment was performed according to previous reports [181-184]. Cells were seeded in a 24-well plate one day before the experiment. After aspirating the culture media, cells were washed once with the HBSS buffer. *D*-Ala-Lys-AMCA (1 mM in HBSS) was then incubated with the cells at 37°C for 1 hour. For the inhibition studies, uptake was studied in the presence of 10 mM of the dipeptide Ser-Leu. The uptake study was terminated by rapidly washing the cells three times with a citrate buffer (150 mM NaCl, 15 mM Citric acid, and 3 mM EDTA, adjusted to pH 7.0). The cellular uptake of *D*-Ala-Lys-AMCA (excitation at 350 nm, emission at 460 nm) was examined by epifluorescence microscopy (Leica Microsystems GmbH, Wetzlar, Germany).

Anti-proliferation assay

To profile the half maximal inhibitory concentration (IC_{50}) of Gly-Sar and BCH, LNCaP, PC-3 and DU145 cells were plated in 96-well plates (BD Falcon™, BD Biosciences) at a density of 5,000 cells/well. After 24 hours, serial dilutions of the drug (final concentration: 0.047-100 mM) were added and incubated with the cells for 72 hours. Cell survival was evaluated using a

MTT assay according to the manufacturer's protocol. IC_{50} was calculated by fitting the concentration-absorbance curve using Graphpad Prism 5 (Graphpad software, Inc., La Jolla, CA).

The knockdown of PEPT1 and PEPT2 expression by siRNAs

Selencer® Select siRNAs targeting PEPT1 and PEPT2 genes were purchased from Life Technologies Corp. (Carlsbad, CA). The sequences of the PEPT1 siRNA are 5'-GCAUCGGAGUAAGGCAUUUtt-3' (sense) and 5'-AAAUGCCUUACUCCGAUGCct-3' (antisense). The sequences of the PEPT2 siRNA are 5'-GAUCGGCCUGAGUCUAAUAtt-3' (sense) and 5'-UAUUAGACUCAGGCCGAUCaa-3' (antisense). siRNA transfection was conducted as we previously reported [185, 186]. Briefly, cells were seeded in Poly-*D*-Lysine pretreated 24-well plates at a density of 7.0×10^4 cells/well 12 hr before transfection. The transfection mixture was prepared by mixing siRNAs and Lipofectamine-2000 in Opti-MEM®-I medium (Invitrogen) and incubating at room temperature for 25 min. The culture medium was replaced with 400 μL of Opti-MEM®-I medium, and 50 μL of the complex was then added into each well to product a final siRNA concentration of 50 nM siRNA per well. After 12 hr incubation, 500 μL complete cell culture medium containing 10% FBS was added to each well, and the cells were incubated for another 24 hr. The cells were then harvested for RNA isolation using Tri reagent (Molecular Research Center, Inc., Cincinnati, OH). The gene knockdown effect was measured by real-time RT-PCR. 18S ribosomal RNA was used as an internal control, and the primers are 5'-GTCTGTGATGCCCTTAGATG-3' (forward) and 5'-AGCTTATGACCCGCACTTAC-3' (reverse). The primers used for the PEPT1 gene are 5'-ATTGTGTTTGTCCTTGGCAGTGGG-3' (forward) and 5'-

Table 5. mRNA expression of peptide transporters in various cell lines.

Cell line	PEPT1	PEPT2	PHT1	PHT2
HeLa	0.32±0.55	2.98±0.06	5.62±0.99	4.54±1.84
Caco-2	37.42±1.77	10.63±0.20	5.14±0.70	4.20±0.28
LNCaP	0.32±0.04	8.51±0.58	5.42±1.00	5.15±1.42
PC-3	9.91±2.14	6.09±2.16	6.19±1.18	17.28±2.84
DU145	1.17±0.34	2.41±0.38	8.40±1.05	8.16±1.14

Expression levels were reported as copy/ng total RNA.

TTTCTCTTTAGCCCAGTCCAGCCA-3' (reverse). The primers for the PEPT2 gene are 5'-TGGCAGATGATGAGGTGAAGGTGA-3' (forward) and 5'-TCTCCTGCACAGAATGCTCAGTGT-3' (reverse).

Statistical Analysis

Data were expressed as the mean ± standard deviation (SD). Differences between any two groups were determined by ANOVA. A p value of <0.05 was considered statistically significant.

4.3. Results

Gene expressing profiles of peptide transporters in prostate cancer cell lines

A quantitative determination of mRNA levels in prostate cancer cell lines was performed using qRT-PCR. A differentiated Caco-2 cell line was used as the positive control and HeLa cells were used as the negative control [187, 188]. The expression levels of four subtypes of peptide transporters were evaluated by measuring the mRNA copy numbers in one nanogram of total RNA (copy/ng). As illustrated in **Table 5**, Caco-2 cells showed the highest mRNA expression level of PEPT1, followed by PC-3 cells. The copy number of PEPT1 mRNA in Caco-

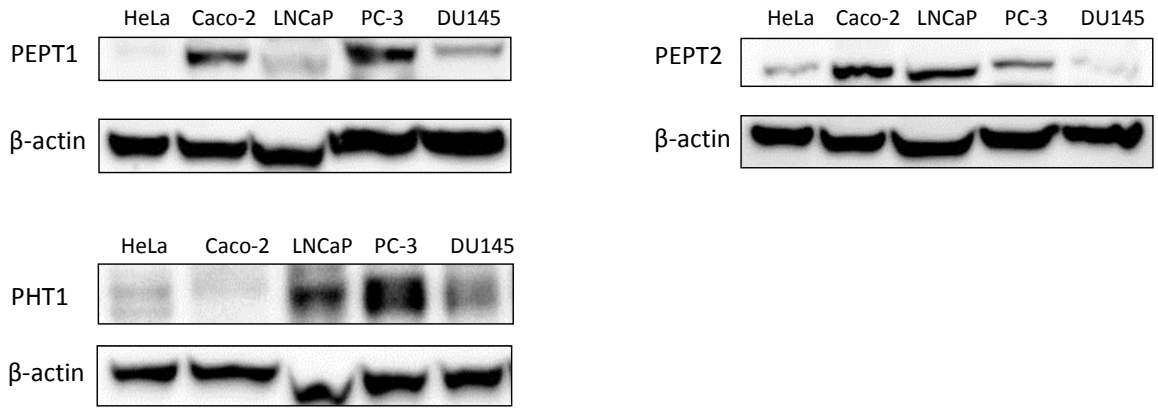

Figure 14. Expression profiles of PEPT1, PEPT2 and PHT1 proteins in five cell lines. Cell lysates of HeLa, Caco-2 (after 21-day differentiation), LNCaP, PC-3 and DU145 cells (orresponding to Lane 1-5) were analyzed by Western blot. Beta-actin was used as an internal control for equal loading. HeLa cells were used as a negative control, and no signal could be spotted at corresponding sites. Caco-2 was used as a positive control, and both PEPT1 and PEPT2 could be detected.

2 cells (~ 37.4 copy/ng) is 3.6 times greater than what is found in PC-3 cells (~ 9.9 copy/ng) and more than 90 times greater than the negative cell lines HeLa and LNCaP. Expression of PEPT2 mRNA was observed in LNCaP, PC-3 and DU145 cells with the levels at 8.5, 6.1 and 2.4 copy/ng. LNCaP had the highest PEPT2 mRNA expression level of all three prostate cancer cell lines. It is slightly lower than what is found in Caco-2 cells (10.6 copy/ng), but much greater than HeLa (~ 2.9 copy/ng) and DU145 cells (~ 2.4 copy/ng). PHT1 and PHT2 are relatively new subtypes of peptide transporters and their expression profiles were also investigated using qRT-PCR. The expression levels of PHT1 mRNA in all five cell lines are similar (5 - 8 copy/ng). As for PHT2, PC-3 cells showed higher mRNA expression (~ 17 copy/ng) than other cell lines (4-8 copy/ng). The finding is partially different from a previous study, in which the authors stated that

the mRNA expression levels of PEPT1 and PEPT2 were negligible *in vitro* in prostate PC-3 cell line but clearly detected *in vivo* in PC-3 xenograft [157]. The discrepancy between these *in vitro* results could be attributed to the different quantitative methods and external standards used in the mRNA copy number study. Instead of using probe-based real-time PCR (hybridization probe sets: Fluorescent probe and LCRed640 probe) in Mitsuoka's study, we used SYBR Green I as the dye to quantify the PCR amplification of target genes. In addition, we used genomic DNA as the universal external standard to calculate the absolute copy numbers of target genes. In contrast, Mitsuoka et al. did not mention which universal external standard was used in their study [157].

To assess the protein expression profile, a Western blot was performed to detect PEPT1, PEPT2 and PHT1 proteins in total cell lysates. The blot confirmed that PEPT1 is expressed at a high level in Caco-2 and PC-3 cells (**Figure 14**). PEPT2 showed similar protein expression profile to that suggested by qRT-PCR. LNCaP cells had the highest expression level in the three prostate cancer cell lines, followed by PC-3 cells. DU145 expressed a negligible amount of PEPT2 protein. All of the prostate cancer cell lines tested expressed PHT1 protein, especially the LNCaP and PC-3 cell lines. Although DU145 cells had the lowest expression of PHT1 protein of the three prostate cancer cell lines, the expression was much greater than what is found in Caco-2 and HeLa cells. PHT2 is a relatively new-identified peptide transporter, and there is only one anti-human PHT2 antibody available. However, we did not observe any PHT2 protein band in all samples in three independent experiments. Because this is the only anti-human PHT2 antibody in the market and we cannot validate the result with other anti-human PHT2 antibodies, we do not know whether this is because of the antibody itself or there is no PHT2 protein expression in these cell lines. Therefore, we did not include the PHT2 western blot result in this report.

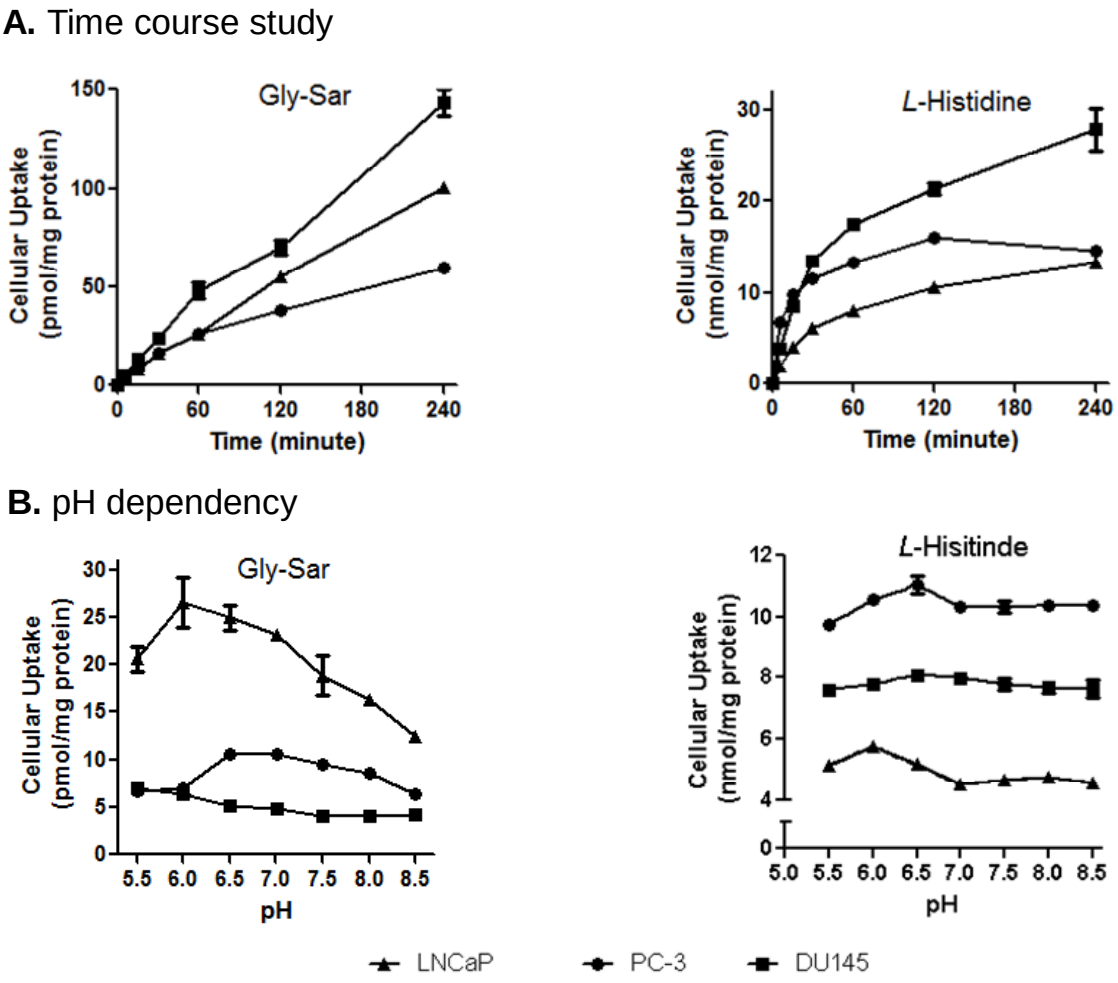

Figure 15. The time course and pH dependency of [^{3}H]Gly-Sar and [^{3}H]*L*-Histidine uptake in three prostate cancer cell lines. (A). Uptakes of [^{3}H]Gly-Sar and [^{3}H]*L*-Histidine at pH 7.4 were measured over a 240 minute time course. (B). The uptakes by prostate cancer cell lines were pH-dependent. Uptake of Gly-Sar was measured after 15 minutes of incubation at various pH values (Range 5.5-8.5). Similar uptake studies were performed for [^{3}H]*L*-Histidine. Data points: mean of three samples; bar: *SD*.

Time course of [^{3}H]Gly-Sar and [^{3}H]*L*-Histidine uptake by prostate cancer cell lines

The time course of Gly-Sar and *L*-Histidine uptake in three prostate cell lines was studied first. As observed from the data in **Figure 15A**, the uptake of 15 μM of Gly-Sar was linear

during the first 60 minutes in all three prostate cancer cell lines. Steady-state uptake was observed at 120 minutes in PC-3 cells. In contrast to PC-3, the uptake of LNCaP and DU145 did not reach plateau even at 240 minutes. Because the uptake of Gly-Sar was linear over the 60 minute incubation period in all three cell lines, the incubation time for all of the subsequent experiments was set at this linear range. The uptake of 100 μM of *L*-Histidine was also linear in the first 30 minutes of the experiment, but steady-state uptake was achieved at approximately 60 minutes in all three cell lines. On the basis of these results, the uptake of *L*-Histidine was determined at 15 minutes in subsequent experiments.

pH dependency of uptake

The effect of extracellular pH on the cellular uptake of Gly-Sar and *L*-Histidine was measured. As shown in **Figure 15B**, the uptake of Gly-Sar was pH dependent. The maximal uptake of Gly-Sar was observed at pH 6.0 in LNCaP cells and pH 6.5 in PC-3 cells. The pH dependency of Gly-Sar uptake on these two cell lines was similar to that observed for PEPT1 positive HT1080 cells and PEPT2 positive mouse astrocytes [171, 189]. The pH dependency of Gly-Sar uptake indicated that PEPT1 and PEPT2 acted as proton-coupled dipeptide transporters, and the inward proton gradient facilitated the uptake of Gly-Sar in LNCaP and PC-3 cells [168]. No significant pH dependency of Gly-Sar uptake was observed in DU145 cells. This is consistent with our observation that the expression levels of PEPT1 and PEPT2 were low in this cell line (**Table 5** & **Figure 14**).

Uptake of *L*-Histidine also demonstrated pH dependency in the three prostate cancer cell lines (**Figure 15B**). Maximal uptake was observed at pH 6.5 in PC-3 cells and DU145 cells and

at pH 6.0 in LNCaP cells. Compared to the pH dependency of Gly-Sar uptake, pH has a much weaker influence on the uptake of *L*-Histidine. The pH dependency observed in *L*-Histidine uptake suggested that PHT1 could operate in a similar manner and be driven by a similar proton-gradient force as PEPT1/PEPT2 [168].

Concentration dependency of uptake and kinetic analysis

To determine the kinetic parameters of Gly-Sar uptake in the three prostate cancer cell lines, the concentration-dependent uptake rate was investigated at pH 7.4 over the substrate concentration range of 62.5 - 2000 μM. The active uptake, which is mediated by peptide transporters, was calculated by subtracting the passive uptake from the total uptake. The passive uptake, which represents passive diffusion and nonspecific binding, was measured in the presence of 200 mM cold Gly-Sar. The excess amount of cold Gly-Sar can efficiently suppress active uptake, but minimally affect diffusion and nonspecific binding [172, 190]. As shown in Figure 3A, the passive uptake was linear over the entire concentration range in all three cell lines. In contrast, the active uptake was found to be hyperbolic over the concentration range (62.5 - 2000 μM), indicating the saturability of the peptide transporter system in LNCaP and PC-3 cell lines. The kinetic parameters were calculated by fitting the active uptake data into the Michaelis-Menten equation using non-linear regression. The LNCaP peptide transporter system exhibited a K_m of 871.2 ± 201.5 μM and a V_{max} of 620.5 ± 64.5 pmol/mg protein/30 min, whereas peptide transporters in PC-3 had a K_m of 603.0 ± 136.7 μM and a V_{max} of 917.9 ± 85.0 pmol/mg protein/30 min. A very weak active uptake was observed in the DU145 cell line (**Figure 16A** & **Table 6**). To further characterize the peptide transporter system, the active uptake data were converted into the Eadie-Hofstee plot (V vs V/S). The straight lines were obtained in both the

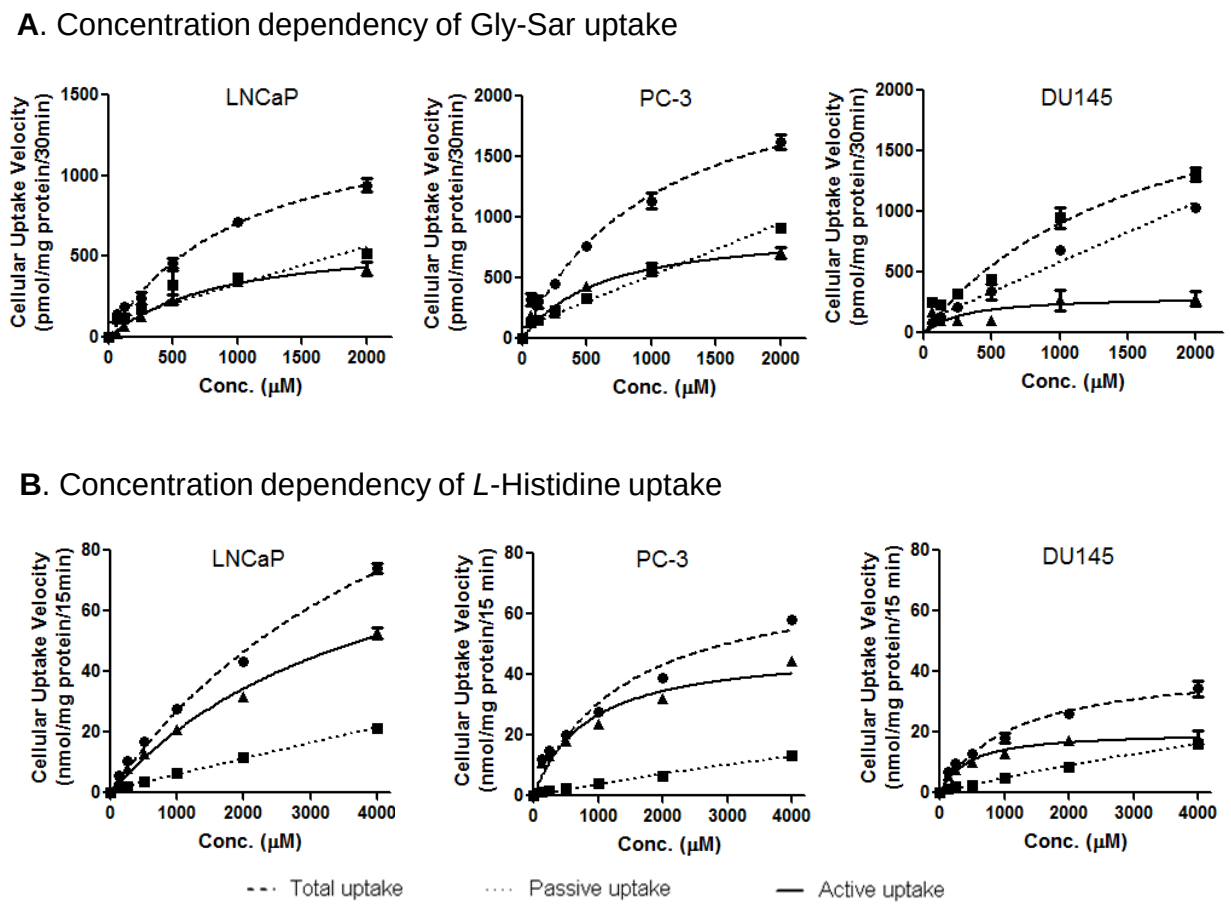

Figure 16. Concentration dependency of [^{3}H]Gly-Sar and [^{3}H]*L*-Histidine uptake. Uptake was measured at pH 7.4 with an incubation time of 30 minutes for [^{3}H]Gly-Sar uptake and 15 minutes for [^{3}H]*L*-Histidine uptake. Passive uptake was determined by measuring the uptake in the presence of 200 mM cold Gly-Sar or *L*-Histidine. Active uptake was obtained by subtracting passive uptake from total uptake. Data points represented mean ± SD for three samples.

LNCaP ($r^2 = 0.857$) and PC-3 ($r^2 = 0.913$) groups, indicating a single transporter system for Gly-Sar uptake (**Figure 17**).

The kinetic parameters of *L*-Histidine uptake were determined using the same method as that of Gly-Sar. The active uptake of *L*-Histidine was also shown as a hyperbolic curve, and the passive uptake is linear over the entire concentration range (**Figure 16B**). The transporter systems exhibited K_m values of 4059.0±615.4 μM, 811.7±149.9 μM and 423.4±91.1 μM in

Table 6. Kinetic parameters of Gly-Sar and *L*-Histidine uptake measured on three prostate cancer cell lines.

Cell lines	Gly-Sar		*L*-Histidine	
	K_m*	V_{max}#	K_m*	V_{max}#
LNCaP	871.2±201.5	620.5±64.5	4059.0±615.4	104.4±9.6
PC-3	603.0±136.7	917.9±85.0	811.7±149.9	48.5±3.3
DU145	300.5±218.9	301.5±72.5	423.4±91.1	20.1±1.3

* Unit for K_m is µM.
\# Unit for V_{max} of Gly-Sar is pmol/mg protein/30 min, while Unit for V_{max} of *L*-Histidine is nmol/mg protein/15 min.

LNCaP, PC-3 and DU145, respectively. The maximum uptake rate (V_{max}) obtained for *L*-Histidine uptake was 104.4±9.6 nmol/mg protein/15 min in LNCaP, 48.5±3.3 nmol/mg protein/15 min in PC-3 and 20.1±1.3 nmol/mg protein/15 min in DU145. As observed in Figure 4, Eadie-Hofstee plots calculated from the active uptake of *L*-Histidine were curvilinear, hence supporting a hypothesis of uptake by two transporter systems in all three cell lines.

Uptake of *L*-Histidine is mediated by two transporter systems

Although both PHT1 and PHT2 have the ability to transport *L*-Histidine, PHT1 was believed to play the major role in the cellular uptake of *L*-Histidine. PHT1 has been proven to be located in the plasma membrane of transiently transfected COS-7 cells [191]. Its active role in cellular uptake of *L*-Histidine has been reported in several studies [191, 192]. In contrast, expression of PHT2 protein was not found on the cell surface, but on the lysosomal membrane, indicating its role in lysosomes function rather than nutrient uptake [193]. In addition to the peptide histidine transporter system, an amino acid transporter system might also mediate the uptake of *L*-Histidine in prostate cancer cells. The Eadie-Hofstee plot has already suggested that

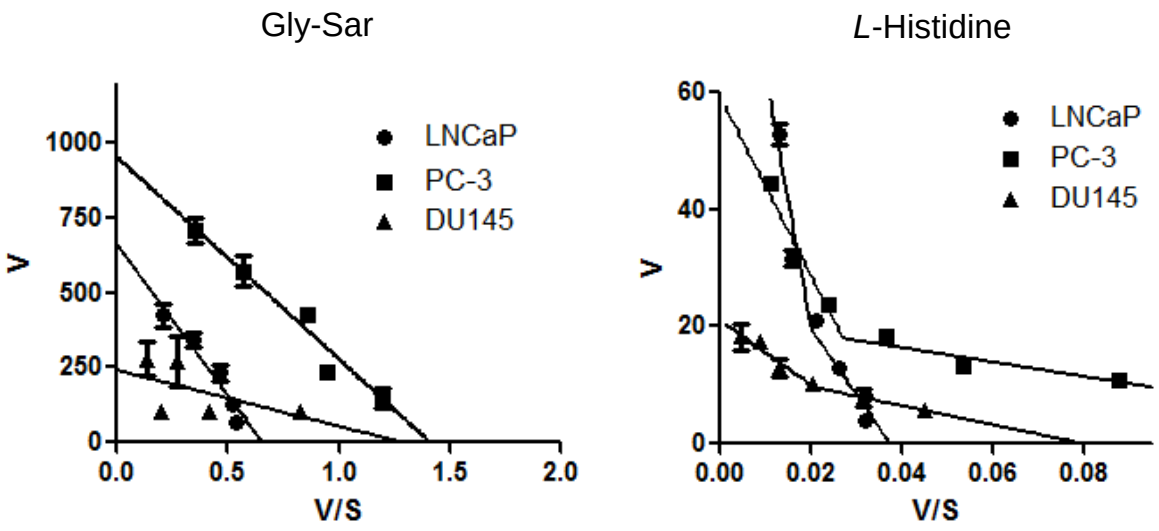

Figure 17. Eadie-Hofstee plots calculated from the active uptake data of [^{3}H]Gly-Sar and [^{3}H]*L*-Histidine in three prostate cancer cell lines. Eadie-Hofstee plot for [^{3}H]Gly-Sar uptake showed straight lines, which indicated a single transporter system. Curvilinear lines were observed in the Eadie-Hofstee plots of [^{3}H]*L*-Histidine uptake, therefore multiple transporter systems mediated the uptake.

multiple *L*-Histidine transporter systems exist in the three prostate cancer cell lines. For further verification, the competitive inhibition of *L*-Histidine uptake was conducted in the presence of various amino acids (competitive inhibitors of amino acid transporters). The uptake of *L*-Histidine can be significantly inhibited by a neutral amino acid *L*-Alanine (Ala), an acidic amino acid *L*-Aspartic acid (Asp), a basic amino acid *L*-Lysine (Lys) and a non-natural amino acid BCH. As shown in **Figure 18A**, *L*-Alanine showed the best inhibition in LNCaP cells, and BCH exhibited the best inhibitory effect in PC-3 and DU145 cells. Overall, *L*-Alanine demonstrated strong competitive inhibition in all three cell lines, with 42.8% in LNCaP, 45.6% in PC-3 and 49.2% in DU145 cells. This is likely because *L*-Alanine and *L*-Histidine possessed similar

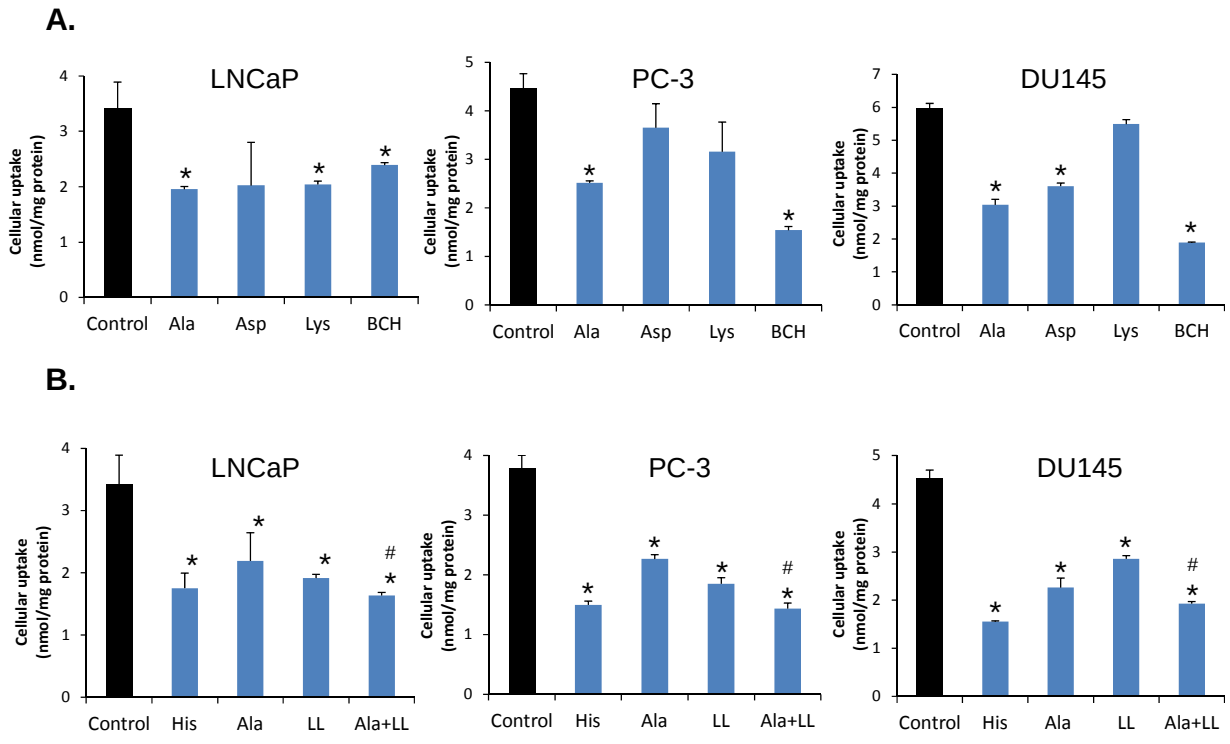

Figure 18. Amino acid transporters are involved in the uptake of [^{3}H]*L*-Histidine in three prostate cancer cell lines. (A) Uptake of [^{3}H]*L*-Histidine can be inhibited by various amino acids; (B) Uptake of [^{3}H]*L*-Histidine can be synergistically inhibited by Ala and LL, which separately represents an amino acid transporter inhibitor and a peptide histidine transporter inhibitor, respectively. (* $P < 0.05$ compared to control; # $P < 0.05$ compared to Ala and LL groups).

molecular geometry and charge, and both have been identified as the predominant substrates of many amino acid transporters, such as sodium-coupled neutral amino acid (system N/A) transporters (SNAT1, SNAT2 and SNAT3) [194]. Additionally, synergistic inhibition of *L*-Histidine uptake was observed when the amino acid transporter and the peptide histidine transporters were simultaneously inhibited by *L*-Alanine and Leu-Leu (Ala + LL in **Figure 18B**). The effect of the synergistic inhibition was significantly higher than those of separate inhibitions

and similar to that of *L*-Histidine (self-inhibition, which can also inhibit both transporter systems). In addition, different levels of synergistic effects were observed in the three prostate cancer cell lines. LNCaP and PC-3 cells exhibited a stronger synergistic effect than DU145 cells, possibly due to the high expression level of PHT1 in LNCaP and PC-3 cells (**Figure 14**).

Substrate specificity of Gly-Sar and *L*-Histidine uptake

The uptake specificity of the three prostate cancer cell lines was investigated by determining the inhibition of Gly-Sar and *L*-Histidine uptake in the presence of transporter inhibitors. As listed in **Table 7**, the uptake of Gly-Sar was dramatically inhibited by various dipeptides in LNCaP and PC-3 cells. Ser-Leu and Leu-Leu are two extremely potent inhibitors in these two cell lines and both can reduce the uptake of Gly-Sar to ~30% and ~60% in LNCaP and PC-3, respectively. Similar to a previous report, cellular uptake of [^{3}H]Gly-Sar (15 μM) in PC-3 cells was slightly inhibited (~15%) by excessive amount of unlabeled Gly-Sar [157]. The pseudopeptide drug Cefadroxil, a 31 β-lactam antibiotic, also inhibited the uptake of Gly-Sar to ~38% in LNCaP cells, but no significant effect was observed on PC-3 cells. This is most likely because Cefadroxil could be recognized and transported by PEPT2 with a much higher affinity than by PEPT1 [195]. Peptide transporters were specific to di/tri-peptides in our study. The tetrapeptide Gly-Gly-Gly-Gly had a minimal inhibitory effect on the uptake of Gly-Sar. The specificity of *L*-Histidine uptake was also studied using the same inhibitors. In addition to *L*-Histidine itself, Ser-Leu and Leu-Leu were the two most potent inhibitors. Both reduced the uptake to 30-50% of control in LNCaP and PC-3 cells, and to 84-86% in DU145 cells. The variation of the inhibitory potency was mainly due to the

Table 7. Substrate specificity of peptide transporters in LNCaP, PC-3 and DU145 cells.

Inhibitors	Conc. (mM)	% Gly-Sar uptake[a]			Conc. (mM)	% *L*-Histidine uptake[a]		
		LNCaP	PC-3	DU145		LNCaP	PC-3	DU145
Gly-Sar	1	46.3±3.3	84.9±7.6	89.3±6.7	10	92.4±6.2	100.1±1.3	99.2±6.9
L-Histidine	1	79.7±1.0	90.1±7.1	103.2±5.8	1	55.0±4.7	39.5±1.7	26.2±0.6
Cefadroxil	1	37.6±8.3	95.1±13.7	85.1±5.0	1	89.8±4.8	92.6±1.2	96.6±2.2
Ala-Ala	1	25.3±2.5	74.6±12.4	92.1±9.5	1	51.8±2.2	61.2±6.1	98.1±2.6
Val-Val	1	36.0±6.3	62.9±5.4	77.8±3.4	1	75.1±0.5	60.0±2.6	82.0±3.2
Ser-Leu	1	31.0±1.9	57.1±5.1	86.1±12.2	1	34.8±3.3	45.4±3.1	84.0±4.0
Leu-Leu	1	28.2±3.9	60.8±10.3	72.8±13.4	1	51.3±1.7	46.5±7.3	85.8±4.1
Gly-Gly	1	42.1±1.9	70.4±11.7	96.0±11.7	1	89.6±3.6	86.9±3.1	88.1±2.7
Gly-Gly-Gly	1	68.6±6.7	91.4±3.8	82.7±6.6	1	87.3±1.7	90.7±2.7	89.4±0.4
Gly-Gly-Gly-Gly	1	91.9±4.9	110.0±18.8	94.8±9.2	1	98.4±3.7	96.6±0.5	94.7±4.8

[a] The uptakes of [^{3}H}Gly-Sar (15μM) and [^{3}H]L-Histidine (100μM) were measured separately at 37^{o}C by incubating for 15 min in HBSS buffer (pH 7.4) at presence of each inhibitor. Each value represents % of control uptake and show as mean ± SD of three experiments.

difference of PHT1 expression levels in the three cell lines.

Visualization of peptide transport in prostate cancer cells by a fluorescent dipeptide probe

The fluorescent dipeptide *D*-Ala-Lys-AMCA is a widely used fluorescent probe to monitor the activity of peptide transporters [196, 197]. It has been proven to be a specific substrate of both PEPT1 and PEPT2 [184, 197]. This fluorescent dipeptide probe could be advantageously used to follow the uptake of the compound either by fluorescence microscopy or by fluorescence plate readers. As shown in **Figure 19**, the visible accumulation of the fluorescent dipeptide probe was observed in both LNCaP and PC-3 cells, but not in DU145 cells. Differences in the intensity of *D*-Ala-Lys-AMCA staining were consistent with the gene expression profiles of peptide transporters in LNCaP, PC-3 and DU145. The uptake of the fluorescent probe can be effectively blocked by the dipeptides Ser-Leu and Leu-Leu.

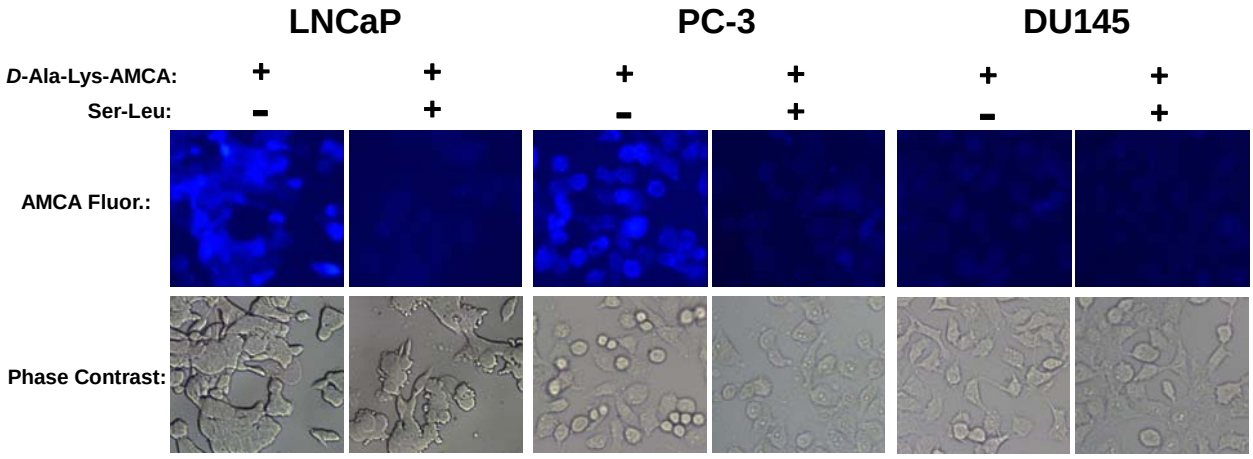

Figure 19. Visualization of peptide transport in prostate cancer cells by the fluorescent dipeptide probe *D*-Ala-Lys-AMCA. The fluorescent dipeptide probe was taken up by LNCaP/PC-3 cells, but not DU145 cells. With the competitive inhibitor Ser-Leu, fluorescence was reduced. Data represents typical results of two independent experiments with triplicate samples.

Inhibition of peptide transporters suppresses prostate cancer cell growth

To examine the role of peptide transporters in the growth of prostate cancer cells, serial concentrations of the non-degradable dipeptide Gly-Sar (0.1-100 mM) were incubated with prostate cancer cells, and IC_{50} was determined after 72 hours using the MTT assay. The inhibition of peptide transporters by Gly-Sar dramatically suppresses the growth of LNCaP and PC-3 cells, but not DU145 cells. Gly-Sar displays IC_{50} values of 9.5 mM in LNCaP cells and 13.9 mM in PC-3 cells (**Figure 20**). No significant inhibition occurred in DU145 cells at low concentrations (< 33 mM), but a minor inhibition was observed at high concentration (100 mM). BCH, a non-metabolizable inhibitor of system *L* amino acid transporters, was used as a positive control. Blockage of amino acid uptake resulted in a depletion of ATP, which causes a cytotoxic

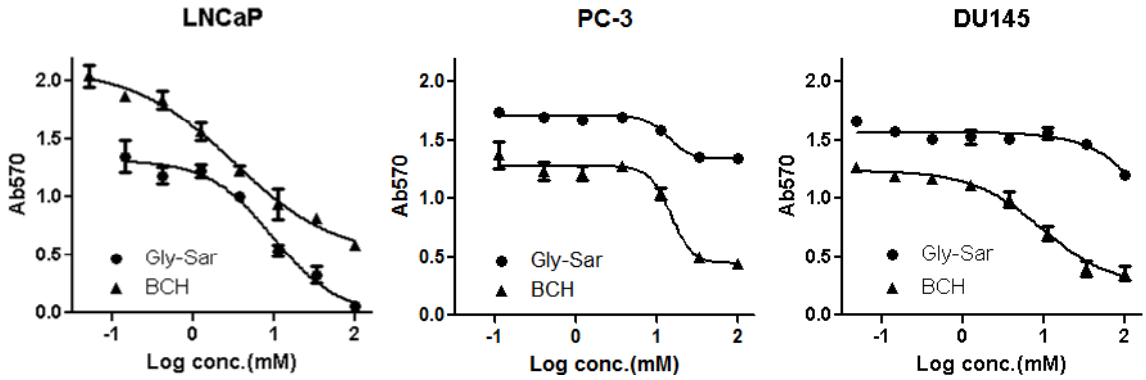

Figure 20. Comparison of growth inhibition of prostate cancer cells by Gly-Sar and BCH. By inhibiting peptide transporters, Gly-Sar suppressed the growth of LNCaP and PC-3 cells.

effect in all cell lines [198]. BCH displayed similar IC_{50} values (~10 mM) and anti-proliferation potency (up to 20-30% of the control) as all three prostate cancer cell lines (**Figure 20**). When prostate cancer cells were treated with Gly-Sar and BCH simultaneously, no combinational anti-proliferation effect was observed when compared to BCH alone (Data not shown). This may be because peptide transporters and amino acid transporters perform the same physiological function (nutrient uptake) in cell growth. Therefore, the anti-proliferation effect of Gly-Sar and BCH is not additive.

Knockdown of PEPT1/PEPT2 gene reduces the transporter activity

We finally investigated whether knockdown of PEPT1 and PEPT2 can affect dipeptide uptake in PC-3 and LNCaP cells (**Figure 21**). *Selencer*® Select siRNAs targeting PEPT1 and PEPT2 genes were used to knockdown PEPT1 and PEPT2 in the cells. As shown in Figure 8, treatment of the cells with these siRNAs knockdown ~74% of PEPT1 in PC-3 cells and ~66% of PEPT2 in LNCaP cells respectively.

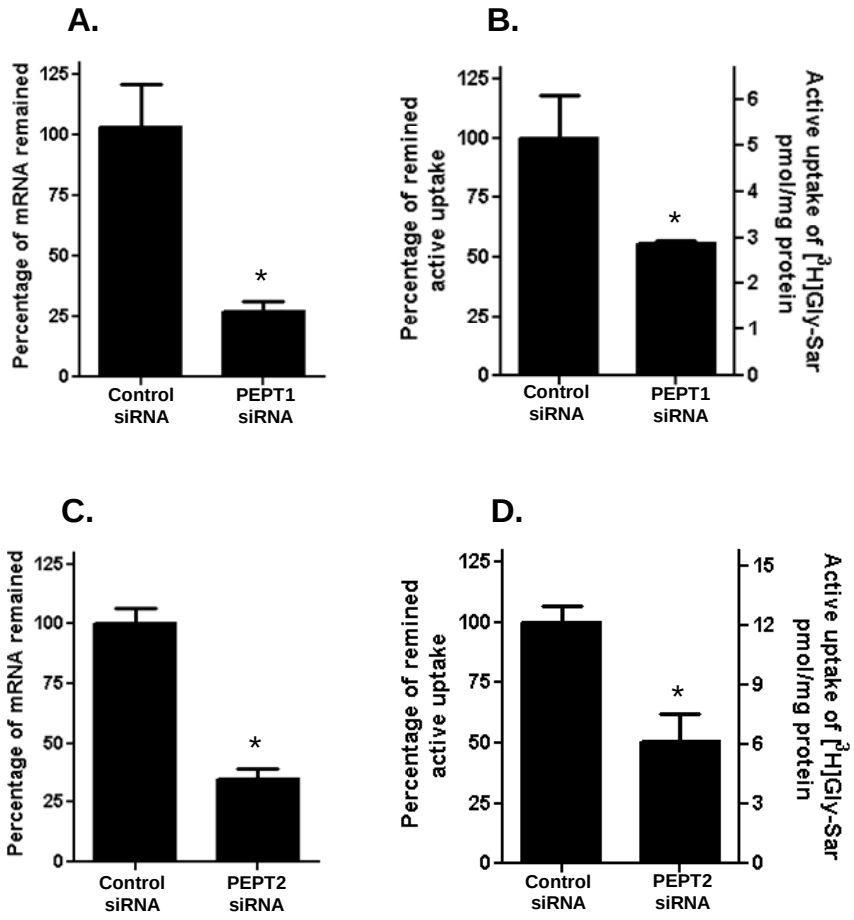

Figure 21. siRNA knockdown of PEPT1/PEPT2 genes and their effects on the active uptake of [^{3}H]Gly-Sar on the PC-3/LNCaP cells. (A). PEPT1 siRNA transfection down-regulates PEPT1 mRNA level in PC-3 cells. (B). PEPT1 knockdown by siRNA can significantly reduce the active uptake of ^{3}H]Gly-Sar on PC-3 cells. (C). PEPT2 mRNA expression was effectively silenced by PEPT2 siRNA mediated RNAi. (D). [^{3}H]Gly-Sar transport activity in LNCaP cells is dramatically decreased when PEPT2 gene is silenced by PEPT2 siRNA. The knockdown of PEPT1/PEPT2 genes was achieved by transfecting siRNA (at 50 nM final concentration) into cancer cells using Lipofectamine 2000. The relative expression of PEPT1 mRNA was determined by real-time RT-PCR 48 hours after transfection. [^{3}H]Gly-Sar uptake (15 µM, 3 µCi/ml) was measured at pH 7.4 with an incubation time of 30 min. The active uptake was obtained by subtracting passive uptake (in the presence of 100 mM unlabeled Gly-Sar) from total uptake. All experiments were conducted in triplicate, and data was expressed as means ± SD. (* $P < 0.05$ versus control siRNA group).

[^{3}H]Gly-Sar uptake (15 μM, 3 μCi/ml) was then measured at pH 7.4 in the PEPT1 and PEPT2 knockdown cells respectively. Active uptake was calculated by subtracting passive uptake from total uptake. After knockdown of the PEPT1 gene, the active uptake of [^{3}H]Gly-Sar in PC-3 cells was accordingly reduced by 47% compared with the control group (**Figure 21B**). The Gly-Sar transport activity in LNCaP cells was also reduced by 50% after the PEPT2 gene was silenced by the PEPT2 siRNA (**Figure 21D**). These results indicate that PEPT1 is the major transporter for Gly-Sar uptake in PC-3 cells and PEPT2 plays the dominant role in LNCaP cells. Our study also suggests that PC-3 can be established as a cell culture model for PEPT1 study and LNCaP as a model for PEPT2 study.

4.4. Discussion

Peptide transporters can transport di- or tri-peptides, peptidomimetic drugs and peptide prodrugs into the cytoplasm of cells. They have been extensively characterized and studied since their discovery two decades ago [165-167]. Although peptide transporters are expressed predominantly in the intestinal and renal epithelial cells, functional expression of peptide transporters is also identified in other normal tissues, such as glia cells, macrophages, and the epithelia of the bile duct, the lungs, and the mammary glands [168]. However, little information is available regarding their presence and role in carcinomas. In this study, we have examined the expression profile and functional activity of peptide transporters in LNCaP, PC-3 and DU145 cells. Although these three cell lines exhibited different expression profiles of peptide transporters, transport activity was observed on the plasma membrane of all three cell lines. The uptakes of Gly-Sar and *L*-Histidine proceeded in a time- and pH-dependent manner (**Figure 15**).

The uptake rates were concentration-dependent, and Michaelis-Menten fitting of the active uptake data gave hyperbolic curves which indicated the saturability of the peptide transporters. Further studies revealed that the uptake of Gly-Sar in LNCaP and PC-3 is mediated by a single transporter system, but multiple transporter systems were involved in *L*-Histidine uptake (**Figure 17** & **18**). In addition, the competitive inhibition study proven that the peptide transporters in the prostate cancer cells exhibited broad substrate specificity with a preference for hydrophobic dipeptides such as Leu-Leu. These results strongly indicate that prostate cancer cells express functionally active peptide transporters on the cytoplasmic membrane.

Because of the pharmaceutical interest and pharmacokinetic importance, peptide transporters have been commonly used for the *in vitro* evaluation of prodrugs [199]. In *in vitro* cell culture model systems, Caco-2 cells and SKPT cells have been widely used for studying PEPT1 and PEPT2 mediated transport [200]. However, Caco-2 needs to grow for 21 days to differentiate into PEPT1 positive cells before they can be used in transport assays [187]. The long differentiation time (~21 Days) dramatically limits the use of Caco-2 cell culture model. SKPT cells are currently the standard cell culture model for PEPT2 studies [195]. As a rat renal cell line, SKPT expresses rat PEPT2, which only shares 83% amino acid identity with human PEPT2 [201]. Our study indicates that PC-3 can be established as a new cell culture model for PEPT1 study and LNCaP as a model for PEPT2 study. As common carcinoma cell lines, PC-3 and LNCaP can be easily obtained and maintained. Moreover, the protein expression of PEPT1 and PEPT2 are continuous, and the cell culture models are ready to use after overnight culture. Lastly, LNCaP cells express natural human PEPT2, which makes it a better model than SKPT cells for PEPT2 study.

In addition to distinguishing PC-3 and LNCaP cells as *in vitro* models for peptide transporter study, the most important impact of our research is revealing the promising potential of peptide transporters in tumor-specific drug delivery. Because of the high expression in intestinal epithelial cells, peptide transporters have been widely utilized to enhance oral absorption of polar drugs by a prodrug approach. However, peptide transporters have not been considered as a specific target for tumor-specific drug delivery. The high expression of peptide transporters on prostate cancer cells provides a new approach for selectively targeting low-molecule anti-cancer drugs to cancer cells through the peptide transporters. Unlike ligand-mediated targeting, low molecular-weight anti-cancer dipeptide prodrugs can function as substrates of peptide transporters to enter into the cytoplasm of prostate cancer cells [202]. Peptide transporters provide a putative uptake pathway to selectively accumulate anti-cancer prodrugs in prostate cancer cells. However, the abundant expression of peptide transporters in the intestine, kidney and other normal tissues might limit their use as a target for drug delivery. Intravenous injection can circumvent some unwanted uptake by epithelial cells in the small intestine, but anti-cancer dipeptide prodrugs may still be taken up by renal and other non-cancer cells [202]. Therefore, it is essential to site-specifically deliver the dipeptide prodrug into the tumor where it could be taken up by cancer cells via peptide transporters. Dipeptide prodrugs would first be specifically delivered into prostate tumors by active targeting or passive targeting via the enhanced permeability and retention (EPR) effect. After accumulation in the interstitial space of the tumor, the dipeptide prodrug would be actively taken up by cancer cells via peptide transporters [177]. Further studies will be needed to evaluate the therapeutic effect of this system *in vivo*.

It is interesting that inhibition of peptide transporters by Gly-Sar suppresses prostate tumor cell growth to some extent (**Figure 20**). The anti-proliferation activity of Gly-Sar is possibly achieved by blocking the supply of nutrients mediated by the peptide transporters. However, it may be difficult to utilize peptide transporters as drug targets for cancer therapy. First, targeting peptide transporters may induce side effects in other tissues because of the wide distribution and important physiological roles of peptide transporters in the intestine and kidney. It has been reported that animals exhibited a remarkable phenotype of malnutrition when PEPT2 was knocked out. The long-term malnutrition in PEPT2-deficient animals also leads to retarded development and small brood size compared to wild-type animals [203]. Second, the anti-tumor effect of Gly-Sar is weak (IC_{50} ~ 10 mM). Another concern is that tumor cells might rely on multiple routes, such as peptide transporter, amino acid transporters, albumin transporters and passive diffusion to absorb nutrients [204, 205]. Simply blocking the peptide transporters may not be efficient enough to suppress tumor cell growth.

4.5. Conclusion

In summary, we have demonstrated that peptide transporters exist in three common prostate cancer cells using qRT-PCR and Western blot. A cellular uptake study of Gly-Sar and *L*-Histidine demonstrated that peptide transporters are functional on the membrane surface of prostate cancer cells. The transport activity observed was also consistent with the expression profiles of peptide transporters. Furthermore, the transportation events were monitored in three prostate cancer cell lines using the fluorescent dipeptide probe *D*-Ala-Lys-AMCA. Inhibition of peptide transporter activity suppresses prostate cancer cell growth, which is consistent with

observations from another PEPT1 overexpressing cancer cell line AsPC-1 [174]. The selective expression of PEPT1 in PC-3 and PEPT2 in LNCaP indicate that these cell lines can be used as new *in vitro* cell culture models for PEPT1 and PEPT2 studies. The discovery of their over-expression in prostate cancer also validates the potential of these peptide transporters for tumor-targeted drug delivery.

CHAPTER 5

DESIGN AND SYNTHESIS OF A RAPAMYCIN CONJUGATE USING A NOVEL POLY(ETHYLENE GLYCOL) MULTIBLOCK COPOLYMER

5.1. Introduction

Rapamycin, also known as sirolimus, is a carboxylic macrolide compound that was originally discovered as a product of a bacteria from soil sample of island Rapa Nui in the south pacific [206]. It was first developed as antifungal drug by Ayerst Research Laboratories, but the potent immunosuppressive and anti-proliferative effects were discovered later [207]. Rapamycin has already been approved as an immunosuppressive agent by the US Food and Drug Administration (FDA) in 1999. Due to its unique cytostatic effect, rapamycin also entered into clinical trials to treat various cancers, including breast cancer, prostate cancer and glioblastoma [208-210]. The molecular mechanism of rapamycin is to inhibit mammalian target of rapamycin (mTOR) signaling pathway by directly binding to FK-binding protein 12 (FKBP12) and mTOR1. Because of the importance of the mTOR signal pathway in cancer development, rapamcyin was found to be active against almost all types of solid tumors [207]. Rapamycin exhibits an exquisite selectivity to mTOR and demonstrates potent anti-tumor activity in the nanomolar range *in vitro*. Besides inhibiting tumor growth, rapamycin can also induce tumor endothelial cell death and vessel thrombosis by acting as a vascular AKT/mTOR inhibitor [211, 212].

Although rapamycin has broad and potent anti-tumor activity, it is insoluble in water and possesses poor distribution *in vivo,* which dramatically limits its pharmacokinetics [213-215]. Structurally rapamycin does not contain any acidic or basic group that can increase aqueous solubility by salt formation [213, 216]. Rapamycin is very hydrophobic and the solubility in

water is only about 33 μg/mL (2.6 μg/mL in some reports) [217]. Moreover, because rapamycin is only slightly soluble in many cosolvents such as ethanol, PEG 400 and polysorbate 80, it is difficult to prepare injectable rapamycin formulations for preclinical/clinical studies [213]. Rapamycin also exhibits a poor distribution profile *in vivo*. Due to the ubiquitous presence of the FK-binding proteins (high affinity to rapamycin) in red blood cells (RBCs), rapamycin in the blood exhibits a preferential distribtion in RBCs. As reported by Yatscoff et al., 95% of rapamycin in the blood is distributed in RBCs compared to 3.1% in the plasma, 1.0% in lymphocytes and 1.0% in granulocytes [214]. Because RBCs can protect rapamycin from hepatic metabolism and renal filtration, rapamycin exhibits a relative long terminal half-life (61-72 hr in humans) compared to other small molecules [218]. Although the distribution in RBCs increases its stability, low partition in the plasma dramatically hinders the diffusion of rapamycin from the blood into tumor cells. In addition, it was reported that rapamycin was extensively distributed among many tissues in rats (tissue to blood partition coefficient Kp > 40 in some cases) because of its lipophilicity nature [219]. The extensive distribution of rapamcyin in tissues is believed to account for its high apparent distribution volume (5.6-17.6 L/kg) and toxic effects [220, 221].

To overcome these limitations, rapamycin has been chemically modified into hydrophilic analogues, such as CCI-779, RAD001 and AP23573 [222]. CCI-779, also known as Temsirolimus (Torisel, Wyeth), is an ester prodrug of rapamycin for treatment of renal cell carcinoma. The introduction of 2,2-bis(hydroxylmethyl) propionic ester at the 42-OH of rapamycin, CCI-779 increases hydrophilicity and makes the analogue readily soluble for intravenous formulation [223]. RAD001, also known as Everolimus (Afinitor,Novartis), is a hydroxyl-ethyl ether of rapamycin with improved aqueous solubility and oral absorption [224].

AP23573 (Deforolimus, Merck/Ariad) is a novel non-prodrug rapamycin analogue in which 42-OH is conjugated with a phosphate group to increase aqueous solubility and oral bioavailability [225]. Even chemically modified, rapamycin analogues (rapalogues), however, have limited aqueous solubility (CCI-779: 0.12mg/mL; RAD001: 0.1mg/mL; AP23573: < 1 mg/mL) [220]. Cosolvent such as ethanol is always required for intravenous formulations [226]. Moreover, it was reported that rapalogue CCI-779 could be quickly hydrolyzed by plasma esterase to rapamycin, which would redistribute into RBCs. Although other two rapalogues, RAD001 and AP23573, cannot be converted into rapamycin *in vivo*, moderate binding to RBCs was still observed in animal studies in rats [227]. Therefore, it is necessary to explore other rapamycin conjugates to improve aqueous solubility and tissue distribution profile, especially to minimize the distribution to RBCs.

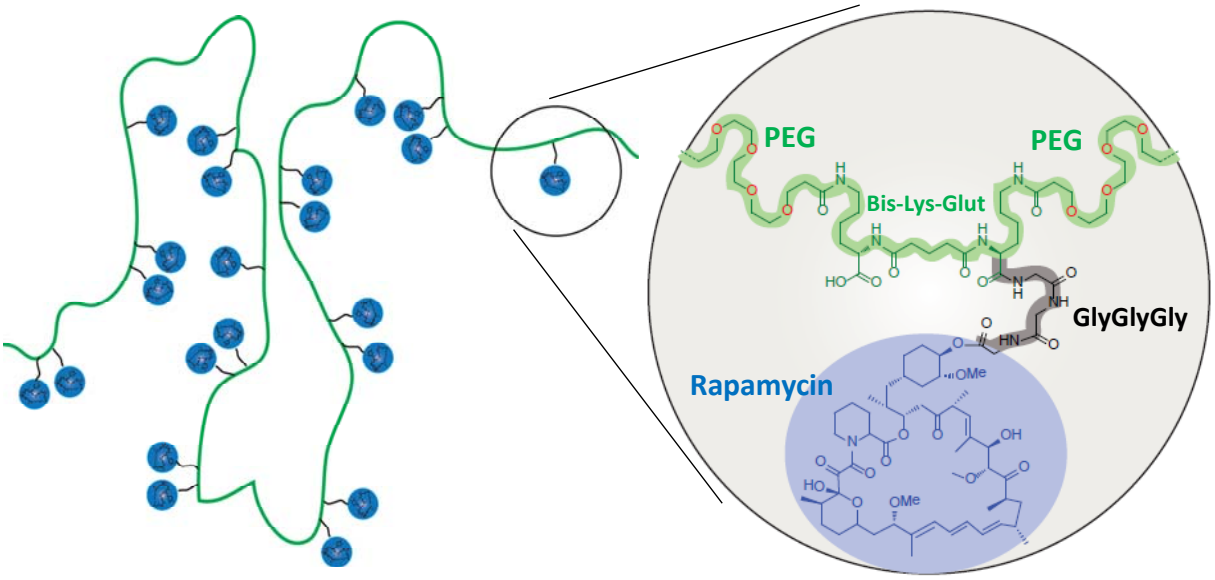

Figure 22. Schematic graph of polymer rapamycin conjugate.

Compared to modification of rapamycin's chemical structure, direct conjugation of rapamycin to polymer may offer a better approach to overcome its limitations. Many hydrophobic drugs, such as paclitaxel and camptothecin, have demonstrated excellent aqueous solubility and pharamcokinetics after being conjugated to hydrophilic polymers [104, 105, 228, 229]. However, rapamycin is sensitive to light, temperature and pH, which make it hard to tolerate many chemical reactions. Although rapamycin has been reported to successfully conjugate with wortmanin and other small molecules under mild reaction conditions, little attempt has been made to conjugate it with macromolecules, such as polymers and antibodies [159, 230, 231]. In this paper, we designed and synthesized a novel, water-soluble, poly(ethylene glycol) (PEG) based multiblock copolymer. To conjugate rapamycin with the polymer, a tri-peptide linker GlyGlyGly was first conjugated with rapamycin at 42-OH and then grafted onto the pendant carboxylic groups in polymer chains. The polymer rapamycin conjugate exhibits an excellent solubility in water and potent anti-tumor activity, suggesting its promising potential for clinical development.

5.2. Materials and Methods

Materials

All reagents listed below were obtained from commercial sources and used without further purification. Rapamycin was purchased from LC laboratories (Woburn, MA). NHS-PEG_{3400}-NHS was purchased from Nanocs Inc. (New York, NJ). 2-(7-Aza-1H-benzotriazole-1-yl)-1,1,3,3-tetramethyluronium hexafluorophosphate (HATU) and N-Hydroxybenzotriazole (HOBT) were ordered from Genscript Inc. (Piscataway, NJ). Thiazolyl Blue was obtained from

RPI Corp. (Prospect, IL). Fmoc-Lys(Boc)-OH and Trt-Gly-OH were purchased from Chem-Impex International Inc. (Wood Dale, IL). TO-PRO-3 stain was obtained from Life Technologies (Grand Island, NY). All solvents, including anhydrous solvents, HPLC grade solvents and other common organic solvents were purchased from commercial suppliers and used without further purification.

Cell Culture

All the cell lines used in this study were obtained from ATCC. LNCaP, PC-3, MCF-7, MCF-7/HER2 and SK-BR-3 cells were grown in RPMI-1640 medium containing 10% Fetal Bovine Serum (FBS), 100 units/mL penicillin, and 100 μg/mL streptomycin. HeLa and DU145 cells were cultured in DMEM medium supplemented with 10% FBS and 100 units/mL penicillin-100 μg/mL streptomycin mixtures. All the cells were grown at 37 ^{o}C in a humidified atmosphere with 5% CO_2. Media were changed every other day, and the cells were passaged when they reached 80~90 % confluency.

Bis-(ε-amino-*L*-Lysine Benzyl ester) Glutaric amide (Bis-Lys(OBn)-Glut), 5

The synthesis of comomomer Bis-Lys(OBn)-Glut **5** started from Fmoc-Lys(Boc)-OH. Fmoc-Lys(Boc)-OH was first esterified with benzyl alcohol, followed by removing Fmoc group by 20% piperidine-DCM according to Agnihotri's report [232]. One gram of NH_2-Lys(Boc)-OBn **3** was dissolved in 50 mL of dry DCM, and then Glutaric acid (0.16 g) and EDCI (0.57 g) were added to the solution. The coupling reaction was initialized by adding 0.52 mL of triethylamine (Et_3N) to the solution. After stiring overnight at room temperature, the reaction

was stopped with 50 mL of saturated NH_4Cl aqueous solution. The organic layer was separated, dried with Na_2SO_4, and concentrated under vacuum. The compound **4** was purified from the pale white residue by silica gel chromatography ($CHCl_3$/MeOH=50/1, v/v). To deprotect the Boc groups, compound **4** (0.5 g) was dissolved in 30 mL of TFA/DCM (v/v, 1/1) and stirred at room temperature for 1 hour. The solvent was evaporated under vacuum, and ice-cold diethyl ether was added to precipitate the product. The white precipitate was collected by filtration and dried under vacuum to get the pure product **5** (~ 60%). ^{1}H NMR (400 MHz, D_2O) δ 7.27 (s, 5H), 5.05 (m, 2H), 4.25 (t, 1H), 2.79 (t, 2H), 1.95 (m, 2H), 1.65 (m, 3H), 1.53 (m, 2H), 1.26 (m, 2H). ESI-MS calcd. for $C_{31}H_{44}N_4O_6$ 568.7; found 569.3 $(M + H)^{1+}$.

Synthesis of Poly(Bis-Lys(OBn)-Glut-PEG$_{3400}$), 6a-d.

Before the reaction, Bis-Lys(OBn)-Glut **5** was dried in a vacuum desiccator for two days. Bis-Lys(OBn)-Glut **5** (19 mg) and NHS-PEG_{3400}-NHS (100 mg) were transferred to a dry 5-mL flask, followed by adding 0.5 mL of extra dry DMF (water < 50 ppm). The suspension was stirred at room temperature for 10 min, and then anhydrous Et_3N was added into the reaction in nitrogen atmosphere. After stirring at room temperature or 50^{o}C for 2-24 hours, the mixture was diluted with 50 mL of water and dialyzed against distilled water using a dialysis tube with MWCO of 14,000. The polymer solution was lyophilized, and pure polymer **6a-d** was collected as white powder (60-80%). As for **6b**, Mw = 31.5 kDa, Mn = 21.9 kDa, Mw/Mn = 1.43. ^{1}H NMR (400 MHz, D_2O) δ 7.30 (s, 5H), 5.08 (m, 2H), 4.26 (t, 1H), 4.07 (m, 2H), 3.61 (m, PEG-CH_2), 3.43 (m, 2H), 2.95 (m, 2H), 2.16 (m, 2H), 2.15-2.18 (m, 5H), 1.35 (m, 2H).

Synthesis of Linker-Drug, Gly-Rapa and GlyGlyGly-Rapa.

*31-O-TMS Rapamycin **10***. 31-Trimethylsilyl Rapamycin was synthesized according to the procedure described by Shaw and Nan [233, 234]. Briefly, Rapamycin (200 mg) and imidazole (150 mg) were dissolved in 25 mL of DCM. After cooling to 0^{o}C, trimethylsilyl chloride (TMSCl) solution in DCM (1M, 1.3 mL) was added into the reaction, slowly. The reaction was stirred for around 10 minutes at 0^{o}C. After the reaction was complete, the mixture was directly applied on silica gel column and eluted with petroleum ether/acetone (v/v, 5/1). The purified intermediate 31,42-bis-O-TMS Rapamycin **9** (210 mg) was then dissolved in 20 mL of DCM, followed by adding 100 mg of imidazole/imidazole·HCl (mole ratio, 1/1). After stirring at room temperature for 3 hours, the reaction was stopped with 50 mL of water. The organic phase was separated, washed and concentrated. 31-O-TMS Rapamycin **10** was purified from the residue by flash chromatography on silica gel (petroleum ether/acetone, v/v = 5/1). The overall yield for the two-step reaction is ~ 60%. ^{1}H NMR (400 MHz, $CDCl_3$) δ 6.41 (m, 2H), 6.17 (q, 1H), 6.05 (d, 1H), 5.59 (q, 1H), 5.33 (d, 1H), 5.22 (d, 1H), 5.05 (q, 1H), 4.73 (s, 1H), 4.07 (d, 1H), 3.85 (m, 2H), 3.72 (m, 1H), 3.66 (d, 1H), 3.41 (s, 3H), 3.38 (m, 3H), 3.27 (s, 3H), 3.14 (s, 3H), 2.93 (m, 1H), 2.68 (m, 3H), 2.31 (m, 2H), 2.11 (m, 1H), 1.98 (m, 3H), 0.60-1.80 (m, 41H), 0.04 (s, 9H). ESI-MS calcd. for $C_{54}H_{87}NO_{13}Si$ 986.4; found 1008.7 $[M + Na]^{+}$.

*Trt-Gly-Rapa **12***. 31-O-TMS Rapamycin **10** (100 mg) and Trt-Gly-OH (64 mg) were dissolved in 5 mL of DCM. After stirring at room temperature for 5 minutes, EDCI (40 mg) and DMAP (2 mg) were added to the reaction. The reaction mixture was continuously stirred for 2 hours at room temperature. Trt-Gly-Rapa(31-O-TMS) **11** was purified from the reaction using silica gel chromatography (petroleum ether/acetone, v/v = 5/1). The TMS group at the 31 site of **11** was

selectively removed using inorganic acid. Briefly, compound **11** was dissolved in 4 mL of ice-cold THF, followed by adding 2 mL of 2N H_2SO_4 solution. The reaction was warmed to room temperature and stirred for 30 minutes. After the reaction was complete, the mixture was poured into 20 g of ice and neutralized by adding excess amount of $NaHCO_3$. The neutralized solution was extracted with AcOEt. The organic phase was washed with brine, dried and concentrated. The residue was applied on a silica gel column and purified using petroleum ether/acetone (v/v = 3/1) as the elution solution (yield, ~ 90%). H NMR (400 MHz, $CDCl_3$) δ 7.46 (d, 6H), 7.28 (m, 6H), 7.26 (t, 3H), 6.36 (m, 2H), 6.13 (q, 1H), 5.95 (d, 1H), 5.55(q, 1H), 5.42 (d, 1H), 5.29 (d, 1H), 5.15(q, 1H), 4.79 (s, 1H), 4.61 (m, 1H), 4.17 (d, 1H), 3.87 (m, 1H), 3.75 (d, 1H), 3.66 (m, 1H), 3.55 (d, 1H), 3.38 (m, 1H), 3.33 (s, 3H), 3.30 (s, 3H), 3.27 (m, 1H), 3.14 (s, 3H), 3.08 (m, 1H), 2.69 (m, 2H), 2.58 (m, 1H), 2.32 (m, 2H), 2.17 (s, 2H), 2.05 (m, 1H), 1.93 (m, 3H), 0.75-1.80 (m, 41H). ESI-MS calcd. for $C_{71}H_{98}N_2O_{13}$ 1213.5; found 1213.7 $[M + H]^+$.

*Gly-Rapa **13***. Protecting group Trt was removed using 0.1 M HOBT in trifluoroethanol (TFE) as reported [235]. Briefly, compound 12 (50 mg) was dissolved in 3 mL of freshly prepared 0.1M anhydrous HOBT in TFE. The reaction was stirred at room temperature for 10 minutes. The process of the reaction was monitored by TLC. After the Trt group was completely removed, 100 mL of water was added to stop the reaction. The white suspension was then extracted with 100 mL of AcOEt. The organic phase was washed with brine, dried by Na_2SO_4 and concentrated under vacuum. Gly-Rapa **13** was purified from the residue using silica gel chromatography ($CHCl_3$/MeOH , v/v = 10/1) and yielded as white powder (~70%). H NMR (400 MHz, $CDCl_3$) δ 6.36 (m, 2H), 6.14 (q, 1H), 5.95 (d, 1H), 5.56(q, 1H), 5.43 (d, 1H), 5.28 (d, 1H), 5.16(q, 1H), 4.97 (s, 1H), 4.73 (m, 1H), 4.18 (d, 1H), 3.86 (m, 1H), 3.75 (d, 1H), 3.66 (m, 1H), 3.55 (d, 1H),

3.43 (m, 2H), 3.37 (s, 3H), 3.33 (s, 3H), 3.14 (s, 3H), 2.81 (m, 1H), 2.69 (m, 2H), 2.59 (m, 1H), 2.32 (m, 2H), 2.12 (s, 1H), 2.04 (m, 2H), 1.99 (m, 3H), 0.75-1.80 (m, 45H). ESI-MS calcd. for $C_{53}H_{82}N_2O_{14}$ 971.2 ; found 971.9 $[M + H]^+$.

*GlyGlyGly-Rapa **15***. Compound **13** (20 mg) and Trt-GlyGly-OH (20 mg) were dissolved in 10 mL of dry DCM. After stirring at room temperature for 5 minutes, EDCI (10 mg) and Et_3N (8 μL) were added to the mixture. After two hours, the reaction was stopped by adding 10 mL of saturated NH_4Cl aqueous solution. The organic phase was then separated, washed with brine, dried by Na_2SO_4 and concentrated under vacuum. The intermediate Trt-GlyGlyGly-Rapa **14** was purified on silica gel column ($CHCl_3$/MeOH, v/v = 50/2.5). The Trt group of **14** was deprotected using the same method as described above. The final product GlyGlyGly-Rapa **15** was purified by silica gel chromatography ($CHCl_3$/MeOH, v/v = 5/1, then 2/1,). The yield for the two steps was 50~ 60%. ^1H NMR (400 MHz, $CDCl_3$) δ 6.35 (m, 2H), 6.13 (q, 1H), 6.00 (d, 1H), 5.51(q, 1H), 5.41 (d, 1H), 5.27 (d, 1H), 5.14(q, 1H), 4.66 (m, 2H), 4.23 (d, 1H), 4.01 (m, 4H), 3.89 (m, 2H), 3.65 (m, 2H), 3.57 (d, 1H), 3.31-3.35 (m, 4H), 3.14 (s, 3H), 2.96 (s, 3H), 2.89 (s, 3H), 2.62 (m, 1H), 2.31 (m, 2H), 0.75-2.00 (m, 53H). ESI-MS calcd. for $C_{57}H_{88}N_4O_{16}$ 1085.3; found 1085.8 $[M + H]^+$.

Synthesis of polymer rapamycin conjugate

*Synthesis of Poly(Bis-Lys-Glut-PEG$_{3400}$) **7**.* Polymer **7** was synthesized by removing the benzyl groups from carboxylic acids of polymer **6** via hydrogenation. Briefly, polymer **6** (150 mg) was dissolved in 50 mL of methanol in nitrogen atmosphere. Twenty milligrams of Pd/C (palladium loading 10%) was transferred into the reaction flask under nitrogen atmosphere. After all the

Pd/C was merged into methanol, nitrogen was changed into hydrogen, and the reaction was stirred at room temperature overnight. The reaction mixture was then filtered to remove Pd/C. The filtrate was concentrated and dried under vacuum overnight to get polymer **7** in quantitative yield. ^{1}H NMR (400 MHz, D_2O) δ 4.20 (m, 1H), 4.10 (m, 2H), 3.61 (m, PEG-CH_2), 3.43 (m, 2H), 3.01 (t, 2H), 2.21 (t, 2H), 1.82 (m, 1H), 1.69 (m, 1H), 1.55 (m, 2H), 1.41 9m, 2H), 1.25 (m, 2H).

*Synthesis of Polymer rapamycin conjugate **8a-c***. Conjugate **8a-c** was synthesized by coupling linker-drugs (rapamycin, Gly-Rapa and GlyGlyGly-Rapa) with polymer **7** using EDCI/Et_3N/NHS. Briefly, polymer **7** (5 mg, 0.0015 mmol of repeat unit) and linker-drug (0.006 mmol) were dissolved in 0.5 mL of dry DMF. EDCI (10 mg), DMAP (2 mg) and NHS (1 mg) were added into the reaction and stirred for 24 hours. The polymer was then precipitated with diethyl ether (20 mL). After centrifugation, ether was poured out and the precipitate was dissolved in 5 mL of water. The insoluble solid was removed by filtering through 0.2 μm filters. The solution was dialyzed against distilled water by 14 kDa MWCO membrane at room temperature for 48 hours. Dialysis water was changed every 8 hours. The solution was free-dried to yield as a white solid (yield, 41-88%).

*Synthesis of Polymer rapamycin conjugate **8d***. Conjugate 8d was synthesized using the same method as described above but the coupling reagent was changed to HATU/DIPEA. Briefly, polymer **7** (5 mg) and GlyGlyGly-Rapa **15** (6 mg) were added into 0.5 mL of dry DMF, followed by HATU (20 mg) and DIPEA (16 μL). The reaction was continuously stirred at room temperature for 24 hours. Twenty milliliter of diethyl ether was poured into the reaction to precipitate the product. The precipitate was collected by centrifugation (4,000 g, 5 min) and re-

dissolved in 5 mL of water. After dialysis and free drying, the pure conjugate **8d** yielded as a light brown powder (yield ~ 50%).

Determination of the percentage of rapamycin conjugated to polymer (wt%)

The percentage of rapamycin conjugated to polymers (wt%) was determined by Ultraviolet-Visible (UV) spectrophotometry. The standard curve was generated with a series of rapamycin solution in water (λ_{max} = 280 nm). Polymer-drug conjugates were diluted in water and UV absorbance at 280 nm was measured. Rapamycin concentration was calculated from the standard curve. The total amount of rapamycin was calculated by the following equation: weight = concentration × volume × molecular weight. The percentage of rapamycin conjugated to polymer (wt%) was calculated by dividing the amount of rapamycin by total weight of polymer-drug conjugates.

Rapamycin release from the polymer conjugates

Aliquots of GlyGlyGly-Rapa and polymer rapamycin conjugate **8c** stock solution (10 mM in DMSO) were diluted to 200 μM in water. The solutions were immediately mixed with 100% human/rat/mouse sera, which gave a final concentration of 100 μM rapamycin in 50% sera. Forty microliters of the solution were divided into 0.2 mL Eppendorf tubes and incubated at 37 ^{o}C. At selected time intervals, serum proteins were precipitated with 120 μL of acetonitrile plus 0.1% TFA. After centrifuging at 12,000 g for 10 mins, 100 μL of the supernatant was collected and analyzed with HPLC for quantification of the released rapamycin. The HPLC system was equipped with a Shimadzu LC-20AT pump, a SIL-10AF autosampler and a SPD-10A UV

detector. The separation was achieved on a Waters C18 column (250 mm × 4.6 mm, 5 μm) at a flow rate of 1.0 mL/min. The mobile phases were consisted of phase A (water, 0.1% formic acid) and B (acetonitrile, 0.1% formic acid), and a gradient of 50% B to 90% B in 20 min. The absorbance of rapamcyin was monitored at 280 nm.

In vitro cytotoxicity

In vitro cytotoxcity of rapamycin, polymer and polymer-drug conjugates was determined according to the method we reported before [177]. Briefly, cells were seeded into 96-well plates at a density of 5,000 cells / well. Twenty-four hours after incubation, a series of drug dilutions ranging from 0.001-1000 nM were added to the wells and cultured for another 72 hours. The relative cell numbers were measured using a MTT assay. To enhance the assay sensitivity, twenty-five microliters of Sorensen's glycine buffer (0.1M glycine, 0.1M NaCl, adjust pH to 10.5 with 0.1N NaOH) was added into wells according to Plumb J. A.'s report [236]. The absorbance was measured using a DTX 880 Multimode Detector (Beckman Coulter,Inc., Fullerton, CA) at the wavelength of 570 nm. IC_{50} was calculated by fitting a concentration – absorbance curve using Graphpad Prism 5 (Graphpad software Inc, La Jolla, CA).

Cellular uptake analysis by confocal laser scanning microscopy

Cellular uptake of FITC-labeled polymer was performed and analyzed by confocal laser scanning microscopy according to the methods reported [237]. Briefly, PC-3 cells were seeded into 8-well Lab-Tek^{TM} chamber slides (Nunc Inc. Rochester, NY) and cultured for 24 hours. The culture medium was discarded, and monolayers were washed once with RPMI-1640 medium.

Polymer-FITC was diluted to 10 μM in RPMI-1640 and added into the chambers. After incubation for 24 hours, the cells were washed six times with DPBS and fixed in 4% buffered formalin at room temperature for 10 min. The cells were washed three times to remove remaining formalin, and the nucleus was stained with TO-PRO-3 (Excitation/Emission: 642/661 nm) according to manufacturer's protocol (Invitrogen, Grand Island, NY). After washing, cell monolayers were mounted onto glass microscope slides using fluorescence mounting medium (Vector Lab, Burlingame, CA). The cellular uptake and distribution was analyzed using Nikon C1 laser scanning confocal microscope (Nikon Instrument Inc., Melville, NY).

Aqueous solubility assay

The aqueous solubilities of rapamycin and its conjugates were assayed by the thermodynamic method as reported before [177]. Briefly, excess amount of rapamycin or its conjugates were suspended in 100 μL of distilled water. The suspension was shaken at room temperature for 24 hours. The suspension was then centrifuged at 12,000 g for 15 min to remove undissolved drug. The supernatant was collected, and the concentration was quantified by UV spectrometry at 280 nm.

Statistical Analysis

Data were expressed as the mean ± standard deviation (SD). Difference between any two groups was determined by ANOVA. $P<0.05$ was considered statistically significant.

5.3. Results

Synthesis of multiblock copolymers Poly(Bis-Lys(OBn)-Glut-PEG$_{3400}$), 6a-e, and Poly(Bis-Lys-Glut-PEG$_{3400}$), 7

The multiblock copolymer Poly(Bis-Lys(OBn)-Glut-PEG$_{3400}$) was synthesized by condensation of monomer NHS-PEG$_{3400}$-NHS with comonomer Bis-Lys(OBn)-Glut **5** in the presence of organic base. Bis-Lys(OBn)-Glut is composed of two *L*-lysine linked at α-amino groups via glutaric acid. The ε-amino group of *L*-Lysine was less sterically hindered and more nucleophilic than α-amino group, therefore making it more reactive to monomer NHS-PEG$_{3400}$-NHS. Comonomer Bis-Lys(OBn)-Glut **5** was synthesized according to the scheme in **Figure 23**. Compound **3** was synthesized from **1** according to Agnihotri's report [232]. Glutaric acid was coupled with at least 2 equivalents of compound **3** using EDCI/DMAP. Compound **4** was carefully purified by silica gel flash chromatography and treated with TFA/DCM to get

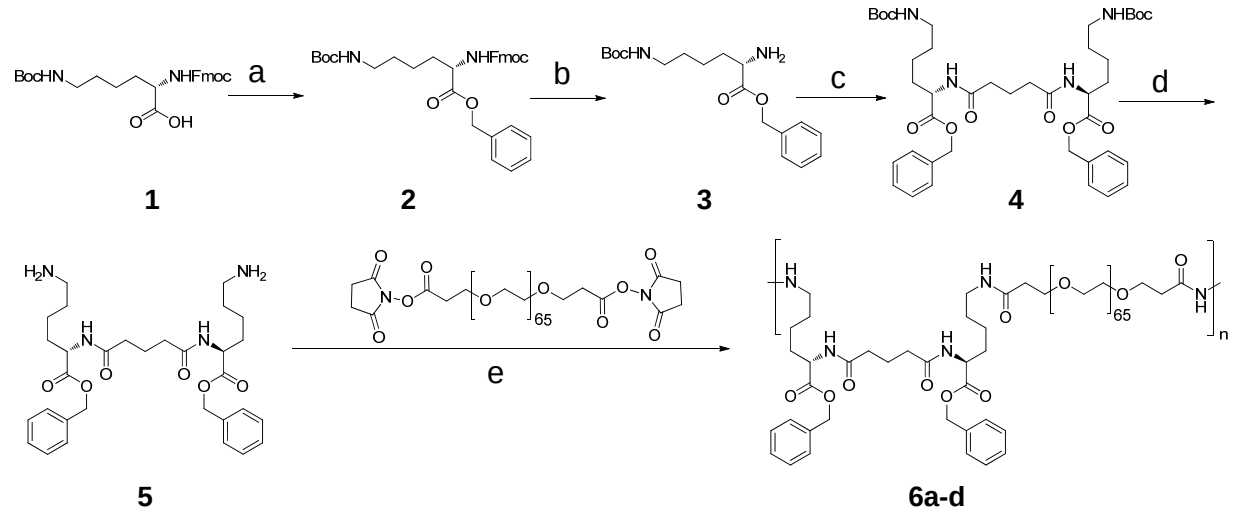

Figure 23. Synthesis of multiblock copolymer Poly(Bis-Lys(OBn)-Glut-PEG$_{3400}$). Reagents and conditions: (a). Benzyl alcohol, EDCI, DMAP; (b). 20% piperidine in DCM; (c). Glutaric acid, EDCI, DMAP; (d). TFA/DCM, rt; (e). Et_3N, DMF.

comonomer Bis-Lys(OBn)-Glut **5**. Polymerization was carried out in anhydrous DMF in nitrogen atmosphere. After the polymerization was initialized by organic base Et_3N, the viscosity of the solution changed dramatically in less than 1 hour. The reaction became very viscous after 24 hours, which indicated successful elongation of the polymer chain. As shown in **Table 8**, polymerization at 50°C can produce higher Mw than that at 25°C. It might be because that high temperature can reduce the viscosity of the polymerization solution and therefore increase the condensation efficiency. Polymer Mw reduced to around 20 kDa when inorganic base $NaHCO_3$ was used. Although both Et_3N and $NaHCO_3$ can deprotonate the ε-amino groups of Bis-Lys(OBn)-Glut **5**, $NaHCO_3$ was partially insoluble in DMF, making it less efficient in polymerization. Polymer **6a-d** are highly soluble in water, THF and chloroform, but insoluble in diethyl ether and petroleum ether.

To graft rapamycin onto polymer, polymer **6b** was deprotected by hydrogenation to liberate the carboxyl groups (**Figure 24**). Polymer **7** is a novel, linear multiblock copolymer containing two carboxyl groups for drug conjugation in each block. This polymer is also soluble in water, DMF, and methanol, slightly soluble in $CHCl_3$, but insoluble in THF and diethyl ether.

Table 8. Polymerization of monomer NHS-PEG_{3400}-NHS with comonomer Bis-Lys-Glut in different conditions.

Polymer	Base	Temperature	Polymerization time	Mw (kDa)	Mn (kDa)	Mw/Mn	Yield (%)
6a	Et_3N	50°C	2h	20.9	15.2	1.37	71
6b	Et_3N	50°C	24h	31.5	21.9	1.43	59
6c	Et_3N	25°C	24h	22.8	16.1	1.41	66
6d	$NaHCO_3$	50°C	24h	19.9	14.1	1.42	79

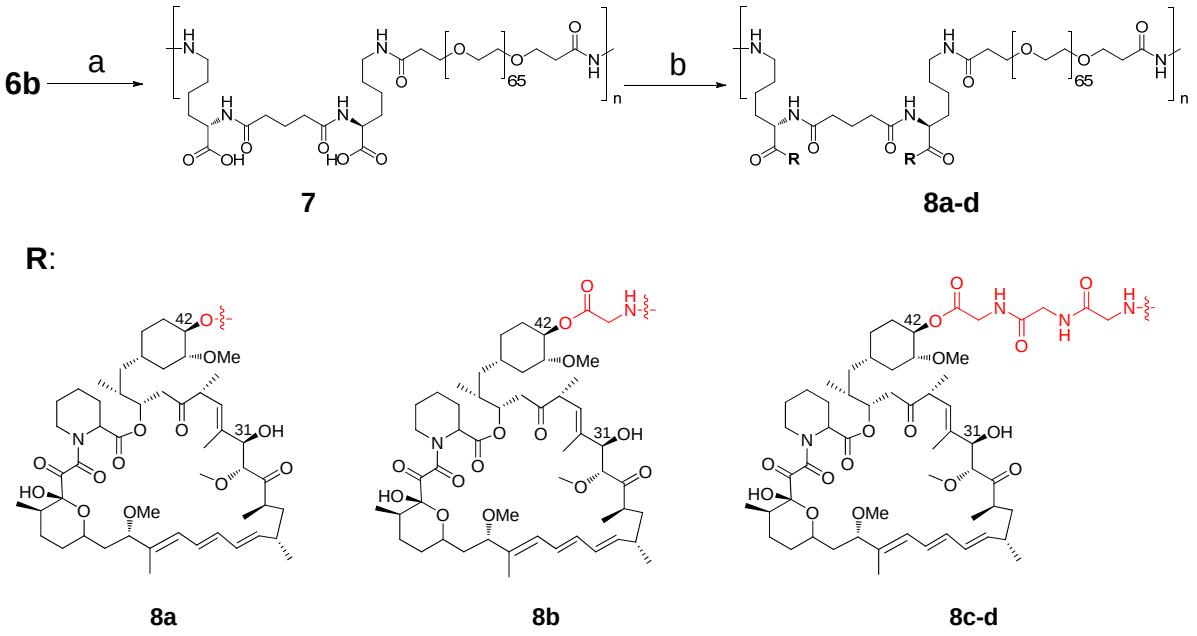

Figure 24. Synthesis of polymer rapamycin conjugate. Reagents and conditions: (a). H_2, Pd/C in methanol; (b). EDCI, Et_3N, NHS.

Synthesis of polymer rapamycin conjugates

Rapamycin was first conjugated with polymer **7** by forming an ester bond between its hydroxyl groups and polymer's carboxyl groups in the presence of EDCI, Et_3N and NHS. Conjugate **8a** was purified by dialysis with a yield around 67%. However, conjugate **8a** had very low drug loading capacity (wt% ~ 0.48). If all the carboxyl groups were conjugated with rapamycin, the theoretical maximal drug loading capacity (wt%) could be as high as 34.1%. Therefore, the hydroxyl group of rapamycin only reacted with around 1.4 percent of all the carboxyl groups in polymer **7**. The low coupling efficiency could be explained partially by the steric hindrance between the polymer and rapamycin. To reduce the steric hindrance, two linkers, Gly and GlyGlyGly, were utilized to link polymer **7** and rapamycin.

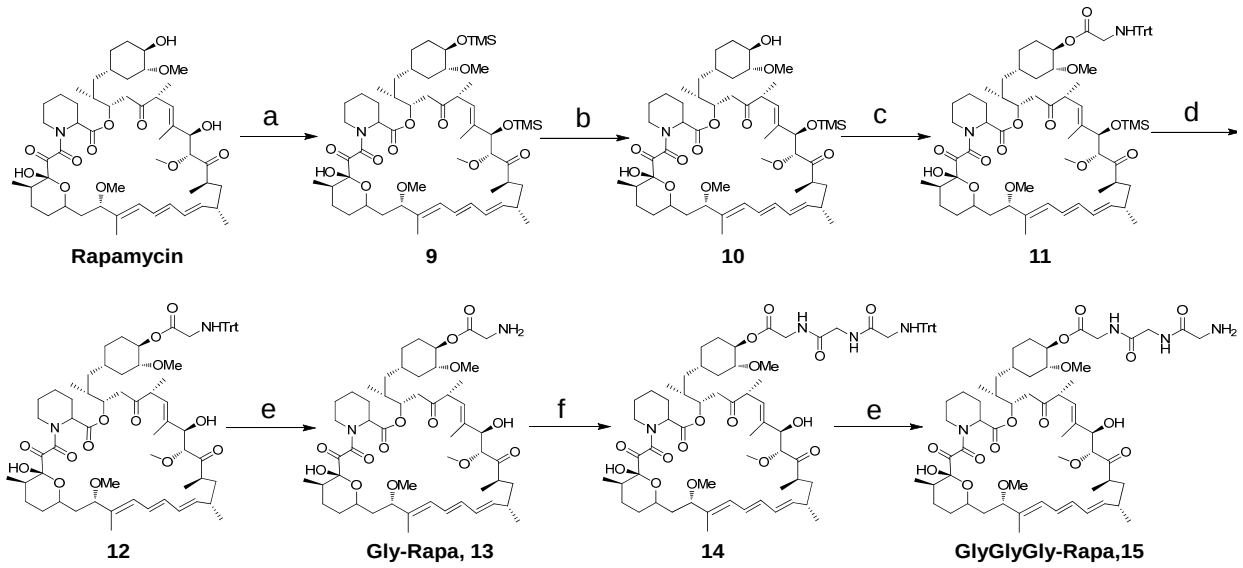

Figure 25. Synthesis of GlyGlyGly-Rapa. Reagents and conditions**:** (a). TMSCl, imidazole, DCM; (b). imidazole/imidazole·HCl, DCM; (c). Trt-Gly-OH, EDCI, DMAP, DCM; (d). THF/2N H_2SO_4 (v/v=2/1); (e). 0.1M HOBT in TFE; (f). Trt-Gly-Gly-OH, EDCI, Et_3N, DCM.

Linker-drugs were synthesized according to the scheme in **Figure 25**. In order to selectively conjugate the linkers at 42-OH, 31-OH of rapamycin was selectively protected with TMS group according to the procedure described by Shaw and Nan [233, 234]. Trt-Gly-OH was then conjugated with 42-OH using conventional coupling method. After removing TMS at 31-OH in diluted inorganic acid H_2SO_4, Trt-Gly-Rapa was deprotected with 0.1M HOBT in TFE to get Gly-Rapa **13**. Since rapamycin is very sensitive to TFA, the routine Trt deprotection methods, such as 1% TFA in DCM, were inapplicable. Gly-Rapa **13** was further coupled with Trt-Gly-Gly-OH using EDCI/Et_3N to give compound **14**. GlyGlyGly-Rapa **15** was finally obtained by removing the Trt group in compound **14**.

Linker-drugs Gly-Rapa **13** and GlyGlyGly-Rapa **15** were conjugated with polymer **7** using the same coupling method as the synthesis of **8a**. Conjugate **8b** was obtained with a yield

Table 9. Properties of polymer rapamycin conjugates.

Polymer-drug conjugate	Conjugation reagents	Linker-Drug	Theoretical maximal drug conjugated (wt%)	Drug conjugated (wt%)	Yield (%)
8a	EDCI/Et_3N/NHS	Rapamycin(Rapa)	34.1	0.68±0.18	57~71
8b	EDCI/Et_3N/NHS	Gly-Rapa	33.4	19.5±1.8	65~88
8c	EDCI/Et_3N/NHS	GlyGlyGly-Rapa	32.1	27.3±5.1	41~63
8d	HATU/DIPEA	GlyGlyGly-Rapa	32.1	24.9±3.1	50~64

of 88%, and the weight percentage (wt%) of rapamycin in the polymer drug conjugate was 19.5%. The highest weight percentage of rapamycin in polymer drug conjugates was observed in conjugate **8c** (wt% ~ 27.3%) where around 80% of carboxyl groups in polymer 7 were conjugated with rapamycin. There was no significant difference in drug loading capacity when other coupling methods, such as HATU/DIPEA, are used (conjugate **8d**, **Table 9**). Therefore, the conjugation efficiency is mainly determined by linkers rather than coupling methods.

Characterizations of polymer rapamycin conjugate

The UV spectrum of conjugate **8c** was scanned over the range of 190 to 400 nm and compared with free rapamycin. As shown in **Figure 26**, The UV spectrum of rapamycin exhibits a maximum peak at 280nm and two smaller peaks on either side. Similar peaks were also observed in the UV spectrum of purified conjugate **8c**, which indicated that rapamycin was conjugated to the polymer chains. Beside three peaks around 280 nm, conjugate **8c** also shows strong absorbance at near ultraviolet region (200 ~ 230 nm). The strong absorbance was proposed to be contributed mainly by polymer 7 and minimally by rapamycin (**Figure 26**). The carboxyl groups in polymer 7 and double bonds in rapamycin were believed to be responsible for the UV absorbance at 200 ~ 230 nm.

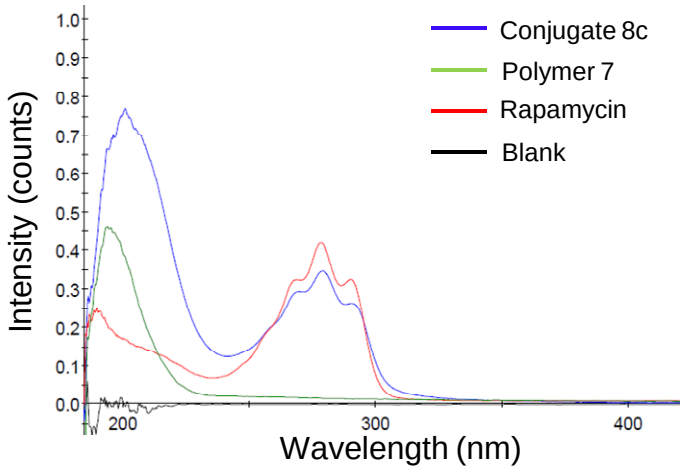

Figure 26. UV spectra of rapamycin, polymer rapamycin conjugate 8c and polymer 7.

Proton NMR (^{1}H NMR) spectroscopy was also determined to prove the presence of rapamycin in polymer rapamycin conjugate **8c**. **Figure 27A** shows the ^{1}H NMR spectrum of rapamycin. The seven groups of peaks (a ~ g) at low field corresponds very well to the protons of double bonds (a ~ e) and carbonyl groups (f, g) in rapamycin. The single peaks (h ~ j), between 3.0 to 3.5 ppm, corresponds to the presence of three CH_3O- groups in rapamycin. The ^{1}H NMR spectrum of polymer rapamycin conjugate **8c** (**Figure 27B**) contains peaks representing both rapamycin and polymer chain. Peaks a ~ j in Figure 5B show the same chemical shifts (ppm) and splitting patterns as that in Figure 36A, indicating the presence of rapamycin in conjugate **8c**. While polymer chain in conjugate 8c corresponds to the peaks a' - c', in which peaks a' - b' represent Bis-Lys-Glut and peak c' represents PEG_{3400}.

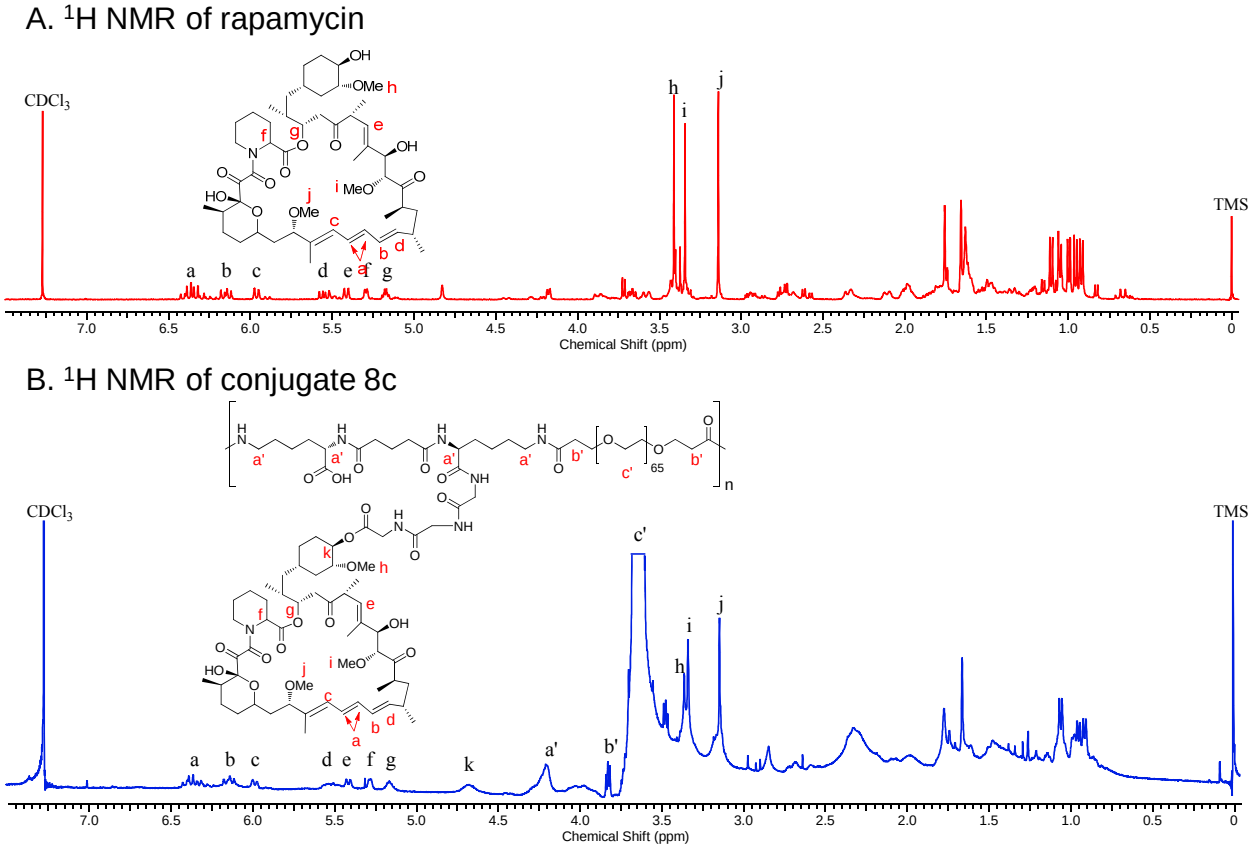

Figure 27. ^{1}H NMR spectra of rapamycin (A) and polymer rapamycin conjugate 8c (B) in $CDCl_3$ solvent.

Release of rapamycin from rapamycin conjugates

The release of rapamycin from two conjugates GlyGlyGly-Rapa and conjugate **8c** was evaluated in mouse, rat and mouse serum. Rapamycin conjugates were incubated with 50% of different serum at 37 ^{o}C for 4~12 hours. The release profile of rapamycin was monitored using HPLC. In mouse serum, the half-life of releasing rapamycin from GlyGlyGly-Rapa is around 0.5 hours. In contrast, the half-life increases to 4 hours in rat serum. A minimal release was observed in human serum where only 10% of rapamycin was released after 4 hours (**Figure 28**). The species-dependent release profile is due to the metabolic differences between species [238]. The

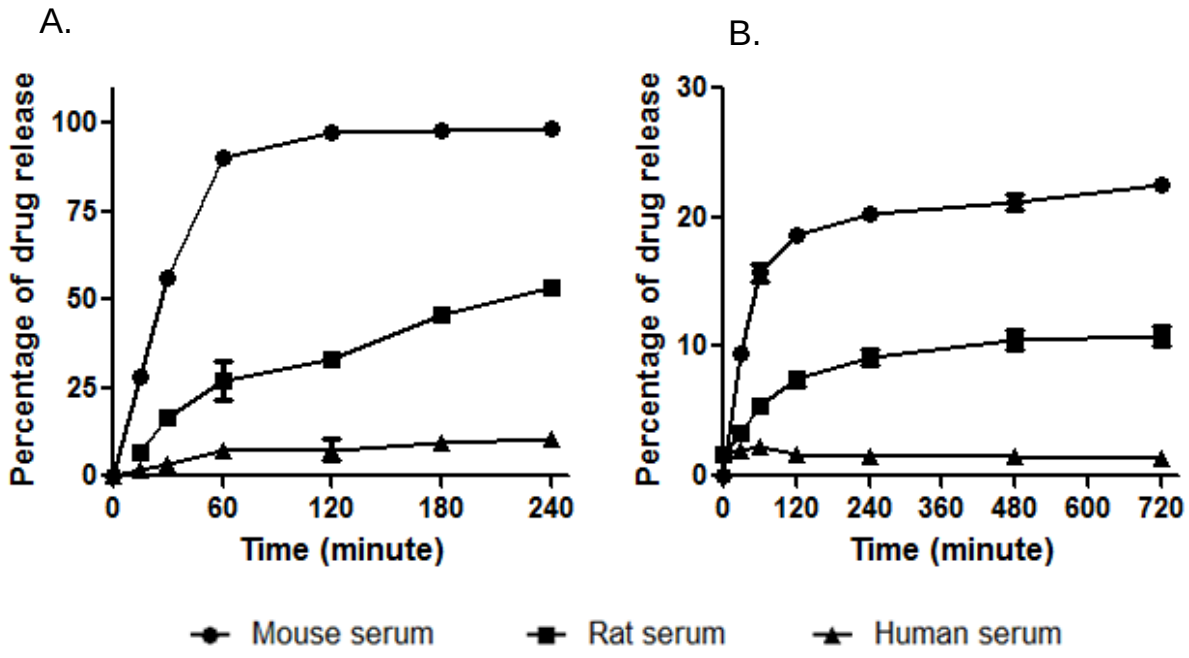

Figure 28. The release of rapamycin from GlyGlyGly-Rapa (A) and conjugate 8c (B) in different sera.

similar phenomenon was also observed in Wortmannin-Rapamycin conjugate [159]. The half-life of releasing rapamycin from polymer rapamycin conjugate **8c** is much longer than that of GlyGlyGly-Rapa. After a 12-hour incubation, only 23%, 11% and 3% of rapamycin was released from conjugate **8c** in mouse, rat and human serum, respectively. The bulky polymer structure in polymer rapamycin conjugate dramatically increased the steric hindrance of the ester linker between rapamycin 42-OH and GlyGlyGly, which makes ester bond less accessible by esterase and therefore decreases the hydrolysis rate [239].

In vitro activity of rapamycin and its conjugates

The *in vitro* cytotoxicity of polymer **7**, rapamycin, GlyGlyGly-Rapa and conjugate **8c** was determined in prostate, breast and cervical cancer cell lines using a MTT assay. No obvious

Table 10. *In vitro* cytotoxicity study (IC_{50}, nM). The cancer cells were treated with the compounds for 72 hours before MTT assay. Values shown are mean ± SD.

Cancer type	Cell line	Polymer 7[a]	Rapamycin	GlyGlyGly-Rapa	Conjugate 8c[b]
Prostate	LNCaP	>100,000	0.9±0.9	4.1±0.3	51.2±0.6
	PC-3	>100,000	0.8±0.7	2.3±0.6	29.9±0.7
	DU145	>100,000	0.1±0.5	5.6±0.5	30.6±0.6
Breast	SK-BR-3	>100,000	4.4±0.3	9.2±0.6	40.7±0.7
	MCF-7	>100,000	5.2±0.3	10.3±0.5	26.3±0.4
	MCF-7/HER2	>100,000	3.3±0.2	3.9±0.4	25.9±0.5
Cervical	HeLa	>100,000	1.0±0.1	36.5±0.1	47.4±0.1

a. IC_{50} is calculated based on molar concentration of repeated units.
b. IC_{50} of polymer rapamycin conjugate 8c is expressed in terms of rapamycin equivalents.

cytotoxicity (IC_{50} > 100 μM) was observed in polymer **7** treated cells, indicating that polymer **7** is not toxic to all these cancer cell lines. Rapamycin showed potent *in vitro* cytotoxicity to all cancer cell lines (**Table 10**). The IC_{50} values of rapamycin in all seven cancer cell lines ranged from 0.1 to 5.2 nM. Compared to breast cancer cell lines, prostate and cervical cancer cell lines were much more sensitive to rapamycin treatment. GlyGlyGly-Rapa was 2- to 36- less potent than rapamycin with the exception of MCF-7/HER2, in which similar potency was observed. Given the fact that GlyGlyGly-Rapa is an ester prodrug of rapamycin ,and the hydrolysis is required for its activity, it is reasonable that GlyGlyGly-Rapa shows lower potency than rapamycin. The IC_{50} values of conjugate **8c** are in a range of 25 to 50 nM. Although it is much less potent than free rapamycin, conjugate **8c** still exhibits low nanomolar IC_{50} values against all cancer cell lines tested.

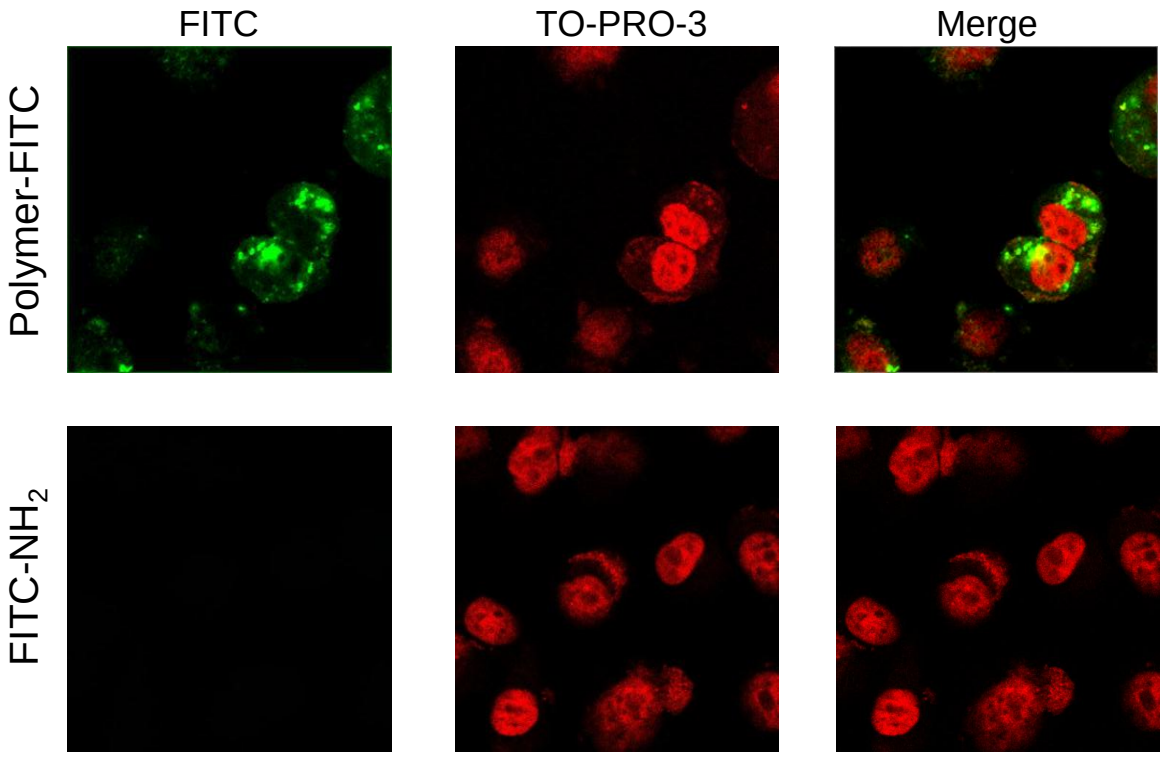

Figure 29. Cellular uptake of FITC labeled polymer (Polymer-FITC) and FITC ethylenediamine (FITC-NH_2) by confocal microscopy. PC-3 cells were treated with Polymer-FITC and FITC-NH_2 in serum free RPMC-1640 media for 1 hour and 24 hours. Cells were then stained for DNA with TO-PRO-3 and imaged in two fluorescent channels.

Cellular uptake and distribution of the polymer rapamycin conjugates

FITC ethylenediamine (FITC-NH_2) was conjugated to polymer **7** using the same coupling method (EDCI/NEt_3/NHS) as conjugate **8a-c**. The weight percentage (wt%) of FITC in the labeled polymer **7** is 4.5% (Data not shown). To determine the cellular uptake and distribution, FITC labeled polymer was incubated with PC-3 cells in serum-free medium for 24 hours. Punctuated staining pattern was exhibited in PC-3 cells after 24-hour treatment (**Figure 29**).

Table 11. Aqueous solubility analysis of polymer **7**, Rapamycin and conjugate **8c** in pure water.

Compound	Aqueous solubility (mg/ml)	Aqueous solubility (Rapamycin equivalents)	
		mg/ml	mM
Polymer 7	100.332±22.278	-/-	-/-
Rapamycin	0.034±0.006	0.034±0.006	0.037±0.007
Conjugate 8c	78.000±12.165	21.061±3.285	23.014±3.594

Other fluorescence labeled polymers, such as β-cyclodextrin polymer and PEG, were reported to share the similar cellular uptake and distribution pattern [237, 240]. Polymers are believed to enter the cells via endocytosis because the punctate vesicular distribution of fluorescence indicated a lysosomal localization. The uptake of FITC-NH_2 in PC-3 cells was also examined. Because FITC-NH_2 was a membrane non-permeable fluorescent dye, no fluorescence was observed even after 24-hour incubation (data not shown) [241].

Conjugation with polymer dramatically enhanced the solubility of rapamcyin

Due to the hydrophilic PEG component, polymer **7** is highly soluble in water (**Table 11**). The aqueous solubility of rapamycin is only around 0.034 mg/mL at room temperature. After conjugated to polymer **7**, its solubility increased to 21.061 mg/mL which is more than 600 fold higher than free rapamycin. The aqueous solubility of polymer rapamycin conjugate **8c** is around 78 mg/ mL.

5.4. Discussion

Rapamycin have been examined alone or in combination with other drugs for treatment of various cancers in clinical studies [208-210]. Although it showed promising therapeutic

effects, its clinical development was interrupted by poor aqueous solubility and preferential distribution in RBCs. Various formulations and conjugates have been developed to overcome the limitations, such as cosolvent system, polymeric micellar formulation and some rapalogues [213, 220, 222]. All these formulations can only partially increase the solubility, which however has little effect on the blood distribution and pharmacokinetics. Therefore, the objective of this study is to develop a polymer rapamycin conjugate that can enhance the solubility and improve the biodistribution profiles of rapamycin.

In this study, rapamycin was conjugated with a novel, linear, PEG containing multiblock copolymer. The polymer was synthesized via the condensation of a difunctionalized PEG monomer (NHS-PEG_{3400}-NHS) with a comonomer (Bis-Lys(OBn)-Glut) containing two pendant carboxyl groups for drug conjugation. Comonomer Bis-Lys(OBn)-Glut is small in size and symmetric in structure, which are expected to enhance the condensation efficiency. The purity of comonomer has a big impact on achieving high M_W polymers. The presence of impurities can terminate the chain elongation, leading to low MW polymers [229]. After precipitation in diethyl ether twice, Bis-Lys(OBn)-Glut was obtained with a purity of ~ 97%. Beside impurity, humility can also dramatically decrease the M_W of the polymer. Polymerization in non-drying solvent or with non-drying comonomer would only generate short polymer chains with M_W of ~18 kDa (data not shown).

This study represents the first attempt to conjugate rapamycin with a polymer. Rapamycin is a complicated natural product, and its structure contains three hydroxyl groups, all of which have the possibility to conjugate with polymers. Although the tertiary alcohol at position 13 is highly hindered and unreactive, rapamycin contains two secondary hydroxyl

groups at position 31 and 42 which are accessible for esterification and etherification. Directly reacting with acrylating agents would produce a mixture of 31,42-bis-acrylated product and 31- or 42-monoacrylated products, which results in inevitable heterogeneity of polymer rapamycin conjugate. In this study, we achieved the regioselective conjugation of rapamycin at 42-OH by first protecting the 31-OH with TMS and then synthesizing 42-monoacrylated rapamycin via esterification. Another challenge in rapamycin conjugation is its instability in acidic/basic conditions which make it intolerable to many chemical reactions. Gly-Rapa was firstly attempted to synthesize from Fmoc-Gly-Rapa, but rapamycin was quickly broken down when deprotecting Fmoc in 10% piperidine in DCM. Removing Boc from Boc-Gly-Rapa was also problematic due to its sensitivity to TFA. Gly-Rapa was finally obtained with a very low yield (~ 10%) from Trt-Gly-Rapa by deprotecting Trt in THF/2N H_2SO_4 (v/v = 2/1). However, the yield was dramatically increased to 60~80% when the deprotecting method was switched to an uncommonly used, but mild condition (0.1N HOBT in TFE).

Conjugation of rapamycin to the polymer was achieved by coupling a linker to rapamycin at position 42-OH, and subsequently grafting the linker-Rapa at the pendant carboxyl groups of this multiblock copolymer. The expected mechanism of drug release from the polymer rapamycin conjugate is that tumor esterase would hydrolyze the 42-ester bond and release free rapamycin from the polymer backbone. Insertion of linkers, such as Gly or GlyGlyGly, between rapamycin and the polymer backbone is believed to accelerate the drug release. Moreover, these amino acids or peptide linkers can transform the hydroxyl group of rapamycin at position 42 to a more reactive amino end group, which could dramatically increase the drug loading capacity. As shown in **Table 9**, directly conjugating rapamycin to polymer can only load very less drug (wt%

~ 0.48). In contrast, the drug loading capacities increased to 19.5% and 27.3%, respectively, by inserting Gly and GlyGlyGly between rapamcyin and the polymer. The use of longer linker, such as GlyGlyGly, resulted in a higher drug loading capacity because the long and flexible linker may reduce the steric hindrance between the polymer and rapamycin during coupling reaction.

The most striking observation of this study is the great solubility of rapamycin after conjugating with the polymer. Rapamycin is practically insoluble in water (0.034 mg/mL), while its solubility increases to 21.061 mg/mL after conjugated with the polymer. This solubility meets the requirement for *i.v.* formulations in animal studies (the desired dose concentration: 3 ~ 6 mg/mL) and clinical studies (the desired dose concentration: 1 mg/mL) [213]. The Backbone of polymer **7** has repeating units of two components, PEG_{3400} and bis-Lys-Glut, in which PEG_{3400} plays the major role in the aqueous solubility. Moreover, PEG_{3400} is also expected to reduce the toxicity and immunogenicity of the polymer [242]. As shown in **Table 10**, polymer **7** does not show obvious toxicity in various cultured tumor cells.

5.5. Conclusion

In conclusion, a novel, linear, PEG based multiblock copolymer was synthesized and utilized as a carrier for hydrophobic drug rapamycin. The polymer rapamycin conjugate showed significantly increased solubility in water, and potent cytotoxicity against a panel of cancer cell lines. It also demonstrated that the rapamycin in the conjugate is releasable in the serum and the polymer drug conjugate could be taken up by tumor cells. The result of the uptake study indicates that the lysosome is the main site of the intracellular localization of the polymer drug conjugate. Thus, in this study we reported a novel rapamycin conjugate which hold great

promising for treatment of a wide variety of tumors. Further studies of this rapamycin conjugate are ongoing in several animal xenograph models to explore its efficacy *in vivo*.

CHAPTER 6

INHIBITION OF BREAST CANCER CELL GROWTH AND INVASION BY DUAL SILENCING OF HER2 AND VEGF

6.1. Rationale

Breast cancer is the most common female malignancy in the United States and accounts for 26% of all cancer cases in women; it is the second leading cause of cancer death in American women [243]. Currently, chemotherapy is the major therapy for breast cancer patients. However, it is limited by nonspecificity, toxicity and inevitable development of resistance. On the other hand, advances in molecular and cell biology have led to elucidation of the molecular mechanism underlying malignant transformation in breast cancer. Due to the fact that mutations and abnormal expression of various genes are involved in tumorigenesis, gene modulation is being explored as a very promising approach to correct those abnormal gene expressions [244, 245]. The present study aims at suppressing two upregulated genes in HER2 positive breast cancer simultaneously.

One of the most certain and commonly amplified genes for breast cancer is the Human Epidermal growth factor Receptor 2 (HER2) gene, also known as Erb-B2, which encodes a transmembrane receptor tyrosine kinase and plays key roles in normal cell differentiation, growth and repair. Over-expression of HER2 usually results in malignant transformation of cells and accounts for ~25% of all breast cancer cases. It is always associated with more aggressive tumor phenotypes, greater likelihood of lymph node involvement, and increased resistance to endocrine therapy [40, 246]. Overall survival rate and time of relapse for HER2 positive breast cancer patients are significantly shorter than patients without HER2 over-expression. Therefore,

HER2 is a logical target for breast cancer therapy and inhibition of HER2 expression leads to the apoptosis of tumor cells [41, 42, 125, 246]. A monoclonal humanized antibody against HER2 (Trastuzumab) has been successfully applied in the treatment of HER2 positive breast cancer.

Additionally, extensive preclinical and clinical evidence indicated the association of angiogenesis with tumor growth and spreading in breast cancer [247, 248]. VEGF is the most potent proangiogenic signal and was identified as the key angiogenic growth factor in breast cancer. High level of VEGF is associated with greater risk of recurrence and decreased response to hormonal therapy and chemotherapy [249]. For example, microvessel density, a measurement of angiogenesis, directly correlates with metastasis potentials of tumor cells [250, 251]. Tumor cells overexpressing VEGF induce disruption of endothelial cell basement membrane, which contributes to the development of metastasis [252]. Therefore, inhibition of VEGF is another effective treatment for breast cancer [253-255]. Furthermore, HER2 positive breast cancer is more likely to over-express VEGF [255-257]. In a clinical study involving 611 breast cancer patients, 87.7% of HER2 positive breast cancers are found associated with overexpressed VEGF [258]. Given all evidence described above, the combination of agents blocking HER2 and antiangiogenic agents will be a very attractive therapeutic approach for HER2 positive breast cancer [246, 254]. Treatment with a combination of VEGF-Trap (a humanized decoy protein targeting VEGF) and monoclonal antibodies directed against HER2 (Trastuzumab) resulted in significant inhibition of HER2 positive BT474 tumor growth than individual agent alone [259]. In addition, a phase I/II clinical trial has been conducted using combinational monoclonal antibodies directed against HER2 (Trastuzumab) and VEGF (Bevacizumab) [260, 261]. The

phase II clinical trial showed promising activity in HER2 positive recurrent or metastatic breast cancer [260].

RNA interference (RNAi) is the phenomenon in which siRNA of 21-23 nt in length silences a target gene by binding to its complementary mRNA and triggering its degradation. Potent knockdown of specific gene sequence makes siRNA a promising therapeutic strategy [262, 263]. In this study, we intended to evaluate the effect of dual silencing of HER2 and VEGF genes on breast cancer cell growth and invasiveness. We have designed and identified potent siRNA which can efficiently silence the target gene. The most potent HER2 and VEGF siRNAs were used to conduct functional studies in HER2 positive breast cancer cells. Tumor invasiveness properties including cell morphology change, *in vitro* migration, spreading, adhesion to ECM were evaluated. In addition, cell proliferation and apoptosis were examined after the treatment with optimized siRNAs.

6.2. Materials and Methods

Materials

Lipofectamine-2000, TRIzol reagent and siRNAs were purchased from Invitrogen Corp. (Carlsbad, CA), while scrambled siRNA control was obtained from Ambion Inc. (Austin, TX). Fetal bovine serum (FBS) was purchased from Atlanta Biologicals, Inc. (Lawrenceville, GA). Other cell culture products including RPMI-1640 medium, Dulbecco's Phosphate Buffered Saline (PBS), penicillin, streptomycin, and G-418 were obtained from Mediatech, Inc. (Manassas, VA). Bovine serum albumin (BSA) was purchased from Sigma-Aldrich corporation (St. Louis, MO). SYBR Green-1 dye universal master mix and Multiscript reverse transcriptase were

purchased from Applied Biosystems, Inc. (Foster City, CA). 6.5mm Transwell® with 8.0μm Pore Polycarbonate Membrane Insert was purchased from Corning Incorporated (Lowell, MA). BD Matrigel™ and BD Pharmingen™ Annexin V-FITC Apoptosis Detection Kit I were obtained from BD Biosciences (San Jose, CA). HER2 and VEGF ELISA (enzyme-linked immunosorbent assay) kits were purchased from R&D Systems, Inc. (Minneapolis, MN). CellTiter-Glo® Luminescent Cell Viability Assay Kit was purchased from Progema Corp. (Madison, WI).

Cell Culture

HER2 positive breast cancer cells, MCF-7/HER2 (kindly provided by Dr. Mien-Chie Hung, Department of Molecular and cellular Oncology, University of Texas), were cultured in RPMI 1640 supplemented with 10% FBS, penicillin (100 unit/mL), streptomycin (100 μg/mL), and G418 (500 μg/mL). The human SK-BR-3 cell line was obtained from American Type Culture Collection (Manassas, VA). SK-BR-3 cells were maintained in RPMI 1640 with 10% FBS, penicillin (100 unit/mL), and streptomycin (100 μg/mL). Cells were cultured at 37 ^{o}C in a humidified atmosphere containing 5% CO_2. The culture medium was changed every other day and the cells were passaged when they reached 80~90% confluency.

siRNA Design and Synthesis

siRNAs targeting HER2 (Accession No. NM_001005862) and VEGF (Accession No. AB021221) were designed using BLOCK-iT™ RNAi Designer (Invitrogen Corp., Carlsbad, CA), siRNA Target Finder (Ambion, Austin, TX), siRNA Target Finder (GeneScript Corp., Piscataway, NJ) and siRNA target Designer (Progema Corp., Madison, WI). All siRNAs were

purchased from Invitrogen Corp. (Carlsbad, CA). siRNAs targeting at different mRNA regions were designed for HER2 and VEGF gene separately (Table 1). These siRNAs are of 19 nt with 2 thymidine deoxynucleotide (T) 3' overhangs. All designed siRNA sequences were blasted against the human genome database to eliminate crosssilence phenomenon with no-target genes. Scrambled siRNA (Ambion, Inc) that does not target any gene was used as the negative control.

Transfection of siRNA

Cells were transfected with siRNA and Lipofectamine 2000 according to manufacturer's instructions. Briefly, cells were seeded in 24 well plate at a density of 5.0×10^4 cells/well with antibiotics-free medium 12 h before transfection. The cells were transfected in RPMI 1640 medium with Lipofectamine 2000 (Invitrogen, Carlsbad, CA). One and a quarter microliters of siRNA duplexes (20 μM) were mixed with 1 μL Lipofectamine 2000 in 50 μl serum-free RPMI 1640 medium and incubated at room temperature for 25 min to form the complex. After washing cells with PBS, the 50 μl transfection mixture were added to each well with 450μl of 10% FBS RPMI 1640 medium at a final concentration of 50 nM siRNA. Twenty-four hours after the transfection, the medium was replaced with fresh 500 μL RPMI 1640 containing 10% FBS. Forty-eight hours after the tansfection, the culture medium was collected for VEGF ELISA assay and cells were collected for RNA or protein isolation.

ELISA for the detection of HER2 and VEGF at the protein level

For the detection of HER2 protein expression, breast cancer cells were lysed with RIPA buffer containing 150mM NaCl, 50mM Tris base pH 8.0, 1mM EDTA, 1% Triton 100, 0.1%

sodium dodecyl sulfate (SDS), 1mM PMSF and 1mM Na_3VO_4. Cell lysis was performed at room temperature for 10 min with rotary shaking. After centrifugation at 12,000 g for 10 min, the supernatant was collected and the total protein content was determined using a BCA protein assay kit (Pierce, Rockford, IL). The supernatant was diluted with a dilution buffer (20mM Tris base pH=8.0, 137mM NaCl, 10% glycerol, 2mM EDTA and 1mM Na_3VO_4) to appropriate concentration for the detection of HER2 protein using the HER2 ELISA kit. The HER2 protein expression was normalized with the total protein content in the sample.

The secretion of VEGF in culture medium by breast cancer cells was determined using Duoset VEGF ELISA kit (R&D system, Minneapolis, MN) according to manufacturer's instruction. Only the second day's culture medium was collected for the ELISA assay.

Real-time RT PCR

Total RNA was isolated from cell pellets using TRIzol reagent (Invitrogen) according to manufacturer's protocol. Two hundred nanograms of RNA were converted to cDNA using random hexamer primer and MultiScribe Reverse Transcriptase Reagent (Applied Biosystems, Inc., Branchburg, NJ). One hundred nanograms of cDNA were amplified by Real Time PCR using SYBR Green-1 dye universal Master mix on ABI Prism 5700 Sequence Detection System (Applied Biosystem, Inc., Fodter City, CA). The primer used for HER2 amplification were 5'–GGACATCTTCCACAAGAACAACCAGC-3' (forward primer) and 5'-TGCTCATGGCA GCAGTCAGT-3' (reverse primer). Primers for the detection of VEGF are 5'-AGGGCAGAA TCATCACGAAGTGGT-3' (forward primer) and 5'-TCTGCATGGTGATGTTGGACTCCT-3' (reverse primer). We used 18s ribosomal RNA as an internal control and the primers are 5'-

GTCTGTGATGCCCTTAGATG-3' (forward primer) and 5'-AGCTTATGACCCGCACTT AC-3' (reverse primer). To confirm the PCR specificity, PCR products were subjected to a melting-curve analysis. Comparative threshold (C_t) method was used to calculate the relative amount of mRNA of treated sample in comparison to control samples [264, 265]. Each sample was performed in triplicate and the mean value was calculated.

Cell Morphology Change

Cell morphology of breast cancer cells was assessed by the shape of cells after the treatment of siRNA. Images of cells were obtained from a LaboMed TCM 400 inverted microscope (Labo America Inc**.,** Fremont, CA) at a magnification of 100×. Cell images were obtained at 24 hours, 48 hours and 72 hours post-transfection.

***In vitro* Cell Migration Assay**

The effect of siRNA treatment on the invasive properties of breast cancer cells was determined using transwell migration assays. Twenty-four hours after the transfection with siRNA, SK-BR-3 cells were trypsinized and resuspended in FBS free RPMI-1640 medium. A total of 1×10^5 cells were plated in the top chamber of the transwell with a non-coated polycarbonate membrane (6.5 mm diameter insert, 8.0 μm pore size, Corning Incorporated). RPMI-1640 medium with 10% FBS was added in the lower chamber as a chemoattractant. After incubation for 48 hours, cells that did not migrate through the pores were mechanically removed by a cotton swab. Cells on the lower surface of the membrane were fixed with 10% formalin, stained with 0.2% crystal violet, followed by counting the number of migrated cells [266]. The

images of migrated cells were obtained by a LaboMed TCM 400 inverted microscope (Labo America Inc., Fremont, CA) with a magnification of 100×. The number of migrated cells was counted from 3 randomly selected fields in a blind way.

Cell Spreading

Cell spreading of breast cancer cells after the siRNA treatment was determined as reported [267, 268]. Briefly, MCF-7/HER2 or SK-BR-3 cells were harvested with PBS buffer containing 0.25% Trypsin at 48 h post-transfection. After centrifugation at 1000 g for 3 min, cell pellets were resuspended in RPMI 1640 medium containing 10% FBS, and then plated onto a Matrigel-treated plate which was coated with 0.5 mg/mL Matrigel (Becton Dickinson, Mountain View, CA) in RPMI 1640 medium overnight at 4 ^{o}C. Cells were allowed to spread for 10~24 h at 37ºC in cell culture incubator. Cell images were taken by LaboMed TCM 400 inverted microscope with 100× magnification at 24 h post-incubation. Spreading cells were defined as cells with extended processes and un-spreading cells were defined as round cells.

Cell Adhesion Assay

Cell adhesion assay was conducted as reported with modifications [269]. Forty-eight hours after the transfecion with siRNA, MCF-7/HER2 cells were harvested with 0.03% Trypsin, followed by centrifugation at 1000g for 3 min at room temperature. The cell pellets were suspended in serum free RPMI 1640 medium at a density of 3×10^5 cells/mL. One hundred microliters of the suspended MCF-7/HER2 cells (30,000 cells/well) were seeded in a 96 well plate which was pre-treated with 30 μg/mL Type I Collagen (Becton Dickinson, Mountain View,

CA) or 1% BSA for 1h at 37 ^{o}C, followed by blocking with 1% BSA at room temperature for 1h. Cells were allowed to adhere for 1h in cell culture incubator and non-attached cells were removed by gently washing twice with 100 μL PBS. Attached cells were fixed with 10% buffered formalin solution for 20 min at room temperature, followed by staining in 0.2% (w/v) crystal violet for 10 min. Stained cells were lysed in 1% SDS and the intensity of stain, which is proportional to the number of adherent cells, was quantitated by a spectrometer at the absorbance of 595nm. SK-BR-3 cells were harvested with 0.25% Trypsin because of the tight attachment between cells and plates. Additionally, after 1 hour's incubation, SK-BR-3 cells were washed five times with 200 μL PBS instead of two times for the cell adhesion assay of MCF-7/HER2.

Cell Proliferation Assay

The effect of siRNA on cell proliferation was measured using CellTiter-Glo® Luminescent Cell Viability Assay Kit (Progema Corp., Madison, WI) according to manufacturer's protocol. SK-BR-3 cells seeded in a 96-well plate (3000 cells/well) were transfected with 50nM siRNA as described above. Seventy-two and ninety-six hours after the transfection, 100 μl of CellTiter-Glo® reagent was added to each well which contained 100 μl of cell culture medium. Cells were lysed by incubating in an orbital shaker for 2 min, followed by incubation at room temperature for another 10 min to stabilize the luminescent signal. The luminescent intensity was measured using a DTX 880 Multimode Detector (Beckman Coulter, Inc., Fullerton, CA) with an integration time of 1 second.

Apoptosis Assay

Flow cytometry was used to analyze apoptosis of breast cancer cells after the treatment of siRNAs. Seventy-two hours after the transfection, cells were trypsinized, stained with Annexin V-FITC and propidium iodide (PI) using the Annexin V-FITC Apoptosis Detection Kit I (BD Biosciences) according to the manufacturer's protocol. The percentage of apoptotic cells was quantified by a BD LSRII flow cytometry (PI-positive indicates cell necrosis, while Annexin-V positive indicates cell apoptosis). Annexin V-FITC negative and PI positive indicates cell necrosis, while Annexin-V positive and PI negative indicates early apoptosis. Viable cells are both Annexin V-FITC and PI negative. Cells in late apoptosis are both Annexin V-FITC and PI positive.

Statistical Analysis

Data were expressed as the mean ± standard deviation (SD). Difference between any two groups was determined by ANOVA. $P < 0.05$ was considered statistically significant.

6.3. Results

Silencing of HER2 and VEGF genes by predesigned siRNAs

Selection of a potent siRNA is the first critical step in developing siRNA therapeutics. Using siRNA designers provided by different biotechnology companies, we designed up to ten synthetic siRNAs (**Table 12**) targeting at different mRNA regions. All these siRNA sequences have not been reported by others. The silencing effect of nine pre-designed HER2 siRNAs was examined in MCF-7/HER2 cells, which are engineered from MCF-7 cells to overexpress HER2.

Table 12. Sequences of HER2 siRNA and VEGF siRNA.

Target Gene	siRNA No.	Start Site	Sense Sequences of siRNAs
HER2	H1	604	5'-AAACCUGGAACUCACCUAC-3'
	H2	748	5'-GCUCUUUGAGGACAACUAU-3'
	H3	936	5'-GGAAGGACAUCUUCCACAA-3'
	H4	1493	5'-GCAGUUACCAGUGCCAAUA-3'
	H5	2394	5'-UCUCUGCGGUGGUUGGCAU-3'
	H6	2396	5'-UCUGCGGUGGUUGGCAUUC-3'
	H7	2560	5'-GCAGAUGCGGAUCCUGAAA-3'
	H8	3481	5'-GGUCGAUGCUGAGGAGUAU-3'
	H9	3962	5'-AAUGGGGUCGUCAAAGACG-3'
VEGF	V1	132	5'-GGAUGUCUAUCAGCGCAGC-3'
	V2	149	5'-GCUACUGCCAUCCAAUCGA-3'
	V3	176	5'-UGGACAUCUUCCAGGAGUA-3'
	V4	190	5'-GAGUACCCUGAUGAGAUCG-3'
	V5	300	5'-CAACAUCACCAUGCAGAUU-3'
	V6	330	5'-ACCUCACCAAGGCCAGCAC-3'
	V7	359	5'-UGAGCUUCCUACAGCACAA-3'
	V8	382	5'-UGUGAAUGCAGACCAAAGA-3'
	V9	418	5'-GAAAAUCCCUGUGGGCCUU-3'
	V10	453	5'-GCAUUUGUUUGUACAAGAT-3'

Cells were transfected with siRNAs at a concentration of 50nM after complex formation with Lipofectamine 2000. A scrambled siRNA that does not target any gene was used as the negative control. The protein expression of HER2 was detected using an ELISA kit. As shown in **Figure 30A**, eight siRNAs significantly inhibited the HER2 expression at the protein level, while the siRNA H4 showed the highest silencing effect up to 76% in comparison to the negative scrambled siRNA. A similar silencing effect (72%) of siRNA H4 was observed at the mRNA level using real time RT-PCR (**Figure 30B**), indicating the consistent silencing effect at protein and mRNA levels. In addition, the silencing effect of siRNA was confirmed in another HER2 positive human breast cancer cell line, SK-BR-3 cells. Similar silencing effects at protein and mRNA levels were observed (data not shown).

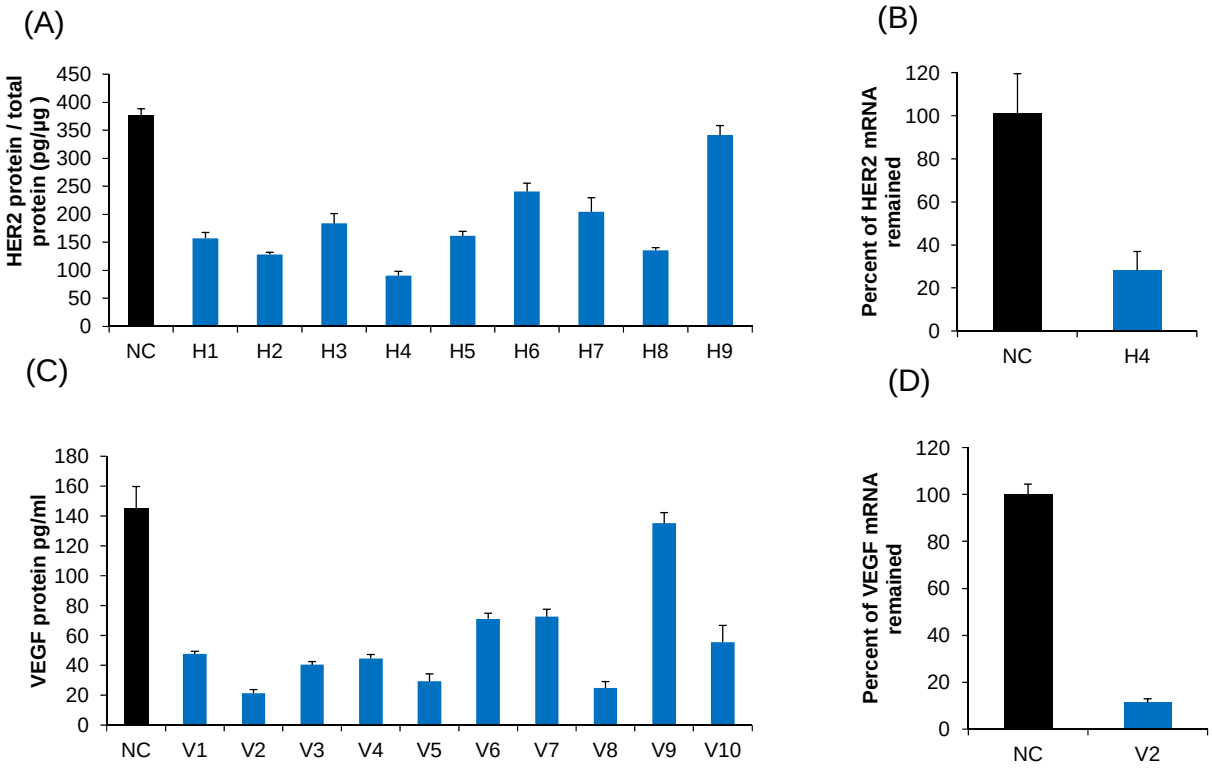

Figure 30. Silencing effect of HER2 siRNA (A&B) and VEGF siRNA (C&D) on MCF-7/HER2 cells. MCF-7/HER2 cells were transfected with predesigned HER2 siRNAs or VEGF siRNAs at a dose of 50nM after complexation with Lipofectamine 2000. A scrambled siRNA that does not target any gene was used as the negative control (NC). (A) Silencing effect of HER2 siRNAs at the protein level was determined using an ELISA kit. The HER2 protein expression was normalized by the total protein expression; (B) Silencing effect of selected HER2 siRNA (H4) at the mRNA level was measured using real time RT-PCR; (C) Silencing effect of VEGF siRNAs at the protein level. The secretion of VEGF in culture medium was determined using an ELISA kit. (D) Silencing effect of selected VEGF siRNA (V2) at the mRNA level was determined using real time RT-PCR. Results were represented as mean±SD (n=3).

Similarly, ten siRNAs targeting at different sites of VEGF mRNA were designed evaluated in MCF-7/HER2 at 50nM. As Fig. 1C showed, most of these siRNAs demonstrated more or less silencing effect at the protein level, while the siRNA V2 showed the highest silencing effect up to 83.5% compared to the negative scrambled siRNA. The silencing effect of V2 at the mRNA level was confirmed using real time RT-PCR (**Figure 30D**). Similar silencing effects at VEGF protein and mRNA levels were also observed in SK-BR-3 cells (data not shown). H4 siRNA (the most potent HER2 siRNA) and V2 siRNA (the most potent VEGF siRNA) were selected for following functional and phenotypic studies in HER2 positive breast cancer cells.

Next, we examined the silencing effect of H4 and V2 siRNAs at different concentrations. As shown in **Figure 31A**, the silencing effect increased with dose in a non-linear relationship in certain range. The silencing effect of H4 siRNA reached the plateau at 50nM, while V2 siRNA reached the plateau at 25nM.

Timecourses of HER2 and VEGF siRNA effect on protein level were also determined by HER2 and VEGF ELISA kit separately. As shown in **Figure 31B**, MCF-7/HER2 cells were transfected with 50nM of siRNA against HER2, VEGF or scrambled siRNA (NC) using Lipofectamine 2000. Silencing effects at 24hr, 48hr and 72hr after transfection was measured by ELISA kits. The highest silencing effects of both H4 and V2 siRNAs was achieved at 48hr after transfection. As for V2 siRNA, silencing effect returned to 54% at 72hr after transfection. Whereas silencing effect of H4 siRNA only slightly reduced from 70% to 67%. The degree of silencing at 48hr and 72hr was sufficient for biological function studies. Most of the following experiments were performed at 48hr or 72hr after transfection.

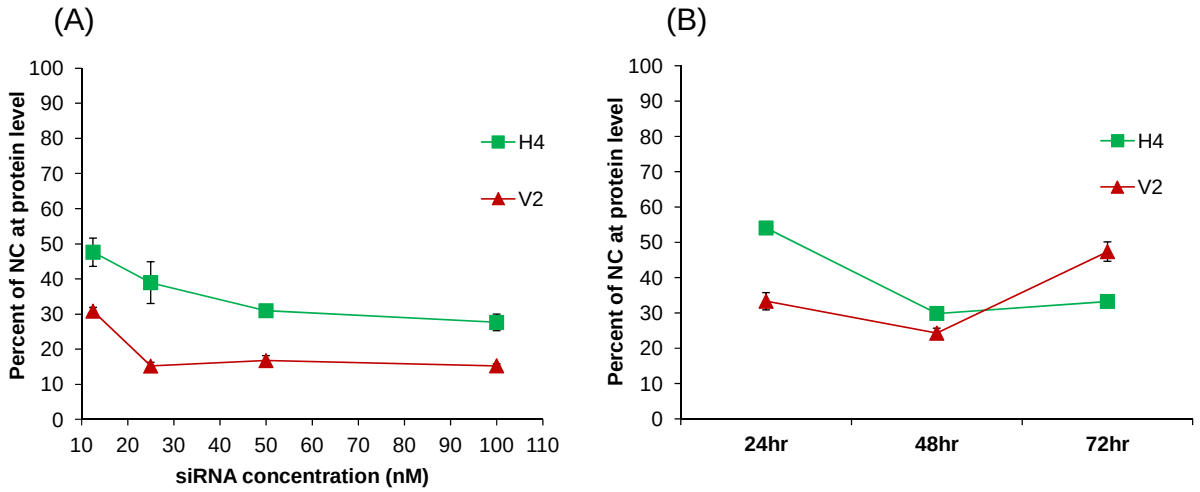

Figure 31. Effect of siRNA concentration and time course on the silencing effect of HER2 and VEGF siRNAs. (A) Concentration effect. MCF-7/HER2 cells were transfected with H4 siRNA at different concentrations (12.5 nM, 25 nM, 50 nM, and 100 nM), and the silencing effect at the protein expression level was measured. The same procedure was used to measure the silencing effect of V2 siRNA at different concentrations (12.5 nM, 25 nM, 50 nM, and 100 nM). (B) Time course effect. After transfection with siRNA at 50 nM, protein samples were collected at indicated time points (24 h, 48 h and 72 h), and then determined using ELISA kits respectively. Silencing effect was calculated in comparison to cells transfected with the negative control siRNA. Both results were represented as mean ± SD (*n* = 3)

The synergistic effect of HER2 and VEGF siRNAs

Activation of HER2 is always associated with up-regulation of VEGF in breast cancers [258]. Both HER2 and VEGF contribute to the aggressive phenotypes of HER2 over-expressed breast cancer. To have better understanding of the interaction of HER2 and VEGF, we examined the synergistic effect of HER2 siRNA (H4) and VEGF siRNA (V2) on HER2 and VEGF expressions respectively. MCF-7/HER2 cells were transfected with H4 siRNA (50nM), V2 siRNA (50nM), combination of H4 and V2 siRNAs (25nM+25nM), and scrambled siRNA

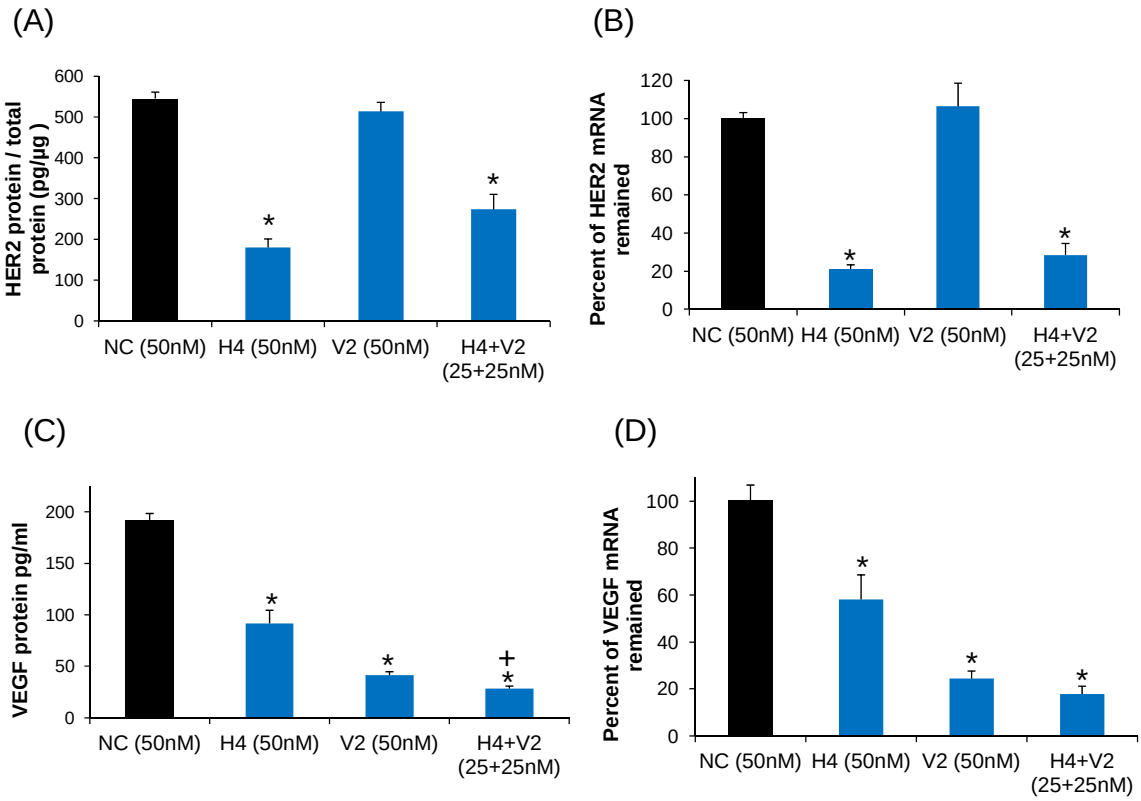

Figure 32. Synergistic effect of HER2 siRNA (H4) and VEGF siRNA (V2) on the HER2 and VEGF expression in MCF-7/HER2 cells. MCF-7/HER2 cells were transfected with H4 siRNA (50 nM), V2 siRNA (50 nM), combination of H4 and V2 siRNAs (25 nM + 25 nM), and negative control siRNA (50 nM). Protein expressions of HER2 (A) and VEGF (C) were measured using ELISA kit, while the mRNA levels of HER2 (B) and VEGF (D) were determined using the real time RT-PCR. Results were represented as mean ± SD (n = 3). * indicates $p < 0.01$ compared to the negative control siRNA (50 nM) group; + indicates $p < 0.01$ compared to the V2 (50 nM) group.

(50nM). Protein expressions of HER2 and VEGF were measured using ELISA kit (**Figure 32A&C**) and mRNA levels were calculated using quantitative real time RT-PCR (**Figure 32B&D**). As **Figure 32A** showed, VEGF specific siRNA (V2) did not show any effect on the HER2 expression at the protein level. The V2/H4 siRNA mixture demonstrated significant silencing effect on HER2 expression, although it was lower than that of H4 siRNA alone, indicating a minor synergistic effect of H4 and V2 siRNAs on the HER2 protein expression.

Similar results were observed at the mRNA level of HER2 (**Figure 32B**). However, the synergistic effect of H4 and V2 siRNAs on HER2 mRNA was more significant because the mixture of H4 and V2 siRNAs showed similar silencing effect as that of H4 siRNA alone.

It is known that HER2 plays an important role in tumor angiogenesis and neutralizing antibody targeting HER2 receptor could down-regulate VEGF production in tumor cells [270]. In Fig. 3C, we found that the HER2 specific siRNA (H4) significantly inhibited VEGF expression at the protein level up to 52%, although it is lower than that of VEGF specific siRNA (V2) which showed a silencing effect of 78%. This result is in accordance with the finding that HER2 signaling increased VEGF expression and subsequently inhibiting HER2 could reduce VEGF expression [257, 271]. Compared to V2 and H4 siRNA alone, the V2/H4 siRNA mixture showed the highest inhibition on VEGF protein expression up to 85%, indicating a dramatic synergistic effect of H4 and V2 siRNAs on VEGF protein expression. The similar, significant synergistic effect on VEGF mRNA expression was also observed using real time RT-PCR (**Figure 30D**).

Cell morphology

One of the earliest changes of tumor cells in the invasiveness evolution is the change in cell shapes to acquire migratory capability, a process called epithelial-mesenchymal transition (EMT) [272]. Therefore, cell morphological changes were examined in MCF-7/HER2 and SK-BR-3 cells after the transfection with H4, V2, H4/V2, and scrambled siRNAs (**Figure 33**). In comparison to cells treated with scrambled siRNA, cells treated with H4 siRNA showed striking changes in morphology from elongated, stretched shape to a round shape, which indicates a low

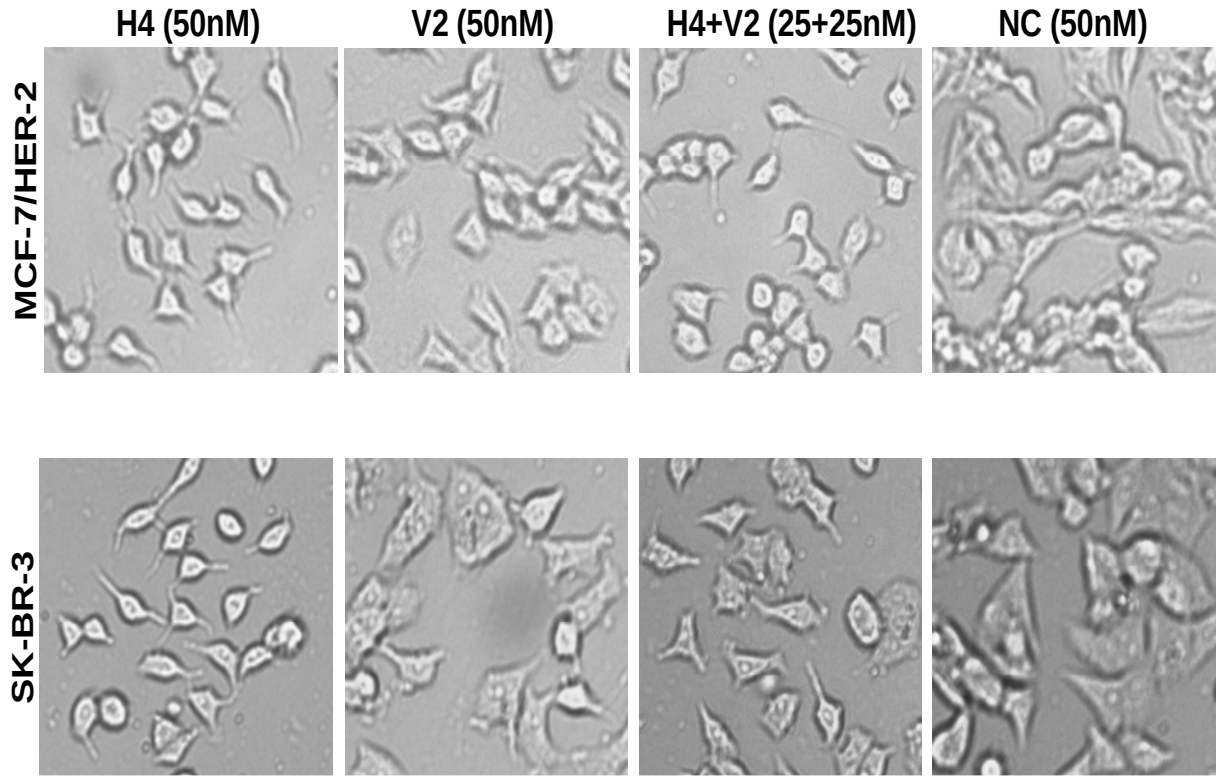

Figure 33. Cell morphology change. MCF-7/HER2 and SK-BR-3 cells were transfected with H4 siRNA (50 nM), V2 siRNA (50 nM), combination of H4 and V2 siRNAs (25 nM + 25 nM), and negative control siRNA (50 nM). Images of cells were obtained at 48 h post-transfection. Cell morphology was assessed by the cell shape

potential for migration and metastasis. V2 siRNA treated cells also showed mild morphological changes compared to the scrambled siRNA group, while the H4/V2 siRNA mixture showed a more significant morphology change.

Inhibition of cell migration by HER2 and VEGF siRNAs

Migration towards a chemoattractant is a distinct cellular phenotype of metastatic tumor cells, and it is an essential step for tumor invasion and metastasis. Since HER2 positive breast

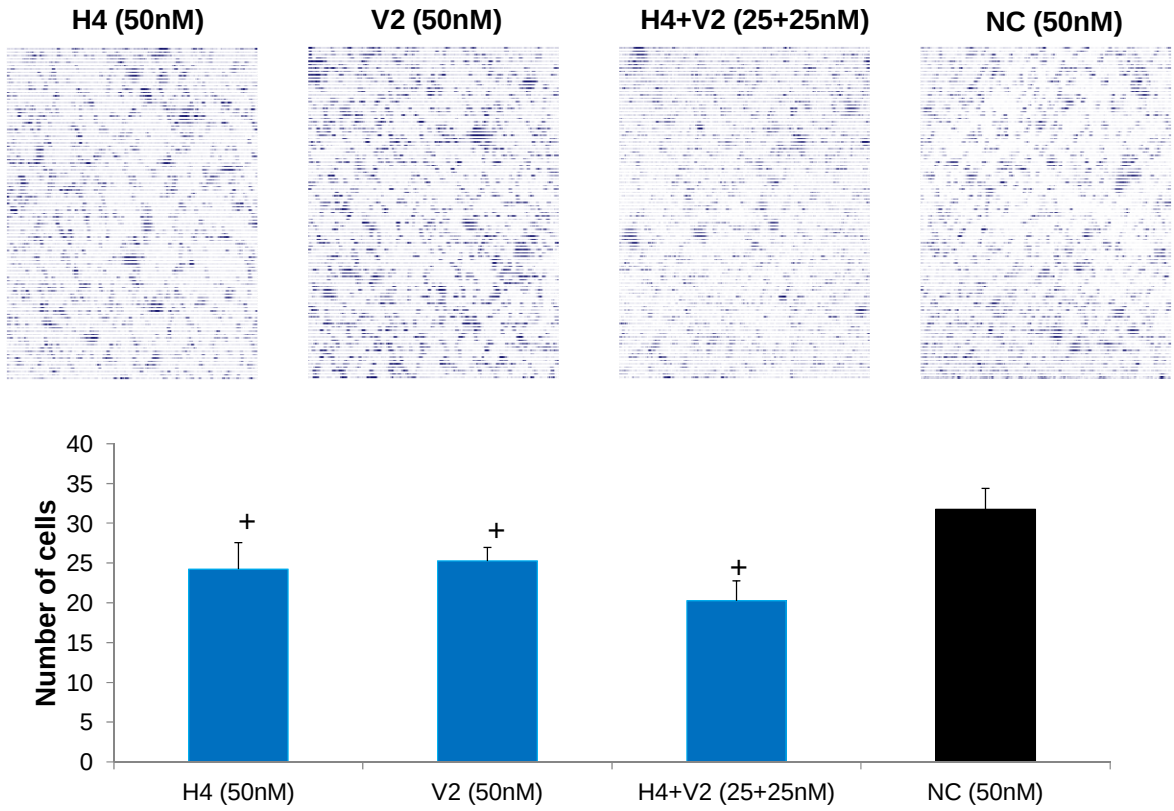

Figure 34. Inhibition of cell migration by HER2 and VEGF siRNAs.MCF-7/HER2 cells were transfected with H4 siRNA (50 nM), V2 siRNA (50 nM), combination of H4 and V2 siRNAs (25 nM + 25 nM), and negative control siRNA (50 nM) in the presence of Lipofectamine 2000. Twenty-four hours after the transfection, cells were trypsinized and plated in the top chamber of the Transwell. RPMI 1640 medium with 10% FBS was added in the lower chamber as a chemoattractant. After incubation for 48 h, cells that did not migrate through the pores were mechanically removed and cells on the lower surface of the membrane were fixed and stained. Images of migrated cells were obtained using an inverted microscope with a magnification of 100×. The number of migrated cells was counted from 3 randomly selected fields in a blind way. + indicates $p < 0.05$ compared to the negative control siRNA (50 mM) group.

cancer is always associated with more aggressive tumor phenotypes, we examined the effect of siRNAs on the migration ability of MCF-7/HER2 (**Figure 34**) and SK-BR-3 (**Figure 35**) cells using an *in vitro* migration assay, which is a simplified model to simulate the *in vivo* metastatic

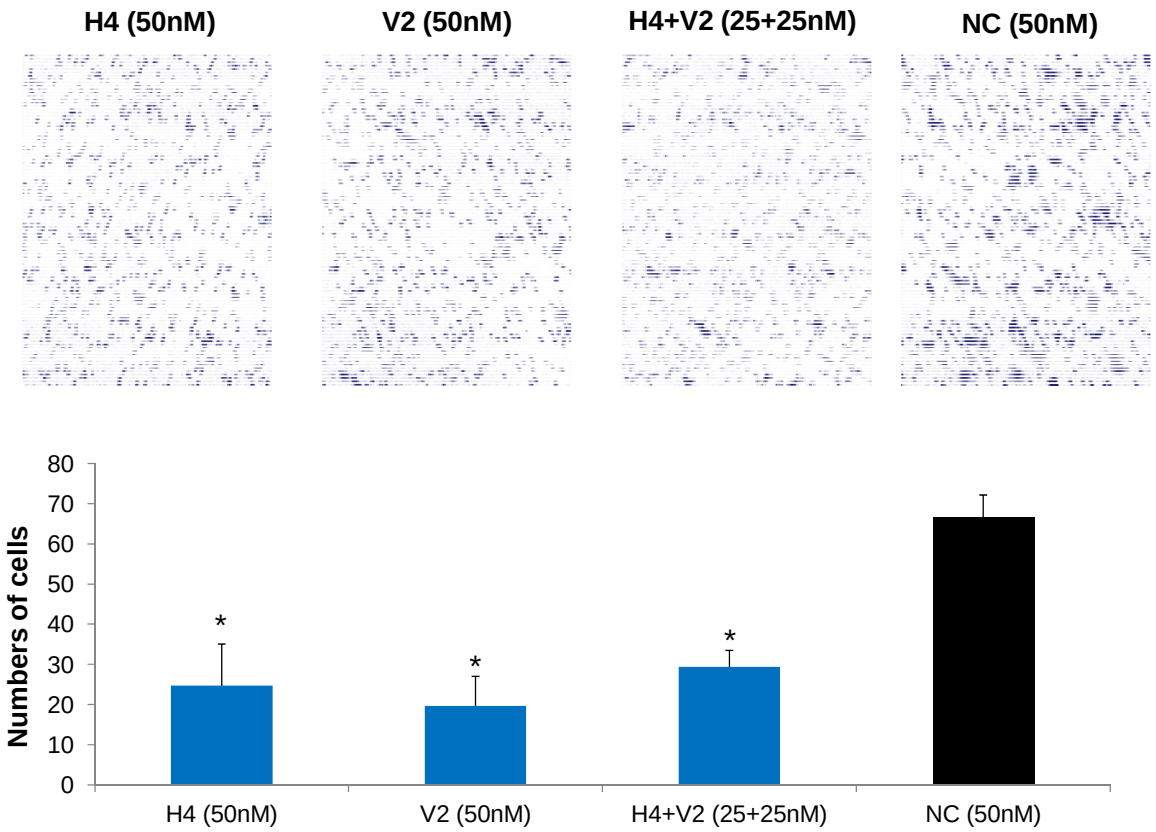

Figure 35. Inhibition of cell migration by HER2 and VEGF siRNAs.SK-BR-3 (B) cells were transfected with H4 siRNA (50 nM), V2 siRNA (50 nM), combination of H4 and V2 siRNAs (25 nM + 25 nM), and negative control siRNA (50 nM) in the presence of Lipofectamine 2000. Twenty-four hours after the transfection, cells were trypsinized and plated in the top chamber of the Transwell. RPMI 1640 medium with 10% FBS was added in the lower chamber as a chemoattractant. After incubation for 48 h, cells that did not migrate through the pores were mechanically removed and cells on the lower surface of the membrane were fixed and stained. Images of migrated cells were obtained using an inverted microscope with a magnification of 100×. The number of migrated cells was counted from 3 randomly selected fields in a blind way. * indicates $p < 0.01$ compared to the negative control siRNA (50 nM) group.

process [273]. As shown in **Figure 35**, there was a dramatic inhibition on SK-BR-3 cells' migration ability after the treatment with H4 siRNA, V2 siRNA, and H4/V2 siRNA mixture. Compared with the scrambled siRNA, silencing of HER2 or VEGF gene caused an average of 63%

and 71% decreased migration ability respectively. The number of migrated cells is similar for cells treated with H4, V2, and H4/V2 siRNAs (**Figure 35**, bottom), indicating there is little synergistic effect on the cell migration ability. The migration ability of MCF-7/HER2 cells was also inhibited by the treatment of siRNA (**Figure 34**), although the inhibition was less than that of SK-BR-3 cells.

Effect of HER2 and VEGF siRNAs on cell spreading and adhesion to ECM

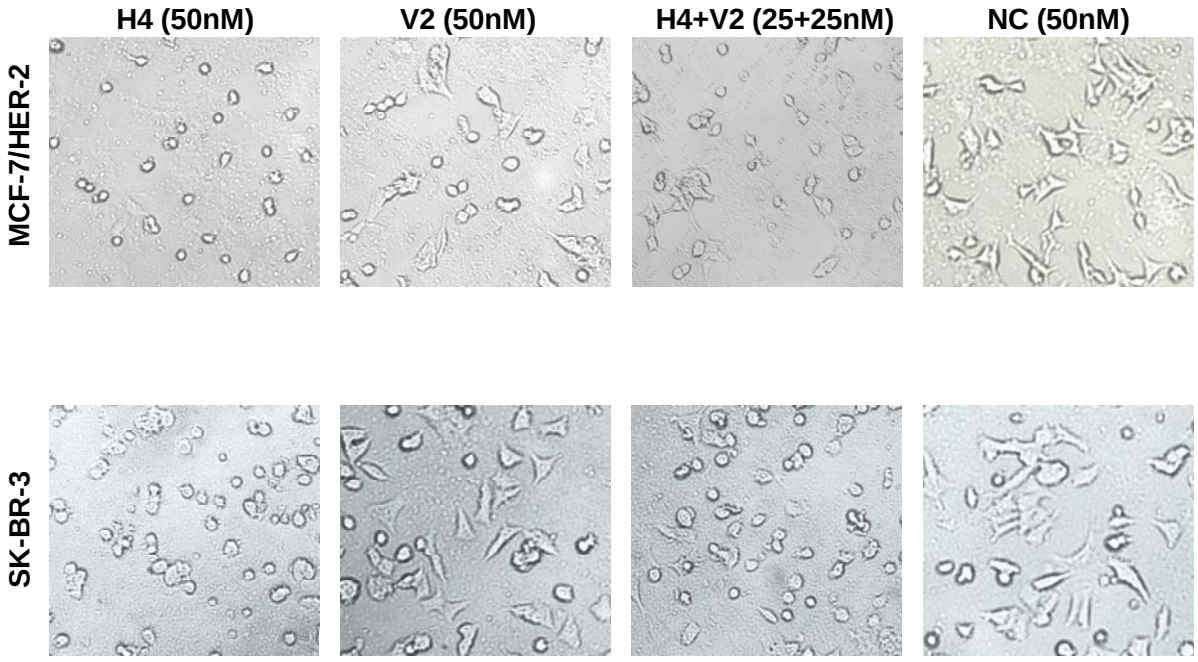

Figure 36. Effect of HER2 and VEGF siRNAs on cell spreading. MCF-7/HER2 and SK-BR-3 cells were transfected with siRNA, and harvested at 48 h post-transfection. Harvested cells were plated onto a Matrigel-treated plate which was coated with Matrigel. Cells were allowed to spread for 10−24 h at 37 °C. Cell images were taken by an inverted microscope with 100× magnification at 20 h postincubation. Spreading cells were defined as cells with extended processes, and unspreading cells were defined as round cells. The representative pictures shown in this figure were taken 20 h after plating.

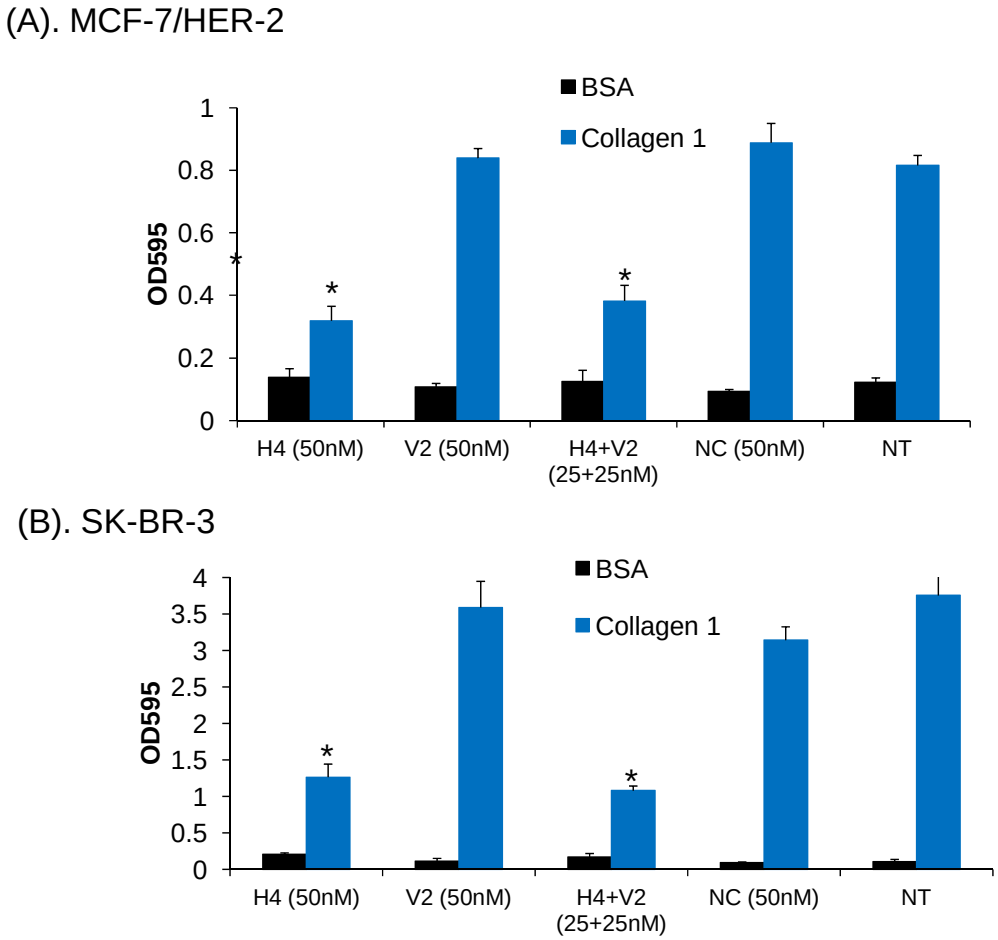

Figure 37. Adhesion of MCF-7/HER2 (A) and SK-BR-3 (B) cells to ECM and BSA after the treatment with siRNA. Forty-eight hours after the transfection, cells were harvested, resuspended, and seeded in a 96 well plate which was pretreated with 30 µg/mL type I collagen or 1% BSA. Cells were allowed to adhere for 1 h and nonattached cells were removed by washing. Attached cells were fixed, stained with crystal violet, followed by measuring the absorbance at 595 nm. * indicates $p < 0.01$ compared to the negative control siRNA (50 nM) group.

Next, we evaluated the influence of siRNA on cellular motility by comparing the spreading ability of cells on Matrigel coated plates. Two HER2 positive cell lines, SK-BR-3 and MCF-7/HER2, were selected to perform the cell spreading assay (**Figure 36**). After seeded on the

Matrigel coated plate, cells treated with scrambled siRNA started to form multiple filopodia and lamellipodia, leading to typical branching and spreading cells. In contrast, most of the H4 siRNA treated cells attached, but remained round shape even after 20 h, indicating the inhibition of spreading ability. The V2 siRNA treated cells showed similar cell spreading phenotype as the cells treated with scrambled siRNA. However, cells treated with H4/V2 siRNA mixture showed very similar phenotype changes as the cells treated with H4 siRNA alone.

HER2 is reported to mediate the adhesion of cells to extra cellular matrix (ECM) as an upstream signal mediator to affect adhesion molecules such as integrins, cadherins and selectins [272]. We examined the adhesion ability of HER2 positive breast cancer cells to ECM after treating with HER2 and VEGF specific siRNAs. As **Figure 37A** indicated, suppression of HER2 expression dramatically inhibit adhesion of MCF-7/HER2 and SK-BR-3 cells to type I collagen, a major component of ECM. VEGF specific siRNA (V2 group) did not show any inhibition on tumor cell adhesion compared to scrambled siRNA and non-treated (NT) group. However, the mixture of H4 and V2 siRNA at low concentration (25+25 nM) showed similar inhibition effect compared to H4 siRNA alone at 50nM. Similar results were observed in SK-BR-3 cells (**Figure 37B**), except that the H4/V2 siRNA mixture showed more significant effect as the H4 siRNA alone, indicating a synergistic effect of HER2 and VEGF siRNAs on tumor cell adhesion. Plates coated with BSA were used as a negative control, and all cells showed negligible adhesion.

Cell proliferation and apoptosis

Since both HER2 and VEGF over-expressions are known to stimulate tumor cell growth [42, 274], we examined cell proliferation of HER2 positive breast cancer cells after the silencing

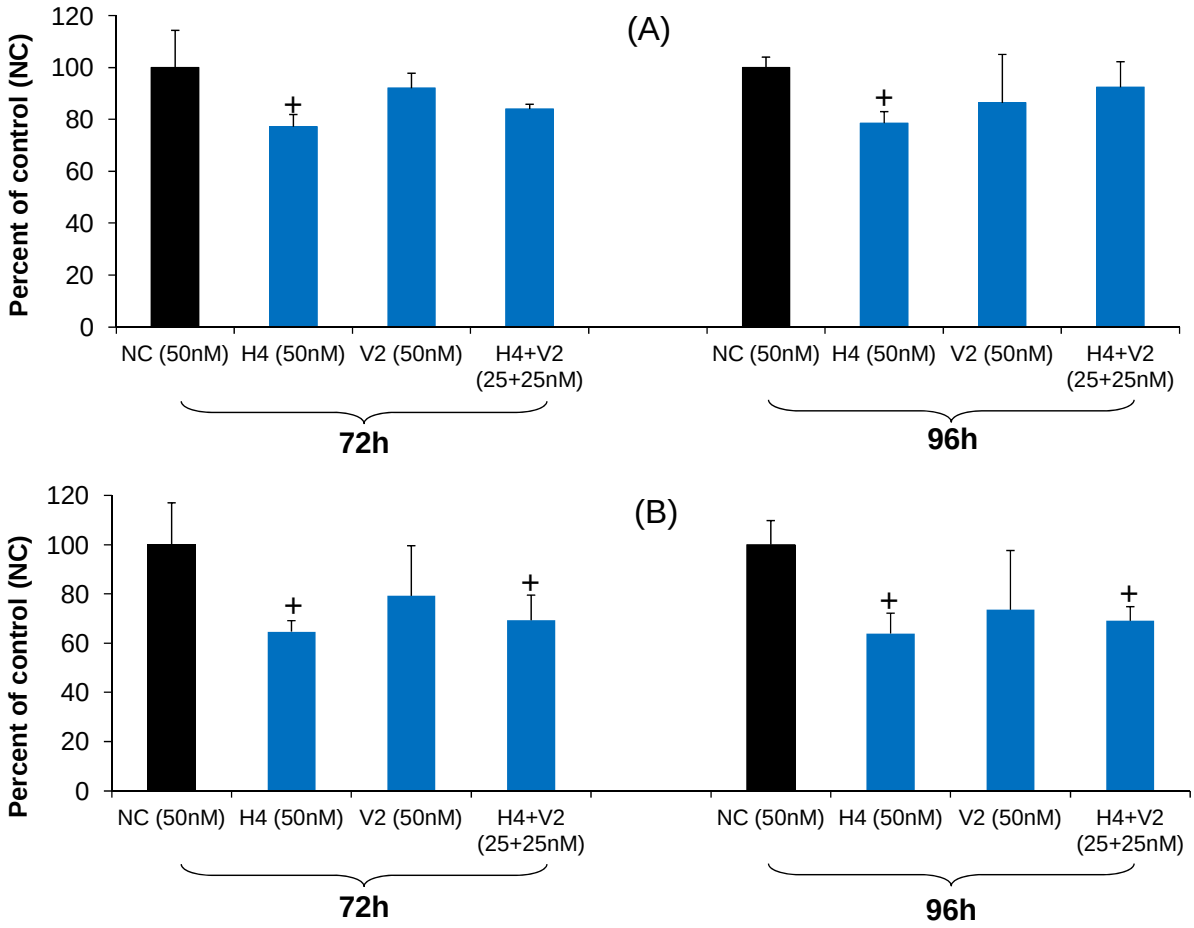

Figure 38. Effect of HER2 and VEGF specific siRNAs on the proliferation of MCF-7/HER2 (A) and SK-BR-3 (B) cells. Cells were transfected with H4, V2, H4 + V2, and negative control siRNAs. The proliferation was assayed in triplicate at 72 h, 96 h post-transfection using CellTiter-Glo Luminescent cell viability kits. Results were represented as mean ± SD (n = 3). * indicates $p < 0.05$ compared to the negative control siRNA (50 nM) group

of HER2 and VEGF genes. Cell proliferation was determined using CellTiter-Glo® Luminescent Cell Viability Assay at 72h and 96h post-transfection. At both time points, the cell proliferation was found inhibited in all three groups (H4, V2, and H4/V2) compared to the scrambled siRNA group (**Figure 38**). The inhibition effect in SK-BR3 cells (**Figure 38B**) was more significant than that in MCF-7/HER2 cells (**Figure 38A**). The H4 siRNA treated group showed the highest

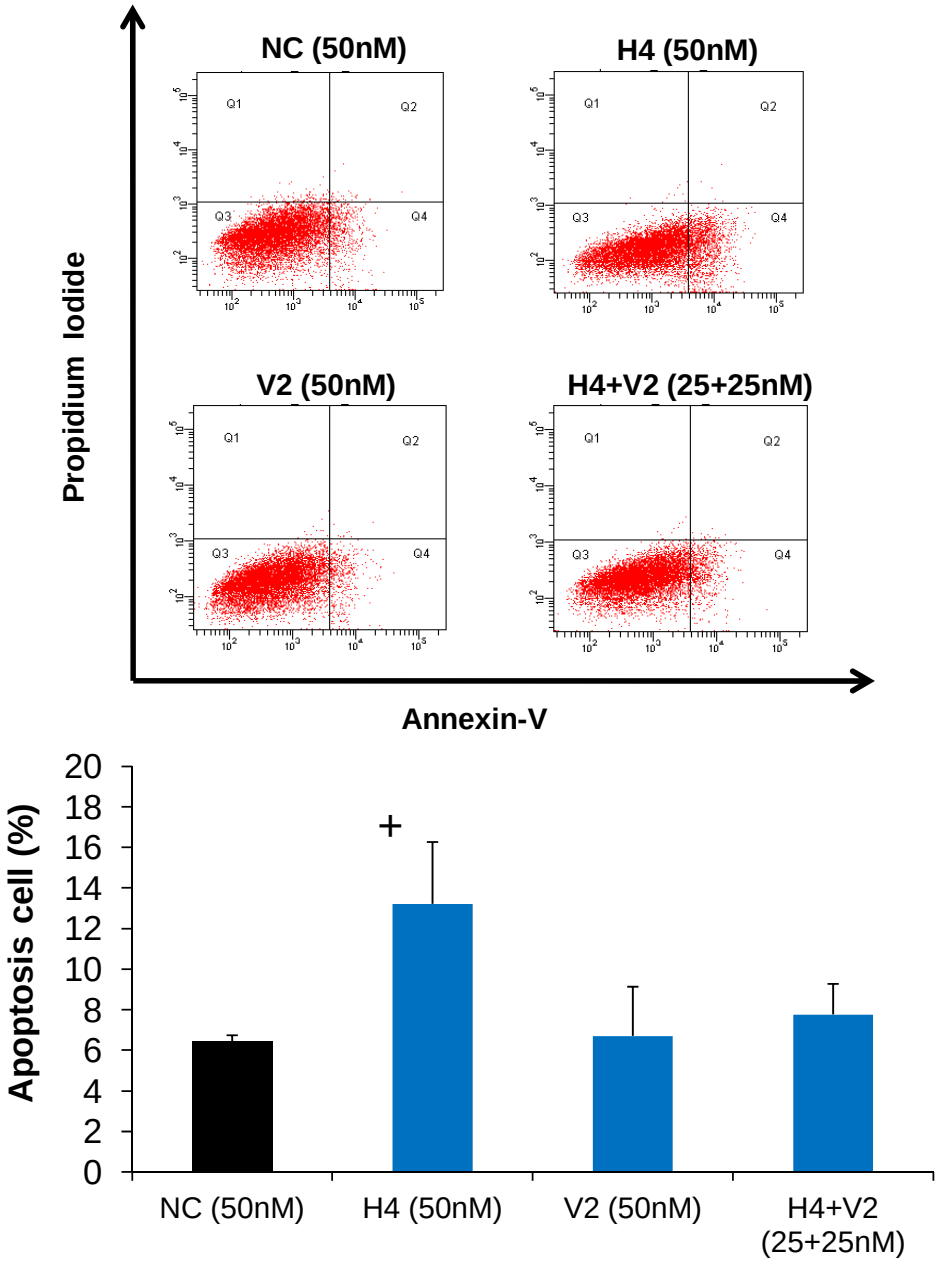

Figure 39. Flow cytometry analysis of cell apoptosis. SK-BR-3 cells were first transfected with H4, V2, H4/V2, and negative control siRNAs. Seventy-two hours after the transfection, cells were trypsinized, stained with Annexin V-FITC and PI using the Annexin V-FITC Apoptosis Detection Kit I. PI positive indicates cell necrosis, while Annexin V positive indicates cell apoptosis. PI positive/Annexin V negative indicates cell necrosis, while Annexin V positive/PI negative and Annexin V positive/PI positive indicate early apoptosis and late apoptosis respectively. * indicates $p < 0.05$ compared to the control siRNA (50 nM) group.

inhibition effect, followed by the H4/V2 siRNA mixture and V2 siRNA alone. This effect is similar to our observation using MTT assay (data not shown). The proliferation inhibition effect at 96h post-transfection is slighter higher than that at 72 h post-transfection.

Furthermore, flow cytometry was used to assay apoptosis of breast cancer cells after the treatment with HER2 and VEGF siRNAs. As **Figure 39** illustrated, we only observed increased apoptosis in H4 siRNA treated cells, but not in V2 and H4/V2 treated cells. Approximately, 12%~16% of cells were identified early apoptosis 72 hours after the H4 siRNA treatment. This is in accordance with the finding that a retrovirus-mediated siRNA against HER2 induced apoptosis of breast and ovarian tumor cells [42]. However, no significant apoptosis was observed in V2 siRNA treated group, which is different from other reports that blockade of VEGF induced apoptosis of breast cancer cells [275, 276]. It was proposed that VEGF acts as an internal autocrine survival factor via binding to VEGF receptor 1 (VEGFR1) [276]. In this study, we used SK-BR-3 cell line, which is VEGFR1 negative [277]. Therefore, the lack of VEGFR1 may abolish the ability of VEGF as the survival factor, leading to little difference after silencing VEGF expression. Although increased apoptosis was observed in H4 treated cells, H4/V2 treated cells only showed slightly increase of apoptotic cells compared to NC siRNA treated cells. Probably it can be explained by different concentration of H4 siRNA in these two groups. As shown in **Figure 31A** & **32A**, higher concentration of H4 siRNA (50nM in H4 group) gave a more potent silencing effect than lower concentration (25nM in H4/V2 group). Sufficient HER2 neutralization by H4 siRNA was essential to induce apoptosis.

6.4. Discussion

HER2 positive breast cancer is always associated with aggressive phenotypes, more likelihood of lymph node involvement and increased resistance to endocrine therapy [40]. On the other hand, over-expression of HER2 is highly associated with up-regulated VEGF, which is the key angiogenic growth factor in breast cancer. Angiogenesis is not only essential for tumor growth, but also essential in tumor cell spreading and migration. Breast cancer cells not only produce VEGF, but also express VEGF receptors on cell surface. This combination of receptor and ligand acts as an autocrine loop to facilitate tumor cell migration, invasion, proliferation, and survive [276, 278]. Early stage breast cancer patients with over-expressed VEGF tend to have increased metastatic potential and significant resistance to systemic chemotherapy and hormonal therapy [279].

Currently, most of the cancer therapeutics targeting HER2 or VEGF focused on monoclonal antibodies. Although there are several reports using antisense oligonucleotide [122] or siRNA[41, 42, 125] to inhibit HER2, our study represents the first report using combination of HER2 and VEGF siRNAs to inhibit the invasiveness and growth of HER2 positive breast cancer cells. Using two different breast cancer cell lines with overexpressed HER2, we demonstrated the significant knockdown of target genes by the predesigned HER2 and VEGF siRNAs. Concurrently, the cells treated with siRNAs displayed a variety of biologic effects including the inhibition of invasiveness and cell growth. The combination of HER2 and VEGF siRNAs holds a great promise for the treatment of HER2 positive breast cancer.

To get precise silencing effect, we adopted ELISA and real time RT-PCR to quantitatively detect the expression of target gene at protein and mRNA levels respectively. The silencing

effect was first evaluated at the protein level using ELISA method due to its accuracy and simplicity. For the siRNA silencing study, selection of a correct control group is very critical to avoid the artificial effects. Currently, most of the *in vitro* siRNA transfections use cationic lipids, and the transfection itself may affect the gene expression profiles of treated cells. Therefore, a scrambled siRNA, which does not target any genes, was incorporated as a negative control (NC) in all siRNA silencing and functional studies to avoid the possible artificial effects. As shown in **Figure 30 A&C**, majority of the predesigned siRNAs showed more or less silencing effect and some of them silenced the protein expression up to 83.5%, indicating the feasibility of designing siRNAs using publicly accessible designers. It also suggested the necessity to screen multiple siRNAs targeting at different mRNA regions to identify the most potent siRNA. To confirm the specificity of these silencing effects, quantitative real time RT-PCR was also conducted for the most potent siRNAs. Silencing effect at the mRNA level was consistent with that at the protein level. We also showed that the silencing effect of H4 and V2 siRNAs reached a plateau when the concentration was increased to 50nm and 25nM respectively. This is in accordance with other reports indicating the non-linear relationship between the dose and silencing effect [264, 280].

It has been shown that HER2 signaling pathway impacts neoangiogenesis, and overexpressed HER2 is correlated with up-regulation of VEGF in breast cancer [272]. HER2 serves as an upstream regulator of VEGF gene expression, although the mechanism is still under controversial. Pak1[281], PI3K[282], HIF-1a[271] and transcription factor SP1[257] probably involves in the regulation. As **Figure 32C&D** showed, HER2 siRNA exhibited significant inhibition on VEGF, which is in agreement with the observation that a murine monoclonal antibody against HER2 reduced VEGF expression in a dose-dependent manner [270]. Moreover,

a significant synergistic silencing effect on VEGF was observed when H4 and V2 siRNAs were used simultaneously at a low concentration, providing a sound rationale for future therapeutic application of this dual silencing strategy. VEGF siRNA alone showed little effect on HER2, but the combination of H4 and V2 siRNAs showed comparable silencing effect on HER2 as the H4 siRNA alone. The synergistic effect of HER2 and VEGF siRNAs is more significant in silencing VEGF than HER2.

For the first time, we conducted numerous studies to evaluate the biological effect of dual HER2 and VEGF siRNAs on invasion and metastasis properties of HER2 positive breast cancer cells. Cell motility is the key step in organ invasion by tumor cells, and the most motile tumor cells acquire the ability to metastasis by dedifferentiation to a mesenchymal cell phenotype, to allow the dissociation from tumour mass and disseminate via bloodstream [283]. We have observed significant morphology change after the treatment with H4 or H4/V2 siRNAs, indicating the reduced motility. However, few changes were found in V2 siRNA alone (**Figure 33**), suggesting that HER2 siRNA has more effect on the cell morphology than that of VEGF siRNA.

We have demonstrated that both HER2 and VEGF siRNAs significantly inhibited the migration ability of breast cancer cells (**Figure 34&35**). The inhibition effect was more significant in SK-BR-3 cells than that in MCF-7/HER2 cells. It may be explained by the fact that MCF-7/HER2 cells are engineered from MCF-7 cells to overexpress HER2, while SK-BR-3 cells are naturally HER2 positive tumor cells. This difference between MCF-7/HER2 and SK-BR-3 cells was also observed in the proliferation assay (**Figure 38**). Although there are several reports using HER2 siRNA to inhibit tumor growth, our data demonstrated for the first time that

HER2 siRNA could inhibit cell migration and invasion abilities. In addition, Timoshenko et al. have reported that endogenous VEGF produced by metastatic breast cancer cells promoted the migratory function [284]. Our finding further proved the role of VEGF in the tumor migration ability, and subsequently demonstrated the potential of using VEGF siRNA to inhibit tumor cell migration.

HER2 plays an important role in the spreading of HER2 positive breast cancer cells. De Corte et al. reported that activation of HER2 by a 50kDa putative HER2 ligand could enhance SK-BR-3 cells' spreading [285]. In contrast, binding of the HER2 extracellular domain with its antibody inhibited cell spreading of HER2 positive tumor cells [285, 286]. In our study, we observed that knockdown of HER2 gene by siRNA inhibited cell spreading of MCF-7/HER2 and SK-BR-3 cells under 10% FBS condition (**Figure 37**). This is also in accordance with a previous finding in which the anti-HER2 antisense oligonucleotide effectively inhibited the spreading activity of an ovarian cancer cell line SK-OV-3 [287]. On the other hand, it has been reported that cell spreading ability was lost in human lung adenocarcinoma cell line A549 cells after the knockdown of HER3 by anti-HER3 siRNAs [267]. Taken together, these observations suggested that HER2/HER3 dimer might play an important role in tumor cell spreading. As a result, blocking HER2 provides an efficient strategy to inhibit cell spreading. No significant difference was observed between V2 and scrambled siRNA treated groups, indicating little influence of VEGF on cell spreading ability.

Several million cells per gram of tumor can be dissociated daily into the lymphatic and blood circulation [288]. In order to metastasize to new organs, disseminated tumor cells in blood circulation must re-establish adhesive connections to endothelium in target tissues [283, 289]. It

is believed that HER2 potentiates metastasis via promoting tumor cell adhesion to endothelial cells and invasion of basement membranes in the metastatic cascade [290]. For example, adhesion of lung tumor cells to ECM protects cells from chemotherapeutic drugs [291]. The role of HER2 in breast cancer cell adhesion is complicated due to its integration with many adhesion signaling systems and associated with cell-cell and cell-ECM adhesion interaction [272]. Our results showed that blocking HER2 expression with siRNA H4 significantly suppressed the adhesion ability of tumor cells to type I collagen, which is a major component of the endothelium [289]. Similar inhibition effect on adhesion ability was reported in breast cancer cells after the treatment with a suppressor gene of HER2 [290]. Although VEGF specific siRNA alone did not show any effect on the cell adhesion to type I collagen, the combination of VEGF and HER2 siRNAs demonstrated dramatic inhibition on cell adhesion ability.

HER2 promotes breast cancer cell proliferation via various signaling pathways. The anti-proliferation effects of HER2 specific siRNA have been reported by several groups using retrovirus-mediated and synthetic siRNAs [41, 42, 125]. However, retrovirus-mediated siRNA will not be suitable for future therapeutic application due to the safety concern. Here, we demonstrated the similar inhibition effect of synthetic HER2 siRNA on cell proliferation in HER2 positive SK-BR-3 cells at a very low concentration using different methods including MTT assay (data not shown) and ATP modulated cell proliferation assay (**Figure 38**). Our and other results strongly confirmed that blockade of HER2 expression could inhibit the proliferation of HER2 positive breast cancer cells. Moreover, we observed that both V2 and V2/H4 siRNAs significantly inhibited breast cancer cell proliferation.

It is well known that VEGF can regulate the proliferation and migration of endothelial cells. Binding of VEGF to its receptors induces the activation of several downstream kinase, including protein kinase C and D, PI3K, and MAPK [292]. VEGF receptors have been initially assumed only express on endothelial cells, recent data indicated its expression is more widespread. It is believed that both VEGFR1 and VEGFR2 are expressed in numerous breast cancer cells, albeit some conclusions are controversial [276, 293]. VEGFR2 is highly expressed in vascular endothelial cells and the VEGF/VEGFR2 mediated signaling loop is mainly responsible for the proliferation response in endothelial cells [294]. It is proved that VEGF promotes proliferation of breast cancer cells via VEGFR2 [274]. We observed anti-proliferative effect of VEGF specific siRNA in SK-BR-3 cells, but not as significant as that of anti-VEGF antibody to MDA-MB-231 which expresses a much higher level of VEGFR2 [295, 296].

We observed a significant increase of apoptosis in SK-BR-3 cells after the treatment with HER2 siRNA (**Figure 39**), which is in agreement with a previous study using retroviral HER2 shRNA [42]. VEGF has been shown as a survival factors for endothelial cells [297]. It also acts as an internal autocrine survival factor via binding to VEGFR1, but not through VEGFR2. Inhibition of VEGF expression induced apoptosis in VEGFR1 positive MDA-MB-231 breast cancer cells [276]. However, we did not observe the apoptosis in SK-BR-3 cells after the treatment with VEGF siRNA. It is probably due to the low expression of VEGFR1 in SK-BR-3 cells [277].

In general, HER2 siRNA showed more effects than VEGF siRNA in inhibiting tumor cell metastasis-associated properties and cell survival. It has been reported that anti-VEGF strategy produced more significant growth inhibition *in vivo* than that *in vitro* because there are no blood

vessels with endothelial cells formed in the *in vitro* system, while antiangiogenesis is one of the major effects of the anti-VEGF therapy [259].

6.5. Conclusion

We have designed and screened potent siRNAs targeting HER2 and VEGF genes respectively. This is the first report to explore the application of dual silencing of HER2 and VEGF genes to inhibit tumor growth and invasiveness. Both HER2 siRNA and VEGF siRNA showed significant inhibition on cell migration and proliferation. HER2 siRNA also demonstrated dramatic suppression on cell spreading and adhesion to ECM, as well as induction of apoptosis. Dual silencing of HER2 and VEGF exhibited substantial suppression effect on cell growth and invasiveness, supporting the hypothesis that HER2 positive breast cancer can be more effectively treated by dual inhibition of HER2 and VEGF gene expressions.

LETTERS OF PERMISSION

RightsLink®

Home | Account Info | Help

Title: Inhibition of Breast Cancer Cell Growth and Invasiveness by Dual Silencing of HER-2 and VEGF

Logged in as: Wanyi Tai

LOGOUT

Author: Wanyi Tai, Bin Qin, and Kun Cheng

Publication: Molecular Pharmaceutics

Publisher: American Chemical Society

Date: Apr 1, 2010

PERMISSION/LICENSE IS GRANTED FOR YOUR ORDER AT NO CHARGE

This type of permission/license, instead of the standard Terms & Conditions, is sent to you because no fee is being charged for your order. Please note the following:

- Permission is granted for your request in both print and electronic formats, and translations.
- If figures and/or tables were requested, they may be adapted or used in part.
- Please print this page for your records and send a copy of it to your publisher/graduate school.
- Appropriate credit for the requested material should be given as follows: "Reprinted (adapted) with permission from (COMPLETE REFERENCE CITATION). Copyright (YEAR) American Chemical Society." Insert appropriate information in place of the capitalized words.
- One-time permission is granted only for the use specified in your request. No additional uses are granted (such as derivative works or other editions). For any other uses, please submit a new request.

BACK | CLOSE WINDOW

PERMISSION/LICENSE IS GRANTED FOR YOUR ORDER AT NO CHARGE

This type of permission/license, instead of the standard Terms & Conditions, is sent to you because no fee is being charged for your order. Please note the following:

- Permission is granted for your request in both print and electronic formats, and translations.
- If figures and/or tables were requested, they may be adapted or used in part.
- Please print this page for your records and send a copy of it to your publisher/graduate school.
- Appropriate credit for the requested material should be given as follows: "Reprinted (adapted) with permission from (COMPLETE REFERENCE CITATION). Copyright (YEAR) American Chemical Society." Insert appropriate information in place of the capitalized words.
- One-time permission is granted only for the use specified in your request. No additional uses are granted (such as derivative works or other editions). For any other uses, please submit a new request.

BACK CLOSE WINDOW

Copyright Clearance Center RightsLink®

Home | Account Info | Help

Title: The role of HER2 in cancer therapy and targeted drug delivery

Author: Wanyi Tai,Rubi Mahato,Kun Cheng

Publication: Journal of Controlled Release

Publisher: Elsevier

Date: 15 September 2010

Logged in as:
Wanyi Tai
Account #:
3000552872

LOGOUT

Order Completed

Thank you very much for your order.

This is a License Agreement between Wanyi Tai ("You") and Elsevier ("Elsevier"). The license consists of your order details, the terms and conditions provided by Elsevier, and the payment terms and conditions.

Get the printable license.

License Number	2964370984503
License date	Aug 08, 2012
Licensed content publisher	Elsevier
Licensed content publication	Journal of Controlled Release
Licensed content title	The role of HER2 in cancer therapy and targeted drug delivery
Licensed content author	Wanyi Tai,Rubi Mahato,Kun Cheng
Licensed content date	15 September 2010
Licensed content volume number	146
Licensed content issue number	3
Number of pages	12
Type of Use	reuse in a thesis/dissertation
Portion	full article
Format	both print and electronic
Are you the author of this Elsevier article?	Yes
Will you be translating?	No
Order reference number	
Title of your thesis/dissertation	Development of drug conjugates for cancer therapy and evaluation of dual siRNA silencing effect on breast cancer growth and invasion
Expected completion date	Aug 2012
Estimated size (number of pages)	190
Elsevier VAT number	GB 494 6272 12
Permissions price	0.00 USD
VAT/Local Sales Tax	0.0 USD / 0.0 GBP
Total	0.00 USD

ORDER MORE... | CLOSE WINDOW

Copyright Clearance Center RightsLink®

Home | Account Info | Help

Title: Prodrugs for improving tumor targetability and efficiency

Author: Rubi Mahato,Wanyi Tai,Kun Cheng

Publication: Advanced Drug Delivery Reviews

Publisher: Elsevier

Date: 18 July 2011

Logged in as:
Wanyi Tai
Account #:
3000552872

LOGOUT

Order Completed

Thank you very much for your order.

This is a License Agreement between Wanyi Tai ("You") and Elsevier ("Elsevier"). The license consists of your order details, the terms and conditions provided by Elsevier, and the payment terms and conditions.

Get the printable license.

License Number	2964380042143
License date	Aug 08, 2012
Licensed content publisher	Elsevier
Licensed content publication	Advanced Drug Delivery Reviews
Licensed content title	Prodrugs for improving tumor targetability and efficiency
Licensed content author	Rubi Mahato,Wanyi Tai,Kun Cheng
Licensed content date	18 July 2011
Licensed content volume number	63
Licensed content issue number	8
Number of pages	12
Type of Use	reuse in a thesis/dissertation
Portion	full article
Format	both print and electronic
Are you the author of this Elsevier article?	Yes
Will you be translating?	No
Order reference number	
Title of your thesis/dissertation	Development of drug conjugates for cancer therapy and evaluation of dual siRNA silencing effect on breast cancer growth and invasion
Expected completion date	Aug 2012
Estimated size (number of pages)	190
Elsevier VAT number	GB 494 6272 12
Permissions price	0.00 USD
VAT/Local Sales Tax	0.0 USD / 0.0 GBP
Total	0.00 USD

ORDER MORE... | CLOSE WINDOW

REFERENCE LIST

1. Jemal, A., et al., *Global cancer statistics.* CA Cancer J Clin, 2011. **61**(2): p. 69-90.
2. Anand, P., et al., *Cancer is a preventable disease that requires major lifestyle changes.* Pharm Res, 2008. **25**(9): p. 2097-116.
3. Jackson, S.P., et al., *PI 3-kinase p110beta: a new target for antithrombotic therapy.* Nat Med, 2005. **11**(5): p. 507-14.
4. Tai, W., R. Mahato, and K. Cheng, *The role of HER2 in cancer therapy and targeted drug delivery.* J Control Release, 2010. **146**(3): p. 264-75.
5. Venter, D.J., et al., *Overexpression of the c-erbB-2 oncoprotein in human breast carcinomas: immunohistological assessment correlates with gene amplification.* Lancet, 1987. **2**(8550): p. 69-72.
6. Blume-Jensen, P. and T. Hunter, *Oncogenic kinase signalling.* Nature, 2001. **411**(6835): p. 355-65.
7. Manning, G., et al., *The protein kinase complement of the human genome.* Science, 2002. **298**(5600): p. 1912-34.
8. Cohen, P., *Protein kinases--the major drug targets of the twenty-first century?* Nat Rev Drug Discov, 2002. **1**(4): p. 309-15.
9. Vieth, M., et al., *Kinomics-structural biology and chemogenomics of kinase inhibitors and targets.* Biochim Biophys Acta, 2004. **1697**(1-2): p. 243-57.
10. Garcia-Echeverria, C. and D. Fabbro, *Therapeutically targeted anticancer agents: inhibitors of receptor tyrosine kinases.* Mini Rev Med Chem, 2004. **4**(3): p. 273-83.
11. Balk, S.P., Y.J. Ko, and G.J. Bubley, *Biology of prostate-specific antigen.* J Clin Oncol, 2003. **21**(2): p. 383-91.
12. O'Keefe, D.S., D.J. Bacich, and W.D. Heston, *Comparative analysis of prostate-specific membrane antigen (PSMA) versus a prostate-specific membrane antigen-like gene.* Prostate, 2004. **58**(2): p. 200-10.
13. Garsky, V.M., et al., *The synthesis of a prodrug of doxorubicin designed to provide reduced systemic toxicity and greater target efficacy.* J Med Chem, 2001. **44**(24): p. 4216-24.
14. Denmeade, S.R., et al., *Prostate-specific antigen-activated thapsigargin prodrug as targeted therapy for prostate cancer.* J Natl Cancer Inst, 2003. **95**(13): p. 990-1000.
15. S. Denmeade1, D.R., S. Christensen2, C. Dionne3 and J. Isaacs1, *A Thapsigargin Prodrug Produces Sustained Growth Inhibition and Substantial Regression of Human Breast Cancers In Vivo with Minimal Host Toxicity.* Thirty-Second Annual CTRC-AACR San Antonio Breast Cancer Symposium, 2009.
16. Van Valckenborgh, E., et al., *Targeting an MMP-9-activated prodrug to multiple myeloma-diseased bone marrow: a proof of principle in the 5T33MM mouse model.* Leukemia, 2005. **19**(9): p. 1628-33.
17. Acker, H., F. Pietruschka, and J. Deutscher, *Endothelial cell mitogen released from HT29 tumour cells grown in monolayer or multicellular spheroid culture.* Br J Cancer, 1990. **62**(3): p. 376-7.
18. Carmeliet, P., *Mechanisms of angiogenesis and arteriogenesis.* Nat Med, 2000. **6**(4): p. 389-95.

19. Eichholz, A., S. Merchant, and A.M. Gaya, *Anti-angiogenesis therapies: their potential in cancer management.* OncoTargets and therapy, 2010. **3**: p. 69-82.
20. Hoeben, A., et al., *Vascular endothelial growth factor and angiogenesis.* Pharmacol Rev, 2004. **56**(4): p. 549-80.
21. Furuya, M., Y. Yonemitsu, and I. Aoki, *III. Angiogenesis: complexity of tumor vasculature and microenvironment.* Current pharmaceutical design, 2009. **15**(16): p. 1854-67.
22. Abdollahi, A., et al., *Transcriptional network governing the angiogenic switch in human pancreatic cancer.* Proc Natl Acad Sci U S A, 2007. **104**(31): p. 12890-5.
23. Nagy, J.A., et al., *Why are tumour blood vessels abnormal and why is it important to know?* Br J Cancer, 2009. **100**(6): p. 865-9.
24. Torchilin, V.P., *Drug targeting.* Eur J Pharm Sci, 2000. **11 Suppl 2**: p. S81-91.
25. Matsumura, Y. and H. Maeda, *A new concept for macromolecular therapeutics in cancer chemotherapy: mechanism of tumoritropic accumulation of proteins and the antitumor agent smancs.* Cancer Res, 1986. **46**(12 Pt 1): p. 6387-92.
26. Jain, R.K., *Determinants of tumor blood flow: a review.* Cancer Res, 1988. **48**(10): p. 2641-58.
27. Blancher, C., et al., *Effects of ras and von Hippel-Lindau (VHL) gene mutations on hypoxia-inducible factor (HIF)-1alpha, HIF-2alpha, and vascular endothelial growth factor expression and their regulation by the phosphatidylinositol 3'-kinase/Akt signaling pathway.* Cancer Res, 2001. **61**(19): p. 7349-55.
28. Vaupel, P. and A. Mayer, *Hypoxia in cancer: significance and impact on clinical outcome.* Cancer Metastasis Rev, 2007. **26**(2): p. 225-39.
29. Ahn, G.O. and M. Brown, *Targeting tumors with hypoxia-activated cytotoxins.* Front Biosci, 2007. **12**: p. 3483-501.
30. McKeown, S.R., R.L. Cowen, and K.J. Williams, *Bioreductive drugs: from concept to clinic.* Clin Oncol (R Coll Radiol), 2007. **19**(6): p. 427-42.
31. Cardone, R.A., V. Casavola, and S.J. Reshkin, *The role of disturbed pH dynamics and the Na+/H+ exchanger in metastasis.* Nat Rev Cancer, 2005. **5**(10): p. 786-95.
32. Kim, J.W. and C.V. Dang, *Cancer's molecular sweet tooth and the Warburg effect.* Cancer Res, 2006. **66**(18): p. 8927-30.
33. Feron, O., *Pyruvate into lactate and back: from the Warburg effect to symbiotic energy fuel exchange in cancer cells.* Radiother Oncol, 2009. **92**(3): p. 329-33.
34. Brahimi-Horn, M.C. and J. Pouyssegur, *Oxygen, a source of life and stress.* FEBS Lett, 2007. **581**(19): p. 3582-91.
35. Sawant, R.M., et al., *"SMART" drug delivery systems: double-targeted pH-responsive pharmaceutical nanocarriers.* Bioconjug Chem, 2006. **17**(4): p. 943-9.
36. Carmeliet, P. and R.K. Jain, *Principles and mechanisms of vessel normalization for cancer and other angiogenic diseases.* Nat Rev Drug Discov, 2011. **10**(6): p. 417-27.
37. Baxter, L.T. and R.K. Jain, *Transport of fluid and macromolecules in tumors. IV. A microscopic model of the perivascular distribution.* Microvasc Res, 1991. **41**(2): p. 252-72.
38. Nguyen, D.X., P.D. Bos, and J. Massague, *Metastasis: from dissemination to organ-specific colonization.* Nat Rev Cancer, 2009. **9**(4): p. 274-84.

39. Balasubramanian, P., et al., *Confocal images of circulating tumor cells obtained using a methodology and technology that removes normal cells.* Mol Pharm, 2009. **6**(5): p. 1402-8.
40. Engel, R.H. and V.G. Kaklamani, *HER2-positive breast cancer: current and future treatment strategies.* Drugs, 2007. **67**(9): p. 1329-41.
41. Faltus, T., et al., *Silencing of the HER2/neu gene by siRNA inhibits proliferation and induces apoptosis in HER2/neu-overexpressing breast cancer cells.* Neoplasia, 2004. **6**(6): p. 786-95.
42. Yang, G., et al., *Inhibition of breast and ovarian tumor growth through multiple signaling pathways by using retrovirus-mediated small interfering RNA against Her-2/neu gene expression.* J Biol Chem, 2004. **279**(6): p. 4339-45.
43. Pils, D., et al., *In ovarian cancer the prognostic influence of HER2/neu is not dependent on the CXCR4/SDF-1 signalling pathway.* Br J Cancer, 2007. **96**(3): p. 485-91.
44. Shawver, L.K., D. Slamon, and A. Ullrich, *Smart drugs: tyrosine kinase inhibitors in cancer therapy.* Cancer Cell, 2002. **1**(2): p. 117-23.
45. Roh, H., J. Pippin, and J.A. Drebin, *Down-regulation of HER2/neu expression induces apoptosis in human cancer cells that overexpress HER2/neu.* Cancer Res, 2000. **60**(3): p. 560-5.
46. Tai, W., B. Qin, and K. Cheng, *Inhibition of breast cancer cell growth and invasiveness by dual silencing of HER-2 and VEGF.* Mol Pharm.
47. Signoretti, S., et al., *Her-2-neu expression and progression toward androgen independence in human prostate cancer.* J Natl Cancer Inst, 2000. **92**(23): p. 1918-25.
48. Scher, H.I., *HER2 in prostate cancer--a viable target or innocent bystander?* J Natl Cancer Inst, 2000. **92**(23): p. 1866-8.
49. Ziada, A., et al., *The use of trastuzumab in the treatment of hormone refractory prostate cancer; phase II trial.* Prostate, 2004. **60**(4): p. 332-7.
50. Liu, Y., et al., *Inhibition of HER-2/neu kinase impairs androgen receptor recruitment to the androgen responsive enhancer.* Cancer Res, 2005. **65**(8): p. 3404-9.
51. Jia, L., et al., *Androgen receptor activity at the prostate specific antigen locus: steroidal and non-steroidal mechanisms.* Mol Cancer Res, 2003. **1**(5): p. 385-92.
52. Craft, N., et al., *A mechanism for hormone-independent prostate cancer through modulation of androgen receptor signaling by the HER-2/neu tyrosine kinase.* Nat Med, 1999. **5**(3): p. 280-5.
53. Yeh, S., et al., *From HER2/Neu signal cascade to androgen receptor and its coactivators: a novel pathway by induction of androgen target genes through MAP kinase in prostate cancer cells.* Proc Natl Acad Sci U S A, 1999. **96**(10): p. 5458-63.
54. Mellinghoff, I.K., et al., *HER2/neu kinase-dependent modulation of androgen receptor function through effects on DNA binding and stability.* Cancer Cell, 2004. **6**(5): p. 517-27.
55. Freeman, M.R., *HER2/HER3 heterodimers in prostate cancer: Whither HER1/EGFR?* Cancer Cell, 2004. **6**(5): p. 427-8.
56. Small, E.J., et al., *Docetaxel, estramustine, plus trastuzumab in patients with metastatic androgen-independent prostate cancer.* Semin Oncol, 2001. **28**(4 Suppl 15): p. 71-6.
57. Beck, A., et al., *The next generation of antibody-drug conjugates comes of age.* Discov Med, 2010. **10**(53): p. 329-39.

58. Teicher, B.A., *Antibody-drug conjugate targets.* Curr Cancer Drug Targets, 2009. **9**(8): p. 982-1004.
59. Hughes, B., *Antibody-drug conjugates for cancer: poised to deliver?* Nat Rev Drug Discov, 2010. **9**(9): p. 665-7.
60. S Sugarman, J.M., M Saleh, AF LoBuglio, D Jones, C Daniel, D LeBherz, H Brewer, D Healey, S Kelley, *A phase I study of BR96-doxorubicin (BR96-Dox) in patients with advanced carcinoma expressing the Lewis(Y) antigen* 1995 ASCO Annual Meeting, 1995. **No. 1532**.
61. A Tolcher, S.S., K Gelmon, R Cohen, M Saleh, C Isaacs, L Young, D Healey, W Slichenmyer *PHASE II RANDOMIZED STUDY OF BMS-182248-1 (BR96-DOXORUBICIN IMMUNOCONJUGATE) VERSUS SINGLE-AGENT DOXORUBICIN IN PATIENTS WITH METASTATIC BREAST CANCER.* 1998 ASCO Annual Meeting, 1998. **No. 438**.
62. H. A. Burris, S.V., H. S. Rugo, C. Vogel, R. Borson, E. Tan-Chiu, M. Birkner, S. N. Holden, B. Klencke, J. O'Shaughnessy *A phase II study of trastuzumab-DM1 (T-DM1), a HER2 antibody-drug conjugate (ADC), in patients (pts) with HER2+ metastatic breast cancer (MBC).* 2008 Breast Cancer Symposium, 2008. **No. 155**.
63. Younes, A., et al., *Brentuximab vedotin (SGN-35) for relapsed CD30-positive lymphomas.* N Engl J Med, 2010. **363**(19): p. 1812-21.
64. Ogura, M., et al., *Phase I study of inotuzumab ozogamicin (CMC-544) in Japanese patients with follicular lymphoma pretreated with rituximab-based therapy.* Cancer Sci, 2010. **101**(8): p. 1840-5.
65. DiJoseph, J.F., et al., *Potent and specific antitumor efficacy of CMC-544, a CD22-targeted immunoconjugate of calicheamicin, against systemically disseminated B-cell lymphoma.* Clin Cancer Res, 2004. **10**(24): p. 8620-9.
66. Sapra, P., et al., *Anti-CD74 antibody-doxorubicin conjugate, IMMU-110, in a human multiple myeloma xenograft and in monkeys.* Clin Cancer Res, 2005. **11**(14): p. 5257-64.
67. Bross, P.F., et al., *Approval summary: gemtuzumab ozogamicin in relapsed acute myeloid leukemia.* Clin Cancer Res, 2001. **7**(6): p. 1490-6.
68. A. Qin, J.W., R. A. Mastico, R. J. Lutz, J. O'Keeffe, S. Zildjian, A. C. Mita, A. T. Phan, A. W. Tolcher *The pharmacokinetics and pharmacodynamics of IMGN242 (huC242-DM4) in patients with CanAg-expressing solid tumors.* 2008 ASCO Annual Meeting
69. Lapusan, S., et al., *Phase I studies of AVE9633, an anti-CD33 antibody-maytansinoid conjugate, in adult patients with relapsed/refractory acute myeloid leukemia.* Invest New Drugs, 2011.
70. Blanc, V., et al., *SAR3419: an anti-CD19-Maytansinoid Immunoconjugate for the treatment of B-cell malignancies.* Clin Cancer Res, 2011. **17**(20): p. 6448-58.
71. Kelly, R.K., et al., *An antibody-cytotoxic conjugate, BIIB015, is a new targeted therapy for Cripto positive tumours.* Eur J Cancer, 2011. **47**(11): p. 1736-46.
72. J. G. Berdeja, S.A., S. D. Weitman, S. Zildjian, J. J. O'Leary, J. O'Keeffe, R. Guild, K. Whiteman, A. A. A. Chanan-Khan; Sarah Cannon Research Institute, Nashville, TN; , *Phase I study of lorvotuzumab mertansine (LM, IMGN901) in combination with lenalidomide (Len) and dexamethasone (Dex) in patients with CD56-positive relapsed or relapsed/refractory multiple myeloma (MM).* 2011 ASCO Annual Meeting

73. D. S. Thompson, A.P., J. C. Bendell, K. Papadopoulos, J. R. Infante, R. A. Mastico, D. Johnson, A. Qin, J. J. O'Leary, A. W. Tolcher; Tennessee Oncology, PLLC, Nashville, TN;, *A phase I dose-escalation study of IMGN388 in patients with solid tumors.* 2010 ASCO Annual Meeting
74. Xie, H., et al., *Pharmacokinetics and biodistribution of the antitumor immunoconjugate, cantuzumab mertansine (huC242-DM1), and its two components in mice.* J Pharmacol Exp Ther, 2004. **308**(3): p. 1073-82.
75. Lewis Phillips, G.D., et al., *Targeting HER2-positive breast cancer with trastuzumab-DM1, an antibody-cytotoxic drug conjugate.* Cancer Res, 2008. **68**(22): p. 9280-90.
76. Jagannath, S., *BT062, An Antibody-Drug Conjugate Directed Against CD138, Shows Clinical Activity in Patients with Relapsed or Relapsed/Refractory Multiple Myeloma.* American Society of Hematology (2011) 2011.
77. Al-Katib, A.M., et al., *Superior antitumor activity of SAR3419 to rituximab in xenograft models for non-Hodgkin's lymphoma.* Clin Cancer Res, 2009. **15**(12): p. 4038-45.
78. J. M. Gudas, M.T., Z. An, X. C. Jia, K. J. Morrison, R. K. Morrison, S. B. Kanner, A. B. Raitano, A. Jakobovits, *AGS-16M8F: A novel antibody drug conjugate (ADC) for treating renal and liver cancers.* 2010 Genitourinary Cancers Symposium
79. Lee, J.W., et al., *EphA2 targeted chemotherapy using an antibody drug conjugate in endometrial carcinoma.* Clin Cancer Res, 2010. **16**(9): p. 2562-70.
80. Keir, C.H. and L.T. Vahdat, *The use of an antibody drug conjugate, glembatumumab vedotin (CDX-011), for the treatment of breast cancer.* Expert Opin Biol Ther, 2012. **12**(2): p. 259-63.
81. Wang, X., et al., *In vitro and in vivo responses of advanced prostate tumors to PSMA ADC, an auristatin-conjugated antibody to prostate-specific membrane antigen.* Mol Cancer Ther, 2011. **10**(9): p. 1728-39.
82. Dan Derwin, D.P., Janette Sung, Daniel Tengco, Brian Lee, Barbara Aguilar, Tim Chen, Qian Zhang, Bilal Sufi, Charlie Cong, Sanjeev Gangwar, and M.H. Adam Salles, Alice Stevens, Chetana Rao, Shrikant Deshpande and Vangipuram Rangan, *Activation of Antibody Drug Conjugate MDX-1203 by Human Carboxylesterase 2.* AACR Annual Meeting 2010.
83. J. A. Thompson, A.F.-T., E. I. Heath, S. M. Ansell, S. K. Pal, J. R. Infante, S. De Vos, P. A. Hamlin, B. Zhao, K. Klussman, N. C. Whiting, *The effect of SGN-75, a novel antibody–drug conjugate (ADC), in treatment of patients with renal cell carcinoma (RCC) or non-Hodgkin lymphoma (NHL): A phase I study.* 2011 ASCO Annual Meeting
84. J. M. Gudas, Z.A., R. K. Morrison, K. J. Morrison, S. M. Duniho, R. Moser, L. Smith, P. Senter, D. Benjamin, A. Jakobovits; Agensys, Inc., Santa Monica, CA, *ASG-5ME: A novel antibody-drug conjugate (ADC) therapy for prostate, pancreatic, and gastric cancers.* 2010 Genitourinary Cancers Symposium
85. Reubi, J.C., *Peptide receptors as molecular targets for cancer diagnosis and therapy.* Endocr Rev, 2003. **24**(4): p. 389-427.
86. Guidoccio, F., et al., *Current role of 111In-DTPA-octreotide scintigraphy in diagnosis of thymic masses.* Tumori, 2011. **97**(2): p. 191-5.

87. Kowalski, J., et al., *Evaluation of positron emission tomography imaging using [68Ga]-DOTA-D Phe(1)-Tyr(3)-Octreotide in comparison to [111In]-DTPAOC SPECT. First results in patients with neuroendocrine tumors.* Mol Imaging Biol, 2003. **5**(1): p. 42-8.
88. Bushnell, D., et al., *Evaluating the clinical effectiveness of 90Y-SMT 487 in patients with neuroendocrine tumors.* J Nucl Med, 2003. **44**(10): p. 1556-60.
89. McStay, M.K., et al., *Large-volume liver metastases from neuroendocrine tumors: hepatic intraarterial 90Y-DOTA-lanreotide as effective palliative therapy.* Radiology, 2005. **237**(2): p. 718-26.
90. Sierra, M.L., et al., *Lymphocytic toxicity in patients after peptide-receptor radionuclide therapy (PRRT) with 177Lu-DOTATATE and 90Y-DOTATOC.* Cancer Biother Radiopharm, 2009. **24**(6): p. 659-65.
91. Reubi, J.C., et al., *Affinity profiles for human somatostatin receptor subtypes SST1-SST5 of somatostatin radiotracers selected for scintigraphic and radiotherapeutic use.* Eur J Nucl Med, 2000. **27**(3): p. 273-82.
92. Reubi, J.C., H.R. Macke, and E.P. Krenning, *Candidates for peptide receptor radiotherapy today and in the future.* J Nucl Med, 2005. **46 Suppl 1**: p. 67S-75S.
93. Scopinaro, F., et al., *Fast cancer uptake of 99mTc-labelled bombesin (99mTc BN1).* In Vivo, 2005. **19**(6): p. 1071-6.
94. Fragogeorgi, E.A., et al., *Spacer site modifications for the improvement of the in vitro and in vivo binding properties of (99m)Tc-N(3)S-X-bombesin[2-14] derivatives.* Bioconjug Chem, 2009. **20**(5): p. 856-67.
95. Breeman, W.A., et al., *Preclinical comparison of (111)In-labeled DTPA- or DOTA-bombesin analogs for receptor-targeted scintigraphy and radionuclide therapy.* J Nucl Med, 2002. **43**(12): p. 1650-6.
96. Dimitrakopoulou-Strauss, A., et al., *68Ga-labeled bombesin studies in patients with gastrointestinal stromal tumors: comparison with 18F-FDG.* J Nucl Med, 2007. **48**(8): p. 1245-50.
97. Ferro-Flores, G., et al., *Peptides for in vivo target-specific cancer imaging.* Mini Rev Med Chem, 2010. **10**(1): p. 87-97.
98. Regina, A., et al., *Antitumour activity of ANG1005, a conjugate between paclitaxel and the new brain delivery vector Angiopep-2.* Br J Pharmacol, 2008. **155**(2): p. 185-97.
99. Thomas, F.C., et al., *Uptake of ANG1005, a novel paclitaxel derivative, through the blood-brain barrier into brain and experimental brain metastases of breast cancer.* Pharm Res, 2009. **26**(11): p. 2486-94.
100. Garlich, J.R., et al., *A vascular targeted pan phosphoinositide 3-kinase inhibitor prodrug, SF1126, with antitumor and antiangiogenic activity.* Cancer Res, 2008. **68**(1): p. 206-15.
101. D. Mahadevan, E.G.C., W. Harris, D. D. Von Hoff, A. Younger, D. M. Rensvold, F. Cordova, W. Qi, C. F. Shelton, M. D. Becker, J. R. Garlich, R. K. Ramanathan, *Phase I evaluation of SF1126, a vascular targeted PI3K inhibitor, administered twice weekly IV in patients with refractory solid tumors.* 2011 ASCO Annual Meeting, 2011. **No. 3015**.
102. Ringsdorf, H., *Structure and properties of pharmacologically active polymers.* J. Polym. Sci. symp., 1975. **51**: p. 135-153.
103. Alconcel, S.N.S., A.S. Baas, and H.D. Maynard, *FDA-approved poly(ethylene glycol)-protein conjugate drugs.* Polymer Chemistry, 2011. **2**(7): p. 1442-1448.

104. Li, C., et al., *Complete regression of well-established tumors using a novel water-soluble poly(L-glutamic acid)-paclitaxel conjugate.* Cancer Res, 1998. **58**(11): p. 2404-9.
105. Li, C., et al., *Biodistribution of paclitaxel and poly(L-glutamic acid)-paclitaxel conjugate in mice with ovarian OCa-1 tumor.* Cancer Chemother Pharmacol, 2000. **46**(5): p. 416-22.
106. Boddy, A.V., et al., *A phase I and pharmacokinetic study of paclitaxel poliglumex (XYOTAX), investigating both 3-weekly and 2-weekly schedules.* Clin Cancer Res, 2005. **11**(21): p. 7834-40.
107. Radha Todd, J.S., Alan V Boddy, Melanie J Griffin, Lesley Robson, James Cassidy, Donald Bissett, Martyn Main, Melvin D Brannan, Suzie Elliott, Kevin Fishwick, Mark Verrill, Hilary Calver, *Phase I and Pharmacological Study of CT-2103, a Poly (L-glutamic Acid)-Paclitaxel Conjugate*, in *2001 ASCO Annual Meeting* p. No. 439.
108. Sanchis, J., et al., *Polymer-drug conjugates for novel molecular targets.* Nanomedicine (Lond), 2010. **5**(6): p. 915-35.
109. Homsi, J., et al., *Phase I trial of poly-L-glutamate camptothecin (CT-2106) administered weekly in patients with advanced solid malignancies.* Clin Cancer Res, 2007. **13**(19): p. 5855-61.
110. Duncan, R., J.K. Coatsworth, and S. Burtles, *Preclinical toxicology of a novel polymeric antitumour agent: HPMA copolymer-doxorubicin (PK1).* Hum Exp Toxicol, 1998. **17**(2): p. 93-104.
111. Hopewel, J.W., et al., *Preclinical evaluation of the cardiotoxicity of PK2: a novel HPMA copolymer-doxorubicin-galactosamine conjugate antitumour agent.* Hum Exp Toxicol, 2001. **20**(9): p. 461-70.
112. Bissett, D., et al., *Phase I and pharmacokinetic (PK) study of MAG-CPT (PNU 166148): a polymeric derivative of camptothecin (CPT).* Br J Cancer, 2004. **91**(1): p. 50-5.
113. Meerum Terwogt, J.M., et al., *Phase I clinical and pharmacokinetic study of PNU166945, a novel water-soluble polymer-conjugated prodrug of paclitaxel.* Anticancer Drugs, 2001. **12**(4): p. 315-23.
114. Rice, J.R., et al., *Preclinical efficacy and pharmacokinetics of AP5346, a novel diaminocyclohexane-platinum tumor-targeting drug delivery system.* Clin Cancer Res, 2006. **12**(7 Pt 1): p. 2248-54.
115. Rademaker-Lakhai, J.M., et al., *A Phase I and pharmacological study of the platinum polymer AP5280 given as an intravenous infusion once every 3 weeks in patients with solid tumors.* Clin Cancer Res, 2004. **10**(10): p. 3386-95.
116. Scott, L.C., et al., *A phase II study of pegylated-camptothecin (pegamotecan) in the treatment of locally advanced and metastatic gastric and gastro-oesophageal junction adenocarcinoma.* Cancer Chemother Pharmacol, 2009. **63**(2): p. 363-70.
117. Sapra, P., et al., *Marked therapeutic efficacy of a novel polyethylene glycol-SN38 conjugate, EZN-2208, in xenograft models of B-cell non-Hodgkin's lymphoma.* Haematologica, 2009. **94**(10): p. 1456-9.
118. Schluep, T., et al., *Pharmacokinetics and biodistribution of the camptothecin-polymer conjugate IT-101 in rats and tumor-bearing mice.* Cancer Chemother Pharmacol, 2006. **57**(5): p. 654-62.

119. Wente, M.N., et al., *DE-310, a macromolecular prodrug of the topoisomerase-I-inhibitor exatecan (DX-8951), in patients with operable solid tumors.* Invest New Drugs, 2005. **23**(4): p. 339-47.
120. Danhauser-Riedl, S., et al., *Phase I clinical and pharmacokinetic trial of dextran conjugated doxorubicin (AD-70, DOX-OXD).* Invest New Drugs, 1993. **11**(2-3): p. 187-95.
121. Roh, H., et al., *Synergistic antitumor effects of HER2/neu antisense oligodeoxynucleotides and conventional chemotherapeutic agents.* Surgery, 1999. **126**(2): p. 413-21.
122. Roh, H., et al., *Antisense oligonucleotides specific for the HER2/neu oncogene inhibit the growth of human breast carcinoma cells that overexpress HER2/neu.* J Surg Res, 1998. **77**(1): p. 85-90.
123. Cheng, K. and B. Qin, *RNA Interference for Cancer Therapy*, in *Pharmaceutical Perspectives of Cancer Therapeutics*, Y. Lu and R.I. Mahato, Editors. 2009, AAPS-Springer publishing program.
124. Cheng, K. and R.I. Mahato, *siRNA delivery and targeting.* Mol Pharm, 2009. **6**(3): p. 649-50.
125. Choudhury, A., et al., *Small interfering RNA (siRNA) inhibits the expression of the Her2/neu gene, upregulates HLA class I and induces apoptosis of Her2/neu positive tumor cell lines.* Int J Cancer, 2004. **108**(1): p. 71-7.
126. Engelman, J.A., J. Luo, and L.C. Cantley, *The evolution of phosphatidylinositol 3-kinases as regulators of growth and metabolism.* Nat Rev Genet, 2006. **7**(8): p. 606-19.
127. Wymann, M.P. and L. Pirola, *Structure and function of phosphoinositide 3-kinases.* Biochim Biophys Acta, 1998. **1436**(1-2): p. 127-50.
128. Marone, R., et al., *Targeting phosphoinositide 3-kinase: moving towards therapy.* Biochim Biophys Acta, 2008. **1784**(1): p. 159-85.
129. Vogt, P.K., A.G. Bader, and S. Kang, *Phosphoinositide 3-kinase: from viral oncoprotein to drug target.* Virology, 2006. **344**(1): p. 131-8.
130. Ayala, G., et al., *High levels of phosphorylated form of Akt-1 in prostate cancer and non-neoplastic prostate tissues are strong predictors of biochemical recurrence.* Clin Cancer Res, 2004. **10**(19): p. 6572-8.
131. Kreisberg, J.I., et al., *Phosphorylation of Akt (Ser473) is an excellent predictor of poor clinical outcome in prostate cancer.* Cancer Res, 2004. **64**(15): p. 5232-6.
132. Le Page, C., et al., *Expression and localisation of Akt-1, Akt-2 and Akt-3 correlate with clinical outcome of prostate cancer patients.* Br J Cancer, 2006. **94**(12): p. 1906-12.
133. Mulholland, D.J., et al., *PTEN and GSK3beta: key regulators of progression to androgen-independent prostate cancer.* Oncogene, 2006. **25**(3): p. 329-37.
134. Steck, P.A., et al., *Identification of a candidate tumour suppressor gene, MMAC1, at chromosome 10q23.3 that is mutated in multiple advanced cancers.* Nat Genet, 1997. **15**(4): p. 356-62.
135. Li, J., et al., *PTEN, a putative protein tyrosine phosphatase gene mutated in human brain, breast, and prostate cancer.* Science, 1997. **275**(5308): p. 1943-7.
136. Lei, Q., et al., *NKX3.1 stabilizes p53, inhibits AKT activation, and blocks prostate cancer initiation caused by PTEN loss.* Cancer Cell, 2006. **9**(5): p. 367-78.

137. Wang, S., et al., *Pten deletion leads to the expansion of a prostatic stem/progenitor cell subpopulation and tumor initiation.* Proc Natl Acad Sci U S A, 2006. **103**(5): p. 1480-5.
138. Cairns, P., et al., *Frequent inactivation of PTEN/MMAC1 in primary prostate cancer.* Cancer Res, 1997. **57**(22): p. 4997-5000.
139. Yoshimoto, M., et al., *FISH analysis of 107 prostate cancers shows that PTEN genomic deletion is associated with poor clinical outcome.* Br J Cancer, 2007. **97**(5): p. 678-85.
140. Jia, S., et al., *Essential roles of PI(3)K-p110beta in cell growth, metabolism and tumorigenesis.* Nature, 2008. **454**(7205): p. 776-9.
141. Zhu, Q., et al., *Phosphoinositide 3-OH kinase p85alpha and p110beta are essential for androgen receptor transactivation and tumor progression in prostate cancers.* Oncogene, 2008. **27**(33): p. 4569-79.
142. Kong, D. and T. Yamori, *Phosphatidylinositol 3-kinase inhibitors: promising drug candidates for cancer therapy.* Cancer Sci, 2008. **99**(9): p. 1734-40.
143. Shaywitz, A.J., et al., *PI3K enters beta-testing.* Cell Metab, 2008. **8**(3): p. 179-81.
144. Bi, L., et al., *Early embryonic lethality in mice deficient in the p110beta catalytic subunit of PI 3-kinase.* Mamm Genome, 2002. **13**(3): p. 169-72.
145. Canobbio, I., et al., *Genetic evidence for a predominant role of PI3Kbeta catalytic activity in ITAM- and integrin-mediated signaling in platelets.* Blood, 2009. **114**(10): p. 2193-6.
146. Oman IA, S.H., Drobnjak M, Morris M, Fazzari M, Cordon-Cardo C, ed. *HER-2/neu membrane overexpression in prostate cancer (PC)*. Proc Am Assoc Cancer Res. Vol. 41. 2000. abstract 4572.
147. Morris MJ, R.V., Kelly WK, Slovin SF, Kenneson KI, Osman I,, *A phase II trial of herceptin alone and with taxol for the treatment of prostate cancer.* Proc ASCO, 2000. **19**: p. abstract 330.
148. Watt, K.W., et al., *Human prostate-specific antigen: structural and functional similarity with serine proteases.* Proc Natl Acad Sci U S A, 1986. **83**(10): p. 3166-70.
149. Shaun, J., *Inhibition Of Phosphoinositide 3-Kinase Beta.* International Patent, 2004. **WO/2004/016607**.
150. Agarwal, S., et al., *Peptide prodrugs: improved oral absorption of lopinavir, a HIV protease inhibitor.* Int J Pharm, 2008. **359**(1-2): p. 7-14.
151. Denmeade, S.R., et al., *Enzymatic activation of a doxorubicin-peptide prodrug by prostate-specific antigen.* Cancer Res, 1998. **58**(12): p. 2537-40.
152. Kumar, S.K., et al., *Targeted inhibition of hedgehog signaling by cyclopamine prodrugs for advanced prostate cancer.* Bioorg Med Chem, 2008. **16**(6): p. 2764-8.
153. Wang, L., et al., *Antitumor effect of an HER2-specific antibody-toxin fusion protein on human prostate cancer cells.* Prostate, 2001. **47**(1): p. 21-8.
154. Agus, D.B., et al., *Response of prostate cancer to anti-Her-2/neu antibody in androgen-dependent and -independent human xenograft models.* Cancer Res, 1999. **59**(19): p. 4761-4.
155. Karasseva, N.G., et al., *Identification and characterization of peptides that bind human ErbB-2 selected from a bacteriophage display library.* J Protein Chem, 2002. **21**(4): p. 287-96.

156. Kumar, S.R., T.P. Quinn, and S.L. Deutscher, *Evaluation of an 111In-radiolabeled peptide as a targeting and imaging agent for ErbB-2 receptor expressing breast carcinomas.* Clin Cancer Res, 2007. **13**(20): p. 6070-9.
157. Mitsuoka, K., et al., *Cancer detection using a PET tracer, 11C-glycylsarcosine, targeted to H+/peptide transporter.* J Nucl Med, 2008. **49**(4): p. 615-22.
158. Terada, T., et al., *Structural requirements for determining the substrate affinity of peptide transporters PEPT1 and PEPT2.* Pflugers Arch, 2000. **440**(5): p. 679-84.
159. Ayral-Kaloustian, S., et al., *Hybrid inhibitors of phosphatidylinositol 3-kinase (PI3K) and the mammalian target of rapamycin (mTOR): design, synthesis, and superior antitumor activity of novel wortmannin-rapamycin conjugates.* J Med Chem, 2010. **53**(1): p. 452-9.
160. Goldstein, D., et al., *Anti-HER2 cationic immunoemulsion as a potential targeted drug delivery system for the treatment of prostate cancer.* Cancer Res, 2007. **67**(1): p. 269-75.
161. Kumar, S.K., et al., *Modulating paclitaxel bioavailability for targeting prostate cancer.* Bioorg Med Chem, 2007. **15**(14): p. 4973-84.
162. DiPaola, R.S., et al., *Characterization of a novel prostate-specific antigen-activated peptide-doxorubicin conjugate in patients with prostate cancer.* J Clin Oncol, 2002. **20**(7): p. 1874-9.
163. Denmeade, S.R., et al., *Concentration of enzymatically active prostate-specific antigen (PSA) in the extracellular fluid of primary human prostate cancers and human prostate cancer xenograft models.* Prostate, 2001. **48**(1): p. 1-6.
164. Kottra, G. and H. Daniel, *Bidirectional electrogenic transport of peptides by the proton-coupled carrier PEPT1 in Xenopus laevis oocytes: its asymmetry and symmetry.* J Physiol, 2001. **536**(Pt 2): p. 495-503.
165. Silbernagl, S., V. Ganapathy, and F.H. Leibach, *H+ gradient-driven dipeptide reabsorption in proximal tubule of rat kidney. Studies in vivo and in vitro.* Am J Physiol, 1987. **253**(3 Pt 2): p. F448-57.
166. Miyamoto, Y., V. Ganapathy, and F.H. Leibach, *Proton gradient-coupled uphill transport of glycylsarcosine in rabbit renal brush-border membrane vesicles.* Biochem Biophys Res Commun, 1985. **132**(3): p. 946-53.
167. Barfuss, D.W., V. Ganapathy, and F.H. Leibach, *Evidence for active dipeptide transport in isolated proximal straight tubules.* Am J Physiol, 1988. **255**(1 Pt 2): p. F177-81.
168. Daniel, H. and G. Kottra, *The proton oligopeptide cotransporter family SLC15 in physiology and pharmacology.* Pflugers Arch, 2004. **447**(5): p. 610-8.
169. Takahashi, K., et al., *Interaction of beta-lactam antibiotics with H+/peptide cotransporters in rat renal brush-border membranes.* J Pharmacol Exp Ther, 1998. **286**(2): p. 1037-42.
170. Rubio-Aliaga, I. and H. Daniel, *Mammalian peptide transporters as targets for drug delivery.* Trends Pharmacol Sci, 2002. **23**(9): p. 434-40.
171. Nakanishi, T., et al., *Carrier-mediated transport of oligopeptides in the human fibrosarcoma cell line HT1080.* Cancer Res, 1997. **57**(18): p. 4118-22.
172. Gonzalez, D.E., et al., *An oligopeptide transporter is expressed at high levels in the pancreatic carcinoma cell lines AsPc-1 and Capan-2.* Cancer Res, 1998. **58**(3): p. 519-25.

173. Inoue, M., et al., *Regulation of human peptide transporter 1 (PEPT1) in gastric cancer cells by anticancer drugs.* Cancer Lett, 2005. **230**(1): p. 72-80.
174. Mitsuoka, K., et al., *Inhibition of oligopeptide transporter suppress growth of human pancreatic cancer cells.* Eur J Pharm Sci, 2010. **40**(3): p. 202-8.
175. Terada, T. and K. Inui, *Peptide transporters: structure, function, regulation and application for drug delivery.* Curr Drug Metab, 2004. **5**(1): p. 85-94.
176. Qin, B., et al., *Identification of a LNCaP-specific binding peptide using phage display.* Pharm Res, 2011. **28**(10): p. 2422-34.
177. Tai, W., et al., *Development of a peptide-drug conjugate for prostate cancer therapy.* Mol Pharm, 2011. **8**(3): p. 901-12.
178. Yun, J.J., et al., *Genomic DNA functions as a universal external standard in quantitative real-time PCR.* Nucleic Acids Res, 2006. **34**(12): p. e85.
179. Patel, M., et al., *Molecular expression and functional activity of sodium dependent multivitamin transporter in human prostate cancer cells.* Int J Pharm, 2012. **436**(1-2): p. 324-331.
180. Jwala, J., et al., *Differential expression of folate receptor-alpha, sodium-dependent multivitamin transporter, and amino acid transporter (B (0, +)) in human retinoblastoma (Y-79) and retinal pigment epithelial (ARPE-19) cell lines.* J Ocul Pharmacol Ther, 2012. **28**(3): p. 237-44.
181. Zimmermann, M. and A.C. Stan, *PepT2 transporter protein expression in human neoplastic glial cells and mediation of fluorescently tagged dipeptide derivative beta-Ala-Lys-Nepsilon-7-amino-4-methyl-coumarin-3-acetic acid accumulation.* J Neurosurg, 2010. **112**(5): p. 1005-14.
182. Otto, C. and K. Bauer, *Dipeptide uptake: a novel marker for testicular and ovarian macrophages.* Anat Rec, 1996. **245**(4): p. 662-7.
183. Otto, C., S. tom Dieck, and K. Bauer, *Dipeptide uptake by adenohypophysial folliculostellate cells.* Am J Physiol, 1996. **271**(1 Pt 1): p. C210-7.
184. Dieck, S.T., et al., *The peptide transporter PepT2 is expressed in rat brain and mediates the accumulation of the fluorescent dipeptide derivative beta-Ala-Lys-Nepsilon-AMCA in astrocytes.* Glia, 1999. **25**(1): p. 10-20.
185. Tai, W., B. Qin, and K. Cheng, *Inhibition of breast cancer cell growth and invasiveness by dual silencing of HER-2 and VEGF.* Mol Pharm, 2010. **7**(2): p. 543-56.
186. Qin, B. and K. Cheng, *Silencing of the IKKepsilon gene by siRNA inhibits invasiveness and growth of breast cancer cells.* Breast Cancer Res, 2010. **12**(5): p. R74.
187. Buyse, M., et al., *PepT1-mediated epithelial transport of dipeptides and cephalexin is enhanced by luminal leptin in the small intestine.* J Clin Invest, 2001. **108**(10): p. 1483-94.
188. Ganapathy, M.E., et al., *Differential recognition of beta -lactam antibiotics by intestinal and renal peptide transporters, PEPT 1 and PEPT 2.* J Biol Chem, 1995. **270**(43): p. 25672-7.
189. Wada, M., et al., *Functional linkage of H+/peptide transporter PEPT2 and Na+/H+ exchanger in primary cultures of astrocytes from mouse cerebral cortex.* Brain Res, 2005. **1044**(1): p. 33-41.
190. Knutter, I., et al., *H+-peptide cotransport in the human bile duct epithelium cell line SK-ChA-1.* Am J Physiol Gastrointest Liver Physiol, 2002. **283**(1): p. G222-9.

191. Bhardwaj, R.K., et al., *The functional evaluation of human peptide/histidine transporter 1 (hPHT1) in transiently transfected COS-7 cells.* Eur J Pharm Sci, 2006. **27**(5): p. 533-42.
192. Yamashita, T., et al., *Cloning and functional expression of a brain peptide/histidine transporter.* J Biol Chem, 1997. **272**(15): p. 10205-11.
193. Sakata, K., et al., *Cloning of a lymphatic peptide/histidine transporter.* Biochem J, 2001. **356**(Pt 1): p. 53-60.
194. Mackenzie, B. and J.D. Erickson, *Sodium-coupled neutral amino acid (System N/A) transporters of the SLC38 gene family.* Pflugers Arch, 2004. **447**(5): p. 784-95.
195. Luckner, P. and M. Brandsch, *Interaction of 31 beta-lactam antibiotics with the H+/peptide symporter PEPT2: analysis of affinity constants and comparison with PEPT1.* Eur J Pharm Biopharm, 2005. **59**(1): p. 17-24.
196. Spence, J.R., et al., *Directed differentiation of human pluripotent stem cells into intestinal tissue in vitro.* Nature, 2011. **470**(7332): p. 105-9.
197. Groneberg, D.A., et al., *Intestinal peptide transport: ex vivo uptake studies and localization of peptide carrier PEPT1.* Am J Physiol Gastrointest Liver Physiol, 2001. **281**(3): p. G697-704.
198. Nawashiro, H., et al., *L-type amino acid transporter 1 as a potential molecular target in human astrocytic tumors.* Int J Cancer, 2006. **119**(3): p. 484-92.
199. Brandsch, M., I. Knutter, and E. Bosse-Doenecke, *Pharmaceutical and pharmacological importance of peptide transporters.* J Pharm Pharmacol, 2008. **60**(5): p. 543-85.
200. Sugawara, M., et al., *Transport of valganciclovir, a ganciclovir prodrug, via peptide transporters PEPT1 and PEPT2.* J Pharm Sci, 2000. **89**(6): p. 781-9.
201. Saito, H., et al., *Molecular cloning and tissue distribution of rat peptide transporter PEPT2.* Biochim Biophys Acta, 1996. **1280**(2): p. 173-7.
202. Mrsny, R.J., *Oligopeptide transporters as putative therapeutic targets for cancer cells.* Pharm Res, 1998. **15**(6): p. 816-8.
203. Barbara Meissner, G.C., Michael Boll, Hannelore Daniel, Ralf Baumeister, *The knock-out of the peptide transporter gene pep-2 results in delayed development and extended life-span in Caenorhabditis elegans* International C. elegans Meeting 2001.
204. Edinger, A.L., *Controlling cell growth and survival through regulated nutrient transporter expression.* Biochem J, 2007. **406**(1): p. 1-12.
205. Francis, G.L., *Albumin and mammalian cell culture: implications for biotechnology applications.* Cytotechnology. **62**(1): p. 1-16.
206. Vezina, C., A. Kudelski, and S.N. Sehgal, *Rapamycin (AY-22,989), a new antifungal antibiotic. I. Taxonomy of the producing streptomycete and isolation of the active principle.* J Antibiot (Tokyo), 1975. **28**(10): p. 721-6.
207. Garber, K., *Rapamycin's resurrection: a new way to target the cancer cell cycle.* J Natl Cancer Inst, 2001. **93**(20): p. 1517-9.
208. H. Zhao, K.C., F. Nie, G. Jin, F. Li, L. Wu, L. Wang, M. Brandl, N. Yilidirim, S. Zhang, A. Sun and S. Wong, *Effects of Rapamycin on Breast Cancer Cell Migration through the Cross-Talk of MAPK Pathway.* Cancer Res 2009. **69**(24 suppl).
209. Armstrong, A.J., et al., *A pharmacodynamic study of rapamycin in men with intermediate- to high-risk localized prostate cancer.* Clin Cancer Res, 2010. **16**(11): p. 3057-66.

210. Cloughesy, T.F., et al., *Antitumor activity of rapamycin in a Phase I trial for patients with recurrent PTEN-deficient glioblastoma.* PLoS Med, 2008. **5**(1): p. e8.
211. Phung, T.L., et al., *Pathological angiogenesis is induced by sustained Akt signaling and inhibited by rapamycin.* Cancer Cell, 2006. **10**(2): p. 159-70.
212. Bruns, C.J., et al., *Rapamycin-induced endothelial cell death and tumor vessel thrombosis potentiate cytotoxic therapy against pancreatic cancer.* Clin Cancer Res, 2004. **10**(6): p. 2109-19.
213. Simamora, P., J.M. Alvarez, and S.H. Yalkowsky, *Solubilization of rapamycin.* Int J Pharm, 2001. **213**(1-2): p. 25-9.
214. Yatscoff, R., et al., *Blood distribution of rapamycin.* Transplantation, 1993. **56**(5): p. 1202-6.
215. Ferron, G.M., W.D. Conway, and W.J. Jusko, *Lipophilic benzamide and anilide derivatives as high-performance liquid chromatography internal standards: application to sirolimus (rapamycin) determination.* J Chromatogr B Biomed Sci Appl, 1997. **703**(1-2): p. 243-51.
216. Serajuddin, A.T., *Salt formation to improve drug solubility.* Adv Drug Deliv Rev, 2007. **59**(7): p. 603-16.
217. Sun, M., et al., *The influence of co-solvents on the stability and bioavailability of rapamycin formulated in self-microemulsifying drug delivery systems.* Drug Dev Ind Pharm, 2011. **37**(8): p. 986-94.
218. Gallant-Haidner, H.L., et al., *Pharmacokinetics and metabolism of sirolimus.* Ther Drug Monit, 2000. **22**(1): p. 31-5.
219. Napoli, K.L., et al., *Distribution of sirolimus in rat tissue.* Clin Biochem, 1997. **30**(2): p. 135-42.
220. Yanez, J.A., et al., *Pharmacometrics and delivery of novel nanoformulated PEG-b-poly(epsilon-caprolactone) micelles of rapamycin.* Cancer Chemother Pharmacol, 2008. **61**(1): p. 133-44.
221. Serkova, N., et al., *Assessment of the mechanism of astrocyte swelling induced by the macrolide immunosuppressant sirolimus using multinuclear nuclear magnetic resonance spectroscopy.* Chem Res Toxicol, 1997. **10**(12): p. 1359-63.
222. Benjamin, D., et al., *Rapamycin passes the torch: a new generation of mTOR inhibitors.* Nat Rev Drug Discov, 2011. **10**(11): p. 868-80.
223. Hidalgo, M. and E.K. Rowinsky, *The rapamycin-sensitive signal transduction pathway as a target for cancer therapy.* Oncogene, 2000. **19**(56): p. 6680-6.
224. Goudar, R.K., et al., *Combination therapy of inhibitors of epidermal growth factor receptor/vascular endothelial growth factor receptor 2 (AEE788) and the mammalian target of rapamycin (RAD001) offers improved glioblastoma tumor growth inhibition.* Mol Cancer Ther, 2005. **4**(1): p. 101-12.
225. G. J. Fetterly, M.M.M., C. D. Britten, E. Poplin, W. D. Tap, A. Carmona, L. Yonemoto, C. L. Bedrosian, E. H. Rubin, A. W. Tolcher *Pharmacokinetics of oral deforolimus (AP23573, MK-8669).* 2008 ASCO Annual Meeting 2008.
226. Rubino, J.T.S., Victoria; Harrison, Maureen M. ; Gandhi, Pooja *Parenteral CCI-779 formulations containing cosolvents, an antioxidant, and a surfactant* US Patent, 2011. **8026276**

227. Laplanche, R., G.M. Meno-Tetang, and R. Kawai, *Physiologically based pharmacokinetic (PBPK) modeling of everolimus (RAD001) in rats involving non-linear tissue uptake.* J Pharmacokinet Pharmacodyn, 2007. **34**(3): p. 373-400.
228. Sapra, P., et al., *Novel delivery of SN38 markedly inhibits tumor growth in xenografts, including a camptothecin-11-refractory model.* Clin Cancer Res, 2008. **14**(6): p. 1888-96.
229. Cheng, J., et al., *Synthesis of linear, beta-cyclodextrin-based polymers and their camptothecin conjugates.* Bioconjug Chem, 2003. **14**(5): p. 1007-17.
230. Umeda, N., et al., *A photocleavable rapamycin conjugate for spatiotemporal control of small GTPase activity.* J Am Chem Soc, 2011. **133**(1): p. 12-4.
231. Naicker, S.K.S.T.W.S., *Rapamycin Peptides Conjugates: Synthesis And Uses Thereof - Patent* 2004. **US Patent: 7659244**.
232. Agnihotri, G., et al., *Structure-activity relationships in nucleotide oligomerization domain 1 (Nod1) agonistic gamma-glutamyldiaminopimelic acid derivatives.* J Med Chem, 2011. **54**(5): p. 1490-510.
233. Shaw, C.-C.S., J.; Noureldin, R.; Cheal, G. K.; Fortier, G., *Regioselective Synthesis of Rapamycin Derivatives.* 2001. **US Patent 6,277,983**.
234. Fajun Nan, J.D., Jianping Zuo, Linqian Yu, Linghua Meng, Yangming Zhang, Na Yang, Min Gu, *Rapamycin carbonic ester analogues, pharmaceutical compositions, preparations and uses thereof.* 2011. **USPTO Applicaton No. 20110166172**
235. Bodanszky, M., M.A. Bednarek, and A. Bodanszky, *Coupling in the absence of tertiary amines.* Int J Pept Protein Res, 1982. **20**(4): p. 387-95.
236. Plumb, J.A., R. Milroy, and S.B. Kaye, *Effects of the pH dependence of 3-(4,5-dimethylthiazol-2-yl)-2,5-diphenyl-tetrazolium bromide-formazan absorption on chemosensitivity determined by a novel tetrazolium-based assay.* Cancer Res, 1989. **49**(16): p. 4435-40.
237. Cheng, J., K.T. Khin, and M.E. Davis, *Antitumor activity of beta-cyclodextrin polymer-camptothecin conjugates.* Mol Pharm, 2004. **1**(3): p. 183-93.
238. Decarie, A., et al., *Serum interspecies differences in metabolic pathways of bradykinin and [des-Arg9]BK: influence of enalaprilat.* Am J Physiol, 1996. **271**(4 Pt 2): p. H1340-7.
239. Chandran, S.S., et al., *A prostate-specific antigen activated N-(2-hydroxypropyl) methacrylamide copolymer prodrug as dual-targeted therapy for prostate cancer.* Mol Cancer Ther, 2007. **6**(11): p. 2928-37.
240. Murthy, N., et al., *Design and synthesis of pH-responsive polymeric carriers that target uptake and enhance the intracellular delivery of oligonucleotides.* J Control Release, 2003. **89**(3): p. 365-74.
241. Sun, Y., et al., *Intracellular labeling method for chip-based capillary electrophoresis fluorimetric single cell analysis using liposomes.* J Chromatogr A, 2006. **1135**(1): p. 109-14.
242. Veronese, F.M. and A. Mero, *The impact of PEGylation on biological therapies.* BioDrugs, 2008. **22**(5): p. 315-29.
243. Greenlee, R.T., et al., *Cancer statistics, 2001.* CA Cancer J Clin, 2001. **51**(1): p. 15-36.
244. Stoff-Khalili, M.A., P. Dall, and D.T. Curiel, *Gene therapy for carcinoma of the breast.* Cancer Gene Ther, 2006. **13**(7): p. 633-47.

245. Takahashi, S., et al., *Gene therapy for breast cancer. --Review of clinical gene therapy trials for breast cancer and MDR1 gene therapy trial in Cancer Institute Hospital.* Breast Cancer, 2006. **13**(1): p. 8-15.
246. Bartsch, R., et al., *HER-2-positive breast cancer: hope beyond trastuzumab.* BioDrugs, 2007. **21**(2): p. 69-77.
247. Hobday, T.J. and E.A. Perez, *Molecularly targeted therapies for breast cancer.* Cancer Control, 2005. **12**(2): p. 73-81.
248. Sobel, M., et al., *The microvasculature of the sesamoid complex: its clinical significance.* Foot Ankle, 1992. **13**(6): p. 359-63.
249. Toi, M., et al., *Tumor angiogenesis in breast cancer: its importance as a prognostic indicator and the association with vascular endothelial growth factor expression.* Breast Cancer Res Treat, 1995. **36**(2): p. 193-204.
250. Uzzan, B., et al., *Microvessel density as a prognostic factor in women with breast cancer: a systematic review of the literature and meta-analysis.* Cancer Res, 2004. **64**(9): p. 2941-55.
251. Hansen, S., et al., *The prognostic value of angiogenesis by Chalkley counting in a confirmatory study design on 836 breast cancer patients.* Clin Cancer Res, 2000. **6**(1): p. 139-46.
252. Weis, S.M. and D.A. Cheresh, *Pathophysiological consequences of VEGF-induced vascular permeability.* Nature, 2005. **437**(7058): p. 497-504.
253. Davidoff, A.M. and A.C. Nathwani, *Antiangiogenic gene therapy for cancer treatment.* Curr Hematol Rep, 2004. **3**(4): p. 267-73.
254. Sledge, G.W., H.S. Rugo, and H.J. Burstein, *The role of angiogenesis inhibition in the treatment of breast cancer.* Clin Adv Hematol Oncol, 2006. **4 Suppl 21**(10): p. 1-12.
255. Zelnak, A.B. and R.M. O'Regan, *Targeting angiogenesis in advanced breast cancer.* BioDrugs, 2007. **21**(4): p. 209-14.
256. Linderholm, B., et al., *Overexpression of c-erbB-2 is related to a higher expression of vascular endothelial growth factor (VEGF) and constitutes an independent prognostic factor in primary node-positive breast cancer after adjuvant systemic treatment.* Eur J Cancer, 2004. **40**(1): p. 33-42.
257. Finkenzeller, G., et al., *Activated Neu/ErbB-2 induces expression of the vascular endothelial growth factor gene by functional activation of the transcription factor Sp 1.* Angiogenesis, 2004. **7**(1): p. 59-68.
258. Konecny, G.E., et al., *Association between HER-2/neu and vascular endothelial growth factor expression predicts clinical outcome in primary breast cancer patients.* Clin Cancer Res, 2004. **10**(5): p. 1706-16.
259. Le, X.F., et al., *Specific blockade of VEGF and HER2 pathways results in greater growth inhibition of breast cancer xenografts that overexpress HER2.* Cell Cycle, 2008. **7**(23): p. 3747-58.
260. Pegram, M., et al., *Phase II combined biological therapy targeting the HER2 proto-oncogene and the vascular endothelial growth factor using trastuzumab (T) and bevacizumab (B) as first line treatment of HER2-amplified breast cancer.* Breast Cancer Res Treat, 2006. **100**(Supplement 1): p. S28-29.

261. Pegram, M.D. and D.M. Reese, *Combined biological therapy of breast cancer using monoclonal antibodies directed against HER2/neu protein and vascular endothelial growth factor.* Semin Oncol, 2002. **29**(3 Suppl 11): p. 29-37.
262. Cheng, K. and R.I. Mahato, *Gene modulation for treating liver fibrosis.* Crit Rev Ther Drug Carrier Syst, 2007. **24**(2): p. 93-146.
263. Mahato, R.I., K. Cheng, and R.V. Guntaka, *Modulation of gene expression by antisense and antigene oligodeoxynucleotides and small interfering RNA.* Expert Opin Drug Deliv, 2005. **2**(1): p. 3-28.
264. Cheng, K., N. Yang, and R.I. Mahato, *TGF-beta1 Gene Silencing for Treating Liver Fibrosis.* Mol Pharm, 2009. **6**(3): p. 772-9.
265. Cheng, K., et al., *Adenovirus-based vascular endothelial growth factor gene delivery to human pancreatic islets.* Gene Ther, 2004. **11**(14): p. 1105-16.
266. Ma, L., J. Teruya-Feldstein, and R.A. Weinberg, *Tumour invasion and metastasis initiated by microRNA-10b in breast cancer.* Nature, 2007. **449**(7163): p. 682-8.
267. Sithanandam, G., et al., *Inactivation of ErbB3 by siRNA promotes apoptosis and attenuates growth and invasiveness of human lung adenocarcinoma cell line A549.* Oncogene, 2005. **24**(11): p. 1847-59.
268. Pouliot, N., et al., *Colon cancer cells adhesion and spreading on autocrine laminin-10 is mediated by multiple integrin receptors and modulated by EGF receptor stimulation.* Exp Cell Res, 2000. **261**(2): p. 360-71.
269. Charboneau, A.L., et al., *Suppression of growth and increased cellular attachment after expression of DAL-1 in MCF-7 breast cancer cells.* Int J Cancer, 2002. **100**(2): p. 181-8.
270. Petit, A.M., et al., *Neutralizing antibodies against epidermal growth factor and ErbB-2/neu receptor tyrosine kinases down-regulate vascular endothelial growth factor production by tumor cells in vitro and in vivo: angiogenic implications for signal transduction therapy of solid tumors.* Am J Pathol, 1997. **151**(6): p. 1523-30.
271. Laughner, E., et al., *HER2 (neu) signaling increases the rate of hypoxia-inducible factor 1alpha (HIF-1alpha) synthesis: novel mechanism for HIF-1-mediated vascular endothelial growth factor expression.* Mol Cell Biol, 2001. **21**(12): p. 3995-4004.
272. Eccles, S.A., *The role of c-erbB-2/HER2/neu in breast cancer progression and metastasis.* J Mammary Gland Biol Neoplasia, 2001. **6**(4): p. 393-406.
273. Lieberthal, J.G., et al., *The role of YY1 in reduced HP1 alpha gene expression in invasive human breast cancer cells.* Breast Cancer Res, 2009. **11**(3): p. R42.
274. Liang, Y., R.A. Brekken, and S.M. Hyder, *Vascular endothelial growth factor induces proliferation of breast cancer cells and inhibits the anti-proliferative activity of anti-hormones.* Endocr Relat Cancer, 2006. **13**(3): p. 905-19.
275. Ge, Y.L., et al., *The mechanisms on apoptosis by inhibiting VEGF expression in human breast cancer cells.* Int Immunopharmacol, 2009. **9**(4): p. 389-95.
276. Lee, T.H., et al., *Vascular endothelial growth factor mediates intracrine survival in human breast carcinoma cells through internally expressed VEGFR1/FLT1.* PLoS Med, 2007. **4**(6): p. e186.
277. Price, D.J., et al., *Role of vascular endothelial growth factor in the stimulation of cellular invasion and signaling of breast cancer cells.* Cell Growth Differ, 2001. **12**(3): p. 129-35.

278. Sledge, G.W., Jr., *VEGF-targeting therapy for breast cancer.* J Mammary Gland Biol Neoplasia, 2005. **10**(4): p. 319-23.
279. Foekens, J.A., et al., *High tumor levels of vascular endothelial growth factor predict poor response to systemic therapy in advanced breast cancer.* Cancer Res, 2001. **61**(14): p. 5407-14.
280. Lu, J.J., R. Langer, and J. Chen, *A novel mechanism is involved in cationic lipid-mediated functional siRNA delivery.* Mol Pharm, 2009. **6**(3): p. 763-71.
281. Bagheri-Yarmand, R., et al., *Vascular endothelial growth factor up-regulation via p21-activated kinase-1 signaling regulates heregulin-beta1-mediated angiogenesis.* J Biol Chem, 2000. **275**(50): p. 39451-7.
282. Wen, X.F., et al., *HER2 signaling modulates the equilibrium between pro- and antiangiogenic factors via distinct pathways: implications for HER2-targeted antibody therapy.* Oncogene, 2006. **25**(52): p. 6986-96.
283. Eccles, S.A. and D.R. Welch, *Metastasis: recent discoveries and novel treatment strategies.* Lancet, 2007. **369**(9574): p. 1742-57.
284. Timoshenko, A.V., S. Rastogi, and P.K. Lala, *Migration-promoting role of VEGF-C and VEGF-C binding receptors in human breast cancer cells.* Br J Cancer, 2007. **97**(8): p. 1090-8.
285. De Corte, V., et al., *A 50 kDa protein present in conditioned medium of COLO-16 cells stimulates cell spreading and motility, and activates tyrosine phosphorylation of Neu/HER-2, in human SK-BR-3 mammary cancer cells.* J Cell Sci, 1994. **107 (Pt 3)**: p. 405-16.
286. Wiechen, K. and M. Dietel, *c-erbB-2 anti-sense phosphorothioate oligodeoxynucleotides inhibit growth and serum-induced cell spreading of P185c-erbB-2-overexpressing ovarian carcinoma cells.* Int J Cancer, 1995. **63**(4): p. 604-8.
287. Chen, X., et al., *p73 is transcriptionally regulated by DNA damage, p53, and p73.* Oncogene, 2001. **20**(6): p. 769-74.
288. Butler, T.P. and P.M. Gullino, *Quantitation of cell shedding into efferent blood of mammary adenocarcinoma.* Cancer Res, 1975. **35**(3): p. 512-6.
289. Cominetti, M.R., et al., *Inhibition of platelets and tumor cell adhesion by the disintegrin domain of human ADAM9 to collagen I under dynamic flow conditions.* Biochimie, 2009. **91**(8): p. 1045-52.
290. Yu, D., et al., *Mechanisms of c-erbB2/neu oncogene-induced metastasis and repression of metastatic properties by adenovirus 5 E1A gene products.* Oncogene, 1992. **7**(11): p. 2263-70.
291. Spangenberg, C., et al., *ERBB2-mediated transcriptional up-regulation of the alpha5beta1 integrin fibronectin receptor promotes tumor cell survival under adverse conditions.* Cancer Res, 2006. **66**(7): p. 3715-25.
292. Olsson, A.K., et al., *VEGF receptor signalling - in control of vascular function.* Nat Rev Mol Cell Biol, 2006. **7**(5): p. 359-71.
293. Mercurio, A.M., E.A. Lipscomb, and R.E. Bachelder, *Non-angiogenic functions of VEGF in breast cancer.* J Mammary Gland Biol Neoplasia, 2005. **10**(4): p. 283-90.
294. Schneider, B.P. and G.W. Sledge, Jr., *Drug insight: VEGF as a therapeutic target for breast cancer.* Nat Clin Pract Oncol, 2007. **4**(3): p. 181-9.

295. Zhang, W., et al., *A monoclonal antibody that blocks VEGF binding to VEGFR2 (KDR/Flk-1) inhibits vascular expression of Flk-1 and tumor growth in an orthotopic human breast cancer model.* Angiogenesis, 2002. **5**(1-2): p. 35-44.
296. Liang, Y. and S.M. Hyder, *Proliferation of endothelial and tumor epithelial cells by progestin-induced vascular endothelial growth factor from human breast cancer cells: paracrine and autocrine effects.* Endocrinology, 2005. **146**(8): p. 3632-41.
297. Bruns, C.J., et al., *Vascular endothelial growth factor is an in vivo survival factor for tumor endothelium in a murine model of colorectal carcinoma liver metastases.* Cancer, 2000. **89**(3): p. 488-99.

VITA

Wanyi Tai was born on December 30, 1981 in Hubei, China. He attended his primary, middle and high schools in Hubei, China and graduated in 2000. He obtained his Bachelor of Science degree from School of Traditional Chinese Pharmacy at China Pharmceutical University in July 2004. He obtained a Master degree in Medicinal Chemistry in Jul. 2007.

In August 2007, Mr. Tai joined the University of Missouri-Kansas City, Division of Pharmaceutical Sciences in pursuit of a Doctor degree of Philosophy. He received Out-Standing Leadship Award from School of Pharmacy in 2010.

Mr. Tai is a member of the American Association of Pharmaceutical Scientists (AAPS) and Controlled Release Society (CRS). He is also a permanent member of the Rho Chi Society (an academic honor society in pharmacy).